SAPIENZA
UNIVERSITÀ DI ROMA

DIPARTIMENTO DI INGEGNERIA ASTRONAUTICA, ELETTRICA ED ENERGETICA

DOTTORATO DI RICERCA IN INGEGNERIA AEROSPAZIALE
CICLO XXV

PRECISE ANGLE AND RANGE MEASUREMENTS:

ADVANCED SYSTEMS FOR DEEP SPACE MISSIONS

Author
Francesco Barbaglio

Advisor
Prof. Luciano Iess

Anno Accademico 2011-2012

Aknowledgements

Working on the Ph.D. has been a wonderful and unforgettable experience. Many people have helped and supported me in innumerable ways, during the 3 years spent to carry out the research and complete this dissertation.

First of all, I am deeply grateful to my advisor Prof. Luciano Iess for his continuos support. His wide knowledge and his enthusiasm have been of great value for me. Moreover he gave me the opportunity to be part of a so exciting scientific community and to have an extraordinary learning experience.

I would like to thank Alessandro Ardito and Gabriele Rapino, who have worked with me in the ΔDOR activities and have become true friends. Our collaboration has been a wonderful experience and their constant support, guidance and generosity have made this work possible. I would like also to thank Mattia Mercolino, from ESOC, for his support, his valuable advice and for the funny moments spent in Darmstadt.

In addition, I have been privileged to get to know and to collaborate with Radioscience laboratory colleagues. I wish to express my thanks to them, for their invaluable support and the fun we had during the working days. A special and warm thank goes to a good friend, Marco Ducci with whom I shared many experiences, professional or otherwise, in these three years. Another particular mention to Mauro di Benedetto, whose friendship and support was important.

I especially thank my Mum, my sister Anna and my nephew Francisco. Their indescribable loving support to me throughout my whole life is invaluable. I am also deeply grateful to my Dad. What I have become and what I have achieved is because of him. I am sure he would be very proud of me. My warm thank goes also to my grandmother and other family members, for their interest and support.

Finally, I owe my loving thanks to Alessandra, for her understanding, endless patience and encouragement. Our love is the best result to me in my life.

Table of Contents

List of Figures iv

List of Tables vi

Introduction viii

1 Earth-based radio tracking systems for deep space missions 1
1.1 Radiometric observables . . . 1
1.2 Error sources . . . 4
1.2.1 Clock Instability . . . 4
1.2.2 Instrumental effects . . . 6
1.2.3 Transmission Media . . . 6
1.2.4 Platform parameters . . . 10

I Delta Differential One Way Ranging (ΔDOR) 12

2 ΔDOR system overview 13
2.1 Spacecraft correlation . . . 17
2.2 Quasar correlation . . . 23
2.3 ΔDOR system accuracy . . . 28
2.3.1 Thermal Noise effect . . . 29
2.3.2 Quasar positioning error . . . 30
2.3.3 Error budget . . . 30
2.3.4 Fragmented correlation . . . 32

3 ΔDOR enhancement: Wideband and Low-SNR 33
3.1 Wideband functionality . . . 33
3.2 Low-SNR functionality . . . 38

4 ΔDOR enhancement: Tests and results 43
4.1 Wideband functionality . . . 44
4.1.1 Quasar only: wideband-like acquisition . . . 44
4.1.2 Venus EXpress: wideband-like acquisition . . . 45

4.1.3 Juno: wideband acquisition 48
4.2 LOW-SNR functionality 50
4.2.1 Real data with added noise 50
4.2.2 Simulated data 51

II Pseudo noise ranging system 57

5 Ranging systems overview 58
5.1 Sequential ranging 60
5.1.1 NASA tone ranging: signal structure 61
5.1.2 ESA code ranging: signal structure 63
5.1.3 Power allocation in a transparent channel 65
5.1.4 Acquisition performance 69
5.2 Pseudo noise (PN) ranging 71
5.2.1 PN code structure and properties 72
5.2.2 PN acquisition, tracking and measurement approaches 74
5.2.3 Power allocation in a regenerative channel 76
5.2.4 Acquisition performance 78
5.3 Ranging system accuracy 85
5.3.1 Ranging jitter 85
5.3.2 Error budget 87

6 Pseudo noise open loop receiver 92
6.1 Simulator 93
6.1.1 Mathematical model 93
6.1.2 SW architecture 97
6.2 Correlator 100
6.2.1 Mathematical model 100
6.2.2 SW architecture 108

7 Pseudo noise open loop receiver: Tests and results 110
7.1 No noise 110
7.2 Thermal noise 112
7.3 Computational optimization 118

8 Conclusions 121

A ESA mission: BepiColombo 123

B Phase estimate through I and Q integration 126

C Chip Tracking Loop performance 130

Bibliography 135

List of Figures

2.1 VLBI technique scheme. . . . 14
2.2 ΔDOR tracking scheme. . . . 15
2.3 ESA ΔDOR acquisition system. . . . 16
2.4 ΔDOR acquisition bandwidths. . . . 17
2.5 Venus EXpress (2012-214) spectra. . . . 18
2.6 Top level diagram of the standard spacecraft correlation method. . . . 20
2.7 Ambiguity removal process. . . . 23
2.8 Quasar S148 spectra. . . . 24
2.9 Top level diagram of the quasar correlation process. . . . 25
2.10 ΔDOR error budget. . . . 32

3.1 GS hardware configuration for ΔDOR acquisition. . . . 33
3.2 ESA ΔDOR error budget with standard and wideband configuration. . . . 37
3.3 Top level diagram of low-SNR spacecraft correlation algorithm. . . . 39

4.1 Different funtionalities for ΔDOR computation. . . . 44
4.2 QUASAR 2012-173: Acquisition configuration. . . . 45
4.3 VEX 2012-214: Acquisition configuration. . . . 46
4.4 VEX 2012-214: Results obtained with two different configurations, standard-narrowband (IFMS2) and wideband-like (IFMS3). Different algorithms used. 48
4.5 Juno 2012-267: Acquisition configuration. . . . 48
4.6 Low-SNR VEX 2012-214: Correlation results. . . . 51
4.7 Low-SNR TEST A: Montecarlo results. . . . 53
4.8 Low-SNR TEST B: Noise configuration. . . . 54
4.9 Low-SNR TEST B: Montecarlo results. . . . 55
4.10 Low-SNR TEST C: Noise configuration. . . . 55

5.1 NASA-DSN sequential ranging spectrum. . . . 62
5.2 ESA code sequential ranging spectrum. . . . 64
5.3 PN Ranging-Sequence waveform. . . . 71
5.4 PN ranging signal spectrum. . . . 74
5.5 Functional block diagram of regenerative ranging channel. . . . 75

5.6 Downlink ranging power gain achievable using regenerative approach instead transparent channel. 78
5.7 Signal-space representation for the decision between the in-phase cyclic shift and one of its out- of-phase cyclic shifts of an arbitrary probing sequence. . . 80
5.8 Range error budget. 91

6.1 Simulator and correlator. 92
6.2 Simulator top-level diagram. 94
6.3 Frequencies on a two-way communications. 95
6.4 Simulator SW diagram. 98
6.5 Data packaging for complex signal. 99
6.6 Open loop range measurement principle. 100
6.7 Open loop range measurement top level diagram. 102
6.8 Correlator SW diagram 108

7.1 No noise TEST: Montecarlo simulations results. 112
7.2 TH. NOISE TEST: Montecarlo results. 116
7.3 TH. NOISE TEST: Montecarlo results. 117
7.4 TIME TEST: Results. 120

C.1 CTL block diagram. 131
C.2 Mid-phase integration. 132
C.3 CTL linearize model. 133

List of Tables

2.1 Parameters used for ΔDOR error budget. 31
2.2 ΔDOR Error budget 31

3.1 ΔDOR Error budget with standard and wideband configuration. 37

4.1 QUASAR 2012-173: Correlation results. 45
4.2 VEX 2012-214: Frequency plan. 46
4.3 VEX 2012-214: Correlation settings. 47
4.4 VEX 2012-214: Correlation results in wideband-like (IFMS3) and narrowband (IFMS2) configuration. 47
4.5 VEX 2012-214: Correlation results in wideband-like configuration (IFMS3). . . 47
4.6 Juno 2012-267: Frequency plan. 49
4.7 Juno 2012-267: Correlation settings. 49
4.8 Juno 2012-267: Correlation results. 49
4.9 Low-SNR VEX 2012-214: Correlation settings. 50
4.10 Low-SNR VEX 2012-214: Correlation results. 50
4.11 LOW-SNR TEST A: Frequency plan. 51
4.12 Low-SNR TEST A: Montecarlo results 52
4.13 Low-SNR TEST B: Frequency plan. 54
4.14 Low-SNR TEST B: Montecarlo results 55
4.15 Low-SNR TEST C: Frequency plan. 56
4.16 Low-SNR TEST C: Montecarlo results 56

5.1 Tones frequencies used in NASA-DSN sequential ranging. 61
5.2 Definition for the modulation scheme. 65
5.3 T2B/T4B PN codes: DC properties. 73
5.4 T2B/T4B PN codes: Correlation properties. 73
5.5 T2B/T4B PN codes: Range clock attenuation. 74
5.6 Definition for the modulation scheme. 77
5.7 T2B/T4B PN codes: Acquisition properties. 82
5.8 T2B/T4B PN codes: Acquisition time. 84
5.9 Range error budget: System configurations. 88
5.10 Range error budget: Radio link configuration and link budget. 89

5.11 Range error budget. 90

6.1 Simulation parameters. 99
6.2 Correlation parameters. 109

7.1 No noise TEST: General parameters setup. 111
7.2 No noise TEST: Residual dynamic setup. 111
7.3 No noise TEST: Montecarlo results. 112
7.4 TH. NOISE TEST: General parameters setup. 113
7.5 TH. NOISE TEST: Residual dynamic setup. 113
7.6 TH. NOISE TEST: Noise setup. 114
7.7 TH. NOISE TEST: Montecarlo results. Dynamic case A. 115
7.8 TH. NOISE TEST: Montecarlo results. Dynamic case B. 115
7.9 TH. NOISE TEST: Montecarlo results. Dynamic case C. 115
7.10 TIME TEST: General parameters setup. 118
7.11 TIME TEST: Results. 119

A.1 BepiColombo scientific instruments. 124

Introduction

The navigation of space vehicles is performed by means of radio waves communication with Earth ground stations. Such radio link permits to send commands, receive telemetry and to track the space probes. The radiometric observables, provided by the radio tracking system, are used to reconstruct, in a process called orbit determination, the space probe position and orbit, whose knowledge is fundamental for navigation as well as for science purposes. In fact, radio science and planetary geodesy experiments need an accurate orbit reconstruction; therefore the quality of radiometric data determines ultimately not only the navigation accuracy but also the science return. For this reason the tracking radio systems are subject to continuous developments and improvements. New and advanced techniques are implemented to reduce the contribution from the many errors sources and therefore to provide highly accurate observables demanded by more challenging navigation performance.

The work here presented regards the radio tracking systems used, in deep space missions, to provide angular and range measurements. In particular, after a chapter about radio tracking systems (ch.1) in general, the work consists in two distinctive parts, involving the enhancements of the European Space Agency (ESA) ΔDOR system and the development of an open loop software correlator for ranging system based on pseudo noise (PN) codes.

Delta differential One-way Ranging (ΔDOR), providing a direct measurement of the angular position of a spacecraft, is a powerful technique used for navigation of interplanetary probes. Its principle, simple but effective, consists in measuring the difference in the arrival time of a spacecraft signal at two ground stations, and calibrating it with an ICRF (International Celestial Reference Frame) quasar signal. In 2005, Sapienza University of Rome undertook the development of a ΔDOR correlator for European Space Agency (ESA). Since the first development, and for the last seven years, that system has been used successfully to navigate the Venus Express and the Rosetta ESA probes. After first enhancements, in 2008 ESA provided support also to NASA (National Aeronautics and Space Administration) mission Phoenix and then to JAXA (Japanese Aerospace Exploration Agency) mission Hayabusa. In 2011, further enhancements of the correlator have been undertaken. The two enhancements presented in this work regard the increase of the ΔDOR system accuracy, extending the bandwidth currently limited by the ground stations hardware, and the operability with signals at very-low signal to noise ratio (SNR). The first part of the work starts with chapter 2, treating the ΔDOR system and in particular the ESA one. The new algo-

rithms and methods designed and implemented to be compliant with the ESA requests are explained in the following chapter 3 while the campaign of tests that has been carried out to validate operatively the new algorithms and functionalities, and to investigate the performance of the ΔDOR correlator, is reported in chapter 4.

The ranging systems are based on the simple principle of measuring the time of flight of an electromagnetic wave in vacuum. In particular, these systems consist, in the most common configuration, in a known ranging signal modulated onto an uplink, retransmitted by the spacecraft and then detected on the downlink. The round-trip light time, measured correlating the received ranging signal with a replica of what was transmitted, yields a measurement of the range. The current ranging system uses as ranging signal a series of tones, or components with different frequencies, transmitted sequentially. The need for greater ranging accuracies required by the new generations of interplanetary space mission, like ESA BepiColombo mission, or the need to travel to more distant planets results in a development of new kind of ranging systems based on PN codes. The ranging signal consists in a code, coming from a logical combination of several sequences, which has particular cross correlation properties. This new system permits to adopt a regenerative approach at the spacecraft. The ranging signal, instead of being only de-modulated and re-modulated (transparent approach) as for sequential ranging, is regenerated, before being retransmitted towards Earth. Removing substantially the uplink noise on the ranging signal, this approach results in an increase of the signal-to-noise ratio at the ground station of up to 30dB and therefore in a better measurements precision achievable. Currently ESA stations don't have receivers capable to operate with PN ranging signal, while NASA Deep Space Network (DSN) has only a limited capability. Given the cost and complexity of closed-loop receiver, a software correlator intrinsic cheapness and flexibility make its development meaningful. The second part of this work regards therefore the design and the development of a software correlator, as part of an open loop receiver, able to provide range measurements by means of an offline processing of the signal acquired at the ground station. After a first general chapter (ch.5) on ranging system, the chapter 6 shows the software architecture of the correlator and that of the simulator of the radio link that has been developed. Then, a campaign of tests carried out to investigate the behavior and the performance of the correlator is reported in the 7th chapter.

Chapter 1

Earth-based radio tracking systems for deep space missions

The deep space probes tracking is accomplished by means of radio and optical techniques. The observables provided by these techniques are fundamental for the probe position estimation and the orbit reconstruction, achieved within an iterative procedure called orbit determination process. Although optical on board images are often used, especially in critical mission phases, the most widely used tracking observables are those provided by Earth based radio tracking systems. Until the 1980s the radio tracking consists only on range and range-rate (Doppler) systems, while in 1970s another kind of system was introduced, the very long baseline interferometry (VLBI). The first paragraph summarizes briefly the radiometric observables provided by Earth-based radio tracking systems used in deep space exploration while in the second chapter, are analyzed the common error sources affecting these observables and limiting their accuracy.

1.1 Radiometric observables

The deep space exploration began in the 1960s. In these years, the Deep Space Network (DSN) developed the S-band[1] capability for uplinks and downlinks and the navigation was based on the estimate of line of sight range and range-rate between a ground station and a spacecraft. The rotation of the earth introduce indeed a diurnal signature on the Doppler that depends on the angular coordinates of the spacecraft, leading to the possibility to navigate a probe with a series of these two types of measurements. In the 1970s the X-band[2] downlink was added and the communications was based on the coherent S/X configuration. In that decade, moreover, the first attempts to use VLBI technique, differencing the ranging data, have been explored. In 1980, the first ΔDOR measurements was made, with the Saturn flyby of the probe Voyager. The great advantage to use that technique consists, when the two stations are in the opposite hemispheres, in its insensitivity to the spacecraft

[1] S-band: Uplink $2.110 - 2.120 GHz$, Downlink $2.290 - 2.300 GHz$

[2] X-band: Uplink $8.400 - 8.450 GHz$, Downlink $7.145 - 7.190 GHz$

declination. In the following years, also the uplink in X-band was developed leading to the 1990s in which all the probes were able to operate in the X/X band except for Cassini that, for the first time, implements a coherent X/Ka band[3] . The following missions, as ESA mission BepiColombo, will be equipped with a full Ka/Ka band capability.
The range and range-rate systems used in deep space mission generally consist in

- sending a signal from the station towards the spacecraft
- receiving the signal at the spacecraft and sending back towards Earth
- receiving the signal at the ground station

If the receiving and transmitting antennae are the same, the measurements is called two-way, otherwise is called three way. The ΔDOR observables are, on the other hand, provided in one-way configuration meaning that the radio link has only one leg: the spacecraft sends a signal which is received by ground stations.

Range

The range observable is based on the simple principle of light time. A radio signal propagates with a finite velocity from a source to a target and therefore the time of flight measurement directly provides the distance travelled by the signal photons. The spacecraft topocentric range ρ is approximately related to the one-way signal transit time τ by the expression

$$\rho = r_{sc}\left(t-\tau\right) - r_{gs}\left(t\right) = \tau c \tag{1.1}$$

where

c is the speed of an electromagnetic wave in the vacuum

r_{sc} is the vector connecting the the spacecraft to the centre of the reference frame

r_{gs} is the vector connecting the ground station to the centre of the reference frame

All ranging methods rely on the measurement of the phase delay of a received tone (clock) with respect to the transmitted one. The phase of the transmitted tone is

$$\Phi_{tx}(t) = 2\pi\ f_0 t + 2\pi \int_0^t R(x)\,dx \tag{1.2}$$

where f_0 is the nominal uplink frequency while the integral of the function $R(t)$ accounts for the eventual uplink ramps that sometimes could be applied to compensate the doppler effect due to relative motion. The received phase is, on the other hand,

$$\Phi_{rx}(t) = 2\pi\ f_0(t-\tau(t)) + 2\pi \int_0^{t-\tau(t)} R(x)\,dx \tag{1.3}$$

[3]Ka Band: Uplink $34.200 - 34.700GHz$, Downlink $31.800 - 32.300GHz$

where $\tau(t)$ is the time delay experienced by the signal at time t. The ranging observable is the difference between the phases of the transmitted and received signal. Thus, subtracting eq. 1.3 from eq. 1.2

$$\Phi_{rx} - \Phi_{tx} = -2\pi f_0 \tau(t) + 2\pi \int_t^{t-\tau(t)} R(x)\, dx \tag{1.4}$$

If the uplink is not tuned the range delay τ can be computed directly from the phase delay

$$\tau(t) = -\frac{(\Phi_{rx} - \Phi_{tx})}{2\pi f_0} = -\frac{\Delta\Phi(t)}{2\pi f_0} \tag{1.5}$$

otherwise an iterative procedure can provide it. The intrinsic modulus 2π ambiguity of the phase measurement is reduced by means of

- other tones with different frequencies (sequential ranging)
- using a code with a certain periodicity (code ranging)

Range-rate

Range-rate observables are based on Doppler effect. A signal transmitted with a certain frequency f_T is received with a different frequency f_R

$$f_R = f_T \sqrt{\frac{1 - v/c}{1 + v/c}} \tag{1.6}$$

if the observer and the radio source are in a relative motion (v is the relative velocity). These radiometric measurements, called also Doppler data, consist in observing the frequency of the received signal, with respect to that of the transmitted one. In a one-way configuration it can be approximated as[4]

$$f_R = f_T \left(1 - \frac{\dot{\rho}}{c}\right) \tag{1.7}$$

where f_T is the transmitted frequency and $\dot{\rho}$ is the spacecraft instantaneous range-rate. The measurement is carried out integrating, for a certain time count, the Doppler tone, obtained differentiating the received and transmitted signal, which is actually the Doppler shift (Thornton and Border, 2000). The integrated doppler tone phase can be expressed as

$$ID(t) = \int_0^{T_c} f_R(t)\, dt - \int_0^{T_c} f_T(t - \tau(t))\, dt \tag{1.8}$$

where T_c is the time count and τ is the time delay experienced by the signal. Assuming a constant uplink frequency, it directly translates to the range change over a certain count interval

$$ID(t) \cdot \frac{c}{f_T} = -\int_0^{T_c} \dot{\rho}(t)\, dt \tag{1.9}$$

[4] $f_R = f_T \sqrt{\frac{1-v/c}{1+v/c}} = f_T \sqrt{\frac{1-v/c}{1+v/c}\frac{1-v/c}{1-v/c}} = f_T \sqrt{\frac{(1-v/c)^2}{1-v^2/c^2}} \approx f_T(1 - v/c)$

As for the range, the most common configuration used is the two-way configuration. The above formulation, written for the one-way case, is still valid, with small changes, for the two- or three-way radio link configurations.

ΔDOR

ΔDOR (Delta-DOR) technique is an evolution of Very Long Baseline Interferometry (VLBI) technique, common used in astronomy. VLBI simple principle is to acquire simultaneously, from two widely separated ground stations, the signal coming from a radio source. The differential phase delay experienced by the signal at the two receiving stations, measured by means of a cross-correlation of the two recorded data streams, directly provides one component of the angular position of the source. The geometric time delay, provided by phase measurements, can be expressed indeed as (Thornton and Border, 2000)

$$\tau_g = \frac{1}{c}\mathbf{B} \cdot \hat{s} \tag{1.10}$$

where $\mathbf{B}$ is the baseline vector between the two stations and $\hat{s}$ is the unit vector in the source direction. That measurement, called Differential One-way Ranging (DOR), has an evident strong sensitivity to systematic or random delays introduced by several sources as instrumentation, media, and baseline models. Moreover, the synchronization of the two stations directly introduce an error, that is the largest by far, on the angle measurement. ΔDOR technique has been developed to face that issues. Differentiating the DOR computed for a spacecraft signal with that of an extragalactic radio source (quasar), whose celestial coordinates are very well known, is possible to cancel out largely the common errors and to obtain a highly accurate angle measurement.

1.2 Error sources

The observables accuracy directly affects the orbit determination and consequently the probes navigation and science returns. An analysis of the main error sources affecting these measurements is therefore mandatory. In this paragraph are briefly reported, and quantitatively evaluated, the main error sources for range and range-rate. Since ΔDOR is the difference between two one-way range measurements, the error model for that kind of observables is directly derived from the range errors models.

1.2.1 Clock Instability

A fundamental source of error in radiometric tracking is the clock instability, affecting range and range-rate data through frequency instability and epoch errors.
Considering the range-rate measurement process, based on the comparison between a received frequency and a reference one, it is clear how any frequency instability, as an offset Δf of the reference frequency from the actual transmitted frequency, will translates directly

into a range-rate measurement error (Thornton and Border, 2000)

$$\Delta\dot{\rho} = c\frac{\Delta f}{f} \tag{1.11}$$

The clock stability is usually expressed, quantitatively, in terms of Allan Deviation [5] , and the range rate error can be expressed, in terms of that parameter, as (Thornton and Border, 2000)

$$\Delta\dot{\rho} \approx \sqrt{2 + log_2 M}\, c\sigma_y(\tau) \tag{1.13}$$

where $M = RTLT/\tau$ is ratio between the round trip light time and the integration time τ. Clock instability is the key parameter in choosing two-way configuration for deep space range-rate tracking. The possibility to use the ground station oscillators (hydrogen masers) is a great advantage as, over typical round trip light time (RTLT), their stability is better of about two magnitude orders than the stability reachable with on-board clocks[6]. Considering a round trip light time of 3600 s, and an allan deviation of $8 \cdot 10^{-15}$ with $\tau = 60s$, typically reachable with hydrogen masers, the range rate error is of about $6\mu m/s$.

On the other hand, the effect of frequency instability on range-data is substantially negligible. The two-way range error can be expressed as (Thornton and Border, 2000)

$$\Delta\rho = \sqrt{2}c\tau\sigma_y(\tau) \tag{1.14}$$

where τ is the RTLT. For a probe at 1AU and considering the use of a hydrogen maser the error is indeed on the order of mm. The error introduced on ΔDOR observables is proportional to the time separating spacecraft and quasar observations T_{sep}, and it can be expressed as (Border and Koukos, 1993):

$$\Delta\tau_{ddor} = \sqrt{2}\sigma_y T_{sep} \tag{1.15}$$

The clock epoch error is another aspect to consider. For what concern range-rate data, its effect can be expressed as

$$\Delta\dot{\rho} = \ddot{\rho}\Delta T \tag{1.16}$$

Considering a time tagging error of $2\mu s$ and a probe with an acceleration of $8\ m/s^2$, the consequent error in range rate is of about $16\mu m/s$. Furthermore, the time tagging error introduces a range bias

$$\Delta\rho = \Delta T\dot{\rho} \tag{1.17}$$

which is, for a time-tag error of $1\mu s$ and a spacecraft velocity of $40km/s$, of about $4cm$. Not only the time tagging error should be considered in the range data. Also any epoch offset between transmitted and received signal is directly translated into a range bias by means

[5] Allan deviation without dead time

$$\sigma_y^2(\tau) = \frac{1}{2} < (\bar{y}_{k+1} - \bar{y}_k)^2 > \tag{1.12}$$

where $\bar{y}_k$ and $\bar{y}_{k+1}$ are adjacent measurements of fractional frequency deviation with averaging time τ.

[6] Ultra Stabe Oscilattors generally have a frequency stability at 1000s of about 10^{-13} (Asmar et al., 2005).

of a multiplication factor of the speed of light c:

$$\Delta\rho = c\Delta T \tag{1.18}$$

In case of a three way configuration, a synchronization of $10ns$ lead to an error of $3m$. For what regards, ΔDOR systems, the error in the syncronization between stations is actually the reason to use a quasar for a complete calibration of it. A clock rate offset translates in a range error of

$$\Delta\rho = cRTLT\Delta\dot{T} \tag{1.19}$$

With an unknown clock rate offset of 10^{-13} causes for a one-hour RTLT a range error of $11cm$. Its evident how the two-way configuration, providing a reference frequency highly stable, permits to reduce drastically all these errors.

1.2.2 Instrumental effects

The instruments used to transmit, receive and manipulate the signals obviously introduce both random and systematic measurement errors. The thermal noise, which is proportional to the receiver operating temperature, introduces a purely white phase noise, thus blue frequency noise, on the signal and therefore in each measurements, being range or range-rate. The quantitatively evaluation of that error depends from the tracking system used and it is also range dependent, being determined by the lowest SNR element in the radio link. The thermal noise effect on range and ΔDOR observables is deeply analyzed in the following chapters. Systematic error on range measurements are introduced by the ground station and spacecraft electronics and by the antenna multi path effect. The group delays at the station are generally called station bias and comprise several effects, some of them not completely identified. Every ground station used for deep space navigation is equipped with a calibration system used before and after each pass. Since the group delays depend from the elevation angle (changes on standing waves and multi path patterns), residual station biases remain and they have to be estimated in the orbit determination process. That uncalibrated errors have seen to be in the order of $1-5m$ (Iess et al., 2012). Also at the spacecraft, multi path and standing waves introduce delays which, however, are not so large. The ground station and spacecraft electronics, for range-rate data, are not dominant error sources in the current deep space missions[7].

1.2.3 Transmission Media

Since the signal doesn't propagates into vacuum, it experiences a delaying effect due to troposphere, ionosphere and solar plasma.

[7]For Cassini the errors have been measured to be on the order of 10^{-16} at 1000s for the ground electronics and of about 10^{-15} for the spacecraft transponder (Asmar et al., 2005).

Troposphere

The troposphere is the lowest portion of Earth's atmosphere. It is a non dispersive medium, in particular for frequency up to $15GHz$, and it affects both range and Doppler radio measurements. The refractive effect of the troposphere results in approximately $2m$ of signal path delay at zenith and $20m$ at $6deg$ of elevation (Thornton and Border, 2000). Signals passing through troposphere experience a group velocity which lengthens the apparent signal path by

$$\Delta_{rho} = \int_{\rho} (n-1)\, d\rho = 10^{-6} \int_{\rho} N\, d\rho \tag{1.20}$$

where n is the refractive index and N the refractivity. The refractivity N is made up of two components, a dry and a wet part. The tropospheric delay can be considered, therefore, as the sum of the contributions of the two parts:

$$\Delta\rho = \Delta\rho_d + \Delta\rho_w \tag{1.21}$$

Furthermore, the delay depends from the elevation angle and can be approximated (for high elevation angles) as

$$\Delta\rho_{w/d} = z_{w/d} \cdot \frac{1}{\sin E} \tag{1.22}$$

where $z_{w/d}$ is the delay at zenith and E is the elevation angle. For ΔDOR measurements, the uncertainty due to the variation (time and space) in tropospheric delay causes the following error at each receiving station (Border and Koukos, 1993) :

$$\Delta\tau_{ddor} = \Delta\tau_{z_{w/d}} \left| \frac{1}{\sin E_{SC}} - \frac{1}{\sin E_{QS}} \right| \tag{1.23}$$

where E_{SC} and E_{QS} are the elevation angles of the spacecraft and quasar and $\Delta\tau_{z_{w/d}}$ is the zenith time delay. In addition to a path delay, troposphere induces a relative frequency shift on the carrier

$$y = \frac{\Delta f}{f} = -\frac{1}{c}\frac{d\rho}{dT} \tag{1.24}$$

The range-rate error, due to fluctuations of the tropospheric delay and variation of the elevation angle, can be found deriving eq. 1.22

$$\Delta\dot{\rho} = \frac{\Delta\rho}{T_c} \cdot \frac{1}{\sin E} - \Delta\rho \frac{\cos E}{\sin^2 E} \cdot \frac{\Delta E}{T_c} \tag{1.25}$$

The scintillation magnitude has been measured to be about $3 - 30 \cdot 10^{-15}$ at 1000s of integration time for winter night observations (Asmar et al., 2005).
The large noise introduced by the troposphere leads to the development of several calibration systems, based on the independent estimate of zenith delay. The total tropospheric effect depends on total pressure p, temperature T and partial pressure of the water vapour e. Measuring the pressure in ,mbar (hPa) and the temperature in Kelvin, the refracritivities

can be well approximated (Smith-weintraub model) up to Ka-band (Iess et al., 2002) as

$$\begin{aligned} N_{dry} &= 77.6 \cdot \frac{p}{T} \\ N_{wet} &= 3.73 \cdot 10^5 \frac{e}{T^2} \end{aligned} \tag{1.26}$$

The dry component, which contributes of about 95% of the total zenith path delay, is close to static equilibrium. This assumption permits to know very well the pressure profile once the ground pressure and temperature are measured. Using these measurements and accurate models, the dry contribution can be calculated to an accuracy of a few millimeters (Thornton and Border, 2000). On the other hand, the wet component, although smaller, is much more difficult to estimate due to its dependance from water vapor density along the ray path. It has indeed a poor mixing and an highly variable magnitude and the calculation through model and local meteorological data doesn't provides accuracy better than $4cm$ (Thornton and Border, 2000). To achieve better accuracy is necessary to use other systems. Global Positioning System (GPS) could provides calibration to about one centimeter while best systems use the Water Vapor Radiometer (WVR), providing accuracy in the order of mm (10/20%). The DSN implemented on 2000 an Advanced Media Calibration (AMC) system for the Cassini radioscience experiment and tested it with the Gravitational Wave Experiment (GWE) on 2001-2002 (Tortora et al., 2004). That system, based on new generation of WVR (Advanced-WVR), digital pressure sensors and microwave temperature profilers, permitted to largely remove ($\approx 90\%$) the wet contribution (Asmar et al., 2005). The differential atmospheric delay fluctuations can be measured, with this calibration system, to an accuracy of between 0.2 to 0.5 mm over time scales of $10s$ to $10000s$ (Resch et al., 2000), and reaching an Allan deviation (at 1000s) of $1.5 \cdot 10^{-15}$(Asmar et al., 2005) under favorable conditions.

Ionosphere and Solar wind

The plasma contained in the Ionosphere, part of the upper atmosphere from about $85km$ to $600km$ altitude, and in the solar wind dramatically affects radio measurements. The charged particles cause indeed a dispersive propagation delays in the radio signals. Plasma refraction index n_r is a function of the signal frequency and the plasma frequency

$$\omega_p = \sqrt{4\pi e^2 n_e / m_e} \tag{1.27}$$

where n_e is the electron number density and m_e is the electron mass. Under the hypothesis of high frequency plasma dynamics, the refractive index of interplanetary plasma and ionosphere may be written as (Bertotti et al., 1993)

$$n_r \approx 1 - \frac{1}{2}\left(\frac{\omega_p}{\omega_o}\right)^2 \tag{1.28}$$

The range delay experienced by the signal, frequency dependent, can be therefore closely approximated as

$$\Delta\rho = -\frac{k}{f^2} \tag{1.29}$$

where k is a positive parameter, proportional to the Total Electron Content (TEC) per unit area along the signal path. The signal delay depends upon:

- The time of transmission during the Sun cycle.
- The signal ray pat relative to Sun. The solar plasma delays can range between $1m$ to $75m$, at X-band, depending on Sun-Earth-probe angles.
- The time of of transmission during the day. The Ionosphere indeed has an effect at X-band during daytime of approximately $20 - 60cm$ (at zenith) and an order of magnitude less at night.
- The elevation of the transmission. The delay experienced at zenith moreover, is about $1/3$ of that at the lowest elevations.

For ΔDOR observables, the error due to ionosphere depends from the angular separation ($\Delta\theta$) of the two radio sources, and it can be expressed quantitatively as (Border and Koukos, 1993; Kinman, 2004)

$$\Delta\tau_{ddor} = \frac{(20.6 + 23.9\Delta\theta) \cdot 10^9}{f_c^2} \tag{1.30}$$

On the other hand, the error due to scintillation acquired by the radio signals as they pass through the solar plasma is given by (Kinman, 2004)

$$\Delta\tau_{ddor} = \frac{1.8 \cdot 10^7}{f_c^2 (\sin\gamma_{SEP})^{1.3}} \cdot \left(\frac{B_p}{\nu_{SW}}^{0.75}\right) \tag{1.31}$$

where

f_c is the carrier frequency in hertz

B_p is the projected baseline

γ_{SEP} is the Sun-Earth-probe angle

ν_{SW} is the solar wind velocity

Random variations of interplanetary plasma (and therefore refractive index) cause frequency fluctuations of the signal (scintillation). For a 1-way coherent link the effect in terms of normalized Doppler shift y can be expressed as

$$y \approx \frac{M}{f^2} \tag{1.32}$$

where M is a term proportional to the variation of the plasma electron content during the Doppler integration time. In terms of Allan deviation at 1000s, the plasma scintillation

effect at X-band has a magnitude varying between 10^{-15} at high SEP, and 10^{-12} at very low SEP (Asmar et al., 2005).

The error introduced by plasma is quite large and, together with troposphere, generally plays the role of dominant error source both in Doppler and range data. Several strategies are therefore adopted to reduce it. The delay frequency dependance permits to reduce the range error increasing the frequency used[8] and also permits to calibrate that error by means of a multiple-links approach (Tortora et al., 2004). A dual frequency link permits to partially calibrate the plasma delay, while a three band link permits to have a complete calibration and therefore plasma-free observables. Since multifrequency links are generally not available in deep space missions, the ionospheric effect can be calibrated using model (for example Klobuchar model) based on sensor readings (Iess et al., 2012).

1.2.4 Platform parameters

Platform parameters are the quantities that define the locations of stations in the inertial reference frame.

Station locations

The station coordinates are defined as r_s (spin radius), λ_s (longitude measured easterly from greenwich) and z_s (height above the equator). An error Δr_s causes a declination error inferred from range-rate data of

$$\Delta\delta = \frac{\Delta r_s}{r_s} cot\delta \tag{1.33}$$

Actually the stations location accuracy is of about $1cm$, which translates into an error of at least $4nrad$. For what regards ΔDOR observable, since the angle measurement is directly referred to the baseline vector, an error on station location directly affects the observable introducing a systematic effect. Assuming an uncertainty in the baseline position coordinates of $1.5cm$, that error is (Kinman, 2004):

$$\Delta\tau_{ddor} = 5 \cdot 10^{-11} \Delta\theta \tag{1.34}$$

where $\Delta\theta$ is the angular separation between spacecraft and quasar, in units of radians.

Earth orientation

The orientation of the terrestrial reference frame relative to the instantaneous axis of rotation and the equinox of date can be defined by three quantities: X and Y pole location parameters and UT correction to time of day. The motion of the solid Earth with respect to Earth's spin axis, polar motion, has to be accurately modeled. It substantially consists in:

- Circular oscillations with amplitudes of 100 and $200mas$ and periods of about one year and 433 days respectively. That effect is due to atmosphere and oceans.

[8] Using Ka instead of X-band permits to have an effect 16 times smaller.

- Long-term drift of few milliarcseconds per year due to postglacial rebound to melting ice in greenland or antarctica.
- Decade time-scale variations with amplitude of $50mas$.
- Fluctuations on time scales of a few weeks to a few months with peak variations of less than $20mas$

The total effect is an excursion of the pole location of $10m$ over a period of one year. Moreover, Earth's rate of rotation is not constant, indeed:

- The length of day varies by several milliseconds over a wide range of time periods.
- Secular increases in LOD of about 1ms per century due to tidal dissipation of lunar forces.
- Secular effects due to the melting of ice.
- Variations up to $5ms$ in LOD over decadal and inter annual time scales, probably due to angular momentum transfer between Earth's solid mantle and fluid core.
- Rapid variations on time scales of less than two years probably due to atmospheric effect.

If left uncorrected in the tracking observable models, UT and polar motion (PM) errors translate directly into spacecraft angular position errors. The current accuracy achievable is of about $2mm$ in the PM parameters and $6mm$ in UT (Thornton and Border, 2000) resulting in an error due to polar motion not relevant both in Doppler and in range. For ΔDOR observables this error is proportional to the angular separation between spacecraft and quasar (Kinman, 2004):

$$\Delta\tau_{ddor} = \Delta\theta\frac{\epsilon_{UTPM}}{c} \tag{1.35}$$

where $\Delta\theta$ is the angular separation between the spacecraft and quasar in units of radians and ϵ_{UTPM} is the positional uncertainty in universal time (UT1) and polar motion at the Earth's surface in units of meters

Precession and Nutation

The orientation of Earth's spin axis continually changes in the inertial space due to the effect on the oblate Earth of the lunar and solar gravitation. These changes are described by

- Long-period rotation of the spin axis, called precession.
- small periodic oscillation superimposed to the precession, called nutation.

The corrections to the parameters describing these phenomenon are obtained from VLBI observations of natural radio scorches. Currently, the accuracy is of about $5nrad$.

Part I

Delta Differential One Way Ranging (△DOR)

Chapter 2

$\triangle$DOR system overview

Very Long Baseline Interferometry (VLBI) is a technique, often used in radioastronomy, that allows the angular position determination of distant radio sources. That is carried out measuring the differential phase delay of a radio signal, recorded simultaneously at two geographically separated ground stations. The observed time delay is called DOR (Differential One-way Range) and in absence of error sources it can be expressed as

$$\tau = \frac{1}{c}\mathbf{B} \cdot \hat{s} = \frac{1}{c} B \cos\theta \tag{2.1}$$

where

$\mathbf{B}$ is the baseline vector between the two stations

$\hat{s}$ is the unit vector in the source direction

θ is the angle between the baseline and the station-spacecraft vector.

Thus, knowing a priori the baseline length and orientation, is possible to infer from the delay measurement (τ) one component (θ) of the source position. Combining different measurements provided with different baseline vectors one can determine the celestial coordinates of a radio source (Iess et al., 2006).

The Delta Differential One Way Ranging (Delta-DOR/ΔDOR) is a an application, and evolution, of the VLBI technique in spacecrafts navigation. Its very simple but effective concept is to use an ICRF (International Celestial Reference Frame) quasar, whose celestial coordinates are very well known, to calibrate the spacecraft DOR. The comparison of the delay measurement of a spacecraft (SC) radio signal and that of an angularly nearby quasar (QS) radio source, permits indeed to enhance the SC angular component measurement removing almost completely the common errors. Although the phase delay theoretically depends only on the geometry of the system (eq. 2.1), it is indeed corrupted by many error sources:

- Clock synchronization of the two ground stations, which is by far the major error. Its magnitude is of about $1\mu s$ using GPS signals (Iess et al., 2006).

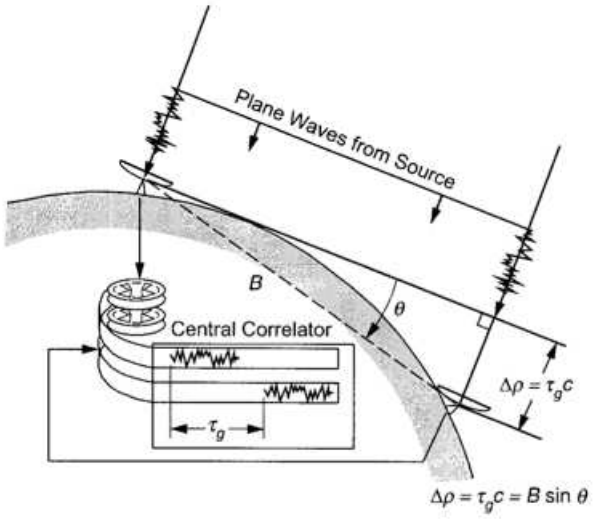

Figure 2.1: VLBI technique scheme. Differential delay τ_g is obtained correlating the signals arriving at the two stations (Thornton and Border, 2000).

- Propagation media, troposphere and ionosphere.
- Clock jitters and other instrumental effects.

The phase delay of the received signal can be schematized therefore as the sum of two phase terms, one accounting the geometrical part and the other accounting for the errors part

$$\phi_{delay} = \phi_{geometric} + \phi_{error} \tag{2.2}$$

For a spacecraft the two phase terms are inseparably and both unknown, while not for a quasar. The first term $\phi_{geometric}$, which is the geometric delay, can be indeed computed within a certain level of accuracy knowing the quasar position[1] and the baseline vector (based on the knowledge of the station locations). Correlating the signal of a quasar, recorded simultaneously at the two stations, is possible therefore to determine quantitatively the effect of the many error sources on its signal (ϕ_{error}). The ΔDOR observable is actually the difference between the spacecraft and quasar DOR. Differencing the two measurements, errors due to station clock offsets and instrumental group delay are almost entirely removed, while the error due to propagation media is quite reduced as it mainly depends upon the commonality of the signal path. For an effective calibration the quasar must be therefore very close, in an angular sense ($< 10deg$), to the spacecraft.

[1]Position knowledge within 50 billionths of a degree (Maddè et al., 2006) for quasar defining International Celestial Reference Frame.

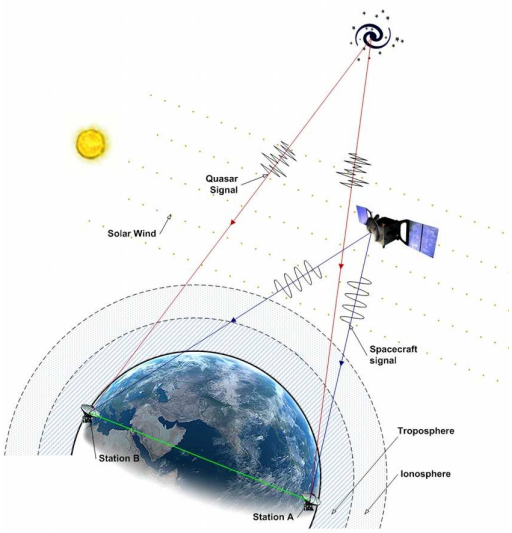

Figure 2.2: Delta-DOR tracking of a deep space probe and a quasar from two ground stations.

In 2004 European Space Agency (ESA) and University of Rome "La Sapienza" undertook the development of a SW correlator to carry out ΔDOR campaign with data acquired by 35-m ESA Deep Space antennae in New Norcia (Australia) and Cebreros (Spain). Since now, ΔDOR technique has been used to successfully navigate the Venus Express spacecraft before the VOI (Venus Orbit Insertion) maneuver, with an achieved accuracy of about $1ns$ (Maddè et al., 2006). It was also used for the support of non-ESA missions such as Phoenix and Hayabusa. What follows refers strictly to the ESA ΔDOR system, even if a large part of it is absolutely general.

A ΔDOR pass consists normally in three scans of data, each of few minutes duration[2]. The observing sequence could be Spacecraft-Quasar-Spacecraft (SQS) or Quasar-Spacecraft-Quasar (QSQ). The use of more than two scans (SC and QS) is need to cancel out clock-epoch and clock-rate offsets, interpolating the two extreme DOR measurements at the time of the central measurement, to which the ΔDOR observable is referred. During each scan, signals, coming from spacecraft (SC) or quasar (QS) are sampled, time tagged and recorded at each antenna (fig.2.3). Then they are processed via software by the central correlator to compute the delay/observable. The received and correlated spacecraft signal is normally the main carrier and a sequence evenly spaced tones (being either dedicated DOR tones or even harmonics of the telemetry subcarrier) while the quasar signal is a broadband signal with nearly flat spectra spread over many gigahertz totally embedded in the antenna receiver noise. Consequently the acquisition scheme used for the spacecraft signal differs from that used for the quasar signal. The ESA back-end receiver Intermediate Frequency Modem System (IFMS), developed by BAE system under ESA contract, provides four complex sub channels of the received spacecraft and quasar signals sampled respectively at a

[2]Typical configuration consists in 5 minutes of SC and 10 minutes of QS.

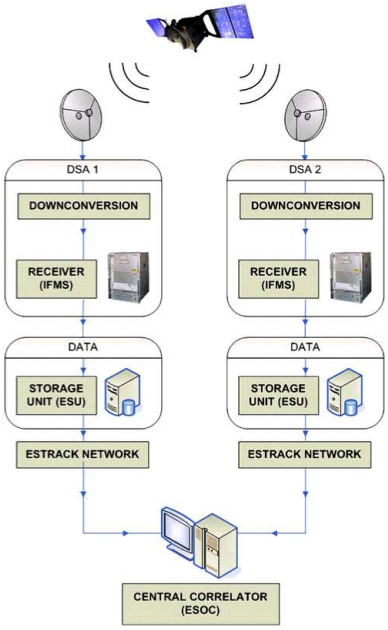

Figure 2.3: ESA ΔDOR acquisition system.

rate close to $50kHz$ and $2MHz$ and with a resolution of 8 and 2 bits[3] (James et al., 2009). The two signals, coming from the two different sources, require not only different acquisition schemes, but also completely different processing algorithms due to their intrinsic different spectral natures. In the next two paragraphs, the correlation algorithms used for spacecraft and quasar data are explained in detail, while in the third paragraph, an analysis of the error budget for ΔDOR system is shown.

[3]Four channels, $50kHz/2MHz$ and $2/8$ bits is the configuration generally used in ESA ΔDOR campaign. However, the IFMS has been developed capable to acquire up to 8 sub channels with bandwidths from $1kHz$ to $2MHz$ and using up to $12bits$ for the signal quantization.

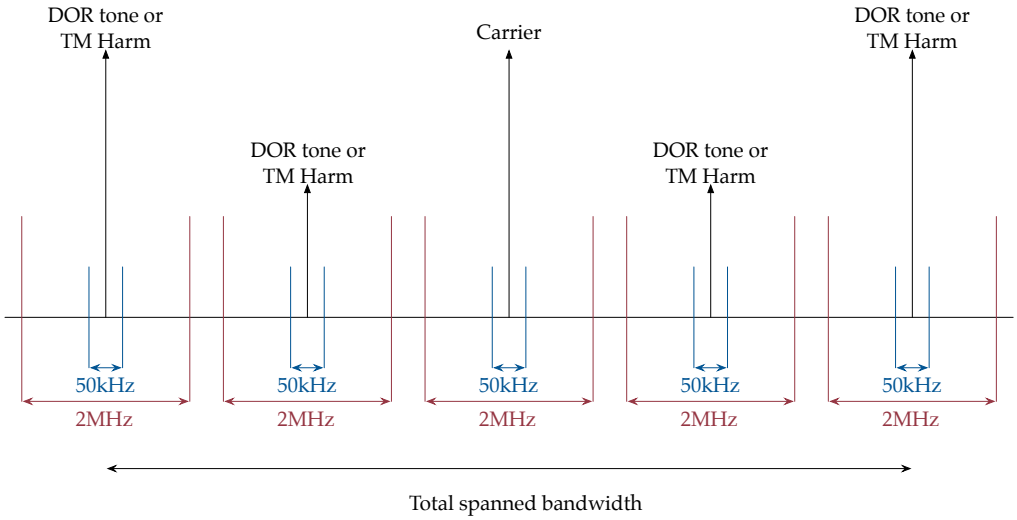

Figure 2.4: Typical acquisition bandwidths of spacecraft (in blue) and quasar (in red) signals.

2.1 Spacecraft correlation

During ΔDOR campaign, the spacecraft telecommunication link is configured in one-way mode. The transmitted signal, which could be the main carrier, a DOR tone or an even telemetry harmonic, is generated by the local on board oscillator and it can be modeled, in the spacecraft reference frame, as

$$s(t) = \mathrm{Re}\left\{s_0 \exp\left[i(\omega_0 t + \phi_0)\right]\right\} \tag{2.3}$$

where ω_0 is the angular frequency and ϕ_0 the initial phase of the transmitted signal.

The signal is not stable in frequency, with jitters of several Hz over short time scales (<1s). Moreover the spectral purity of the signal is poor ($5Hz$ is a typical value of the Mars Express line broadening) and thermal drifts can easily cause offsets of several tens of Hz with respect to the predicted frequency over time scales of days. The emitted frequency can be represented therefore by a constant plus a jitter (which may include a slow drift as well) assumed to be the same for all telemetry harmonics

$$\omega_0 = \langle\omega_0\rangle + \Delta\omega \tag{2.4}$$

The stations, A and B, receive an attenuated, delayed and Doppler shifted replica of the spacecraft signal

$$\begin{aligned} s_A(t) &= \mathrm{Re}\left\{s_{0A} \exp\left[i\left(\omega_0 t + \phi_0 + \mathbf{k_A}\cdot(\mathbf{r_A}(t) - \mathbf{r_{SC}}(t-\tau_A))\right)\right]\right\} \\ s_B(t) &= \mathrm{Re}\left\{s_{0B} \exp\left[i\left(\omega_0 t + \phi_0 + \mathbf{k_B}\cdot(\mathbf{r_B}(t) - \mathbf{r_{SC}}(t-\tau_B))\right)\right]\right\} \end{aligned} \tag{2.5}$$

where

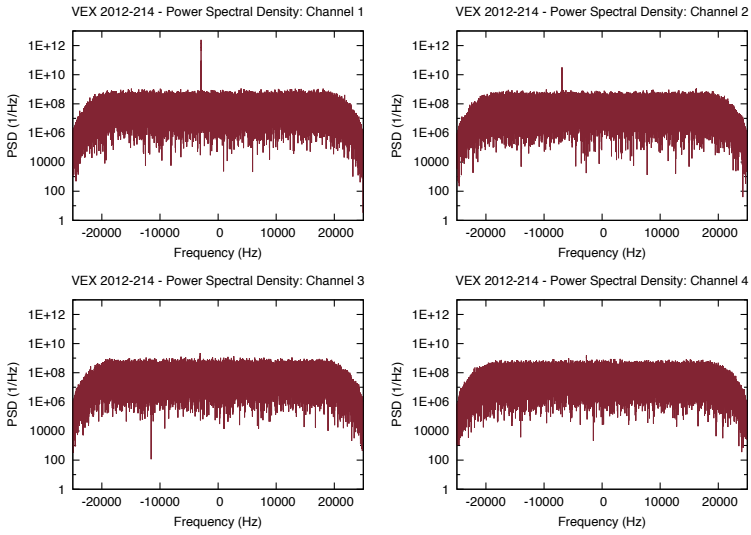

Figure 2.5: Venus EXpress (2012-214) spectra (over 1 second data) of the four $50kHz$ channels.

s_{0A}, s_{0B} are the received signals amplitude at the ground stations

$\mathbf{k}_A$,$\mathbf{k}_B$ are the wavevectors of the e.m. signal ($|\mathbf{k}| = \omega_0/c$) at the two stations, computed accounting for light time and angular aberrations

$\mathbf{r}_A$,$\mathbf{r}_B$ are the position vectors of stations A and B in the intertial frame

$\mathbf{r}_{SC}$ is the position vector of the spacecraft in the intertial frame

τ_A,τ_B are the light times between spacecraft and ground stations

The last term in the exponential is effectively the number of wavelengths (multiplied by 2π) contained in a distance travelled by photons to reach the spacecraft and accounts for the Doppler shift and the delay. In general it is preferred to refer all quantities to the solar system barycenter (SSB) frame of reference, with the time t being coordinate time.

The signal phase may be decomposed into a rapidly varying part ($\omega_0 t$) and a slowly varying part due to the orbital dynamics and media:

$$\begin{aligned} \Phi_A(t) &= \omega_0 t + \phi_0 + \Psi_A\left(t, \tau_A(t)\right) \\ \Phi_B(t) &= \omega_0 t + \phi_0 + \Psi_B\left(t, \tau_B(t)\right) \end{aligned} \tag{2.6}$$

Before being recorded the signal is down-converted (fixed frequency) by a X-band converter and a L-band converter. At the start of the recording session, it is ulteriorly beaten against a complex signal of suitable and constant frequency and brought to nearly zero frequency

after low-pass filtering. The phase of the total down-converting signal is

$$\begin{aligned} \Phi_{LO_A} &= -\hat{\omega}_0 t - \hat{\omega}_{DS_A} t \\ \Phi_{LO_B} &= -\hat{\omega}_0 t - \hat{\omega}_{DS_B} t \end{aligned} \tag{2.7}$$

where

$\hat{\omega}_0$ is the a priori prediction of the transmitted angular frequency

$\hat{\omega}_{DS_{A,B}}$ is an a priori prediction of the angular frequency shift (Doppler effect) induced by relative motion (station-spacecraft)

The resulting signal

$$\begin{aligned} S_A(t) &= S_{0A} \exp\left[i\left(\Omega_A t + \phi_{A_0} + \Psi_A\right)\right[\\ S_B(t) &= S_{0B} \exp\left[i\left(\Omega_B t + \phi_{B_0} + \Psi_B\right)\right[\end{aligned} \tag{2.8}$$

is sampled at $50kHz$ and quantized with 8 bits. It is impossible to obtain a zero beat frequency ($(\Omega_{A,B}+\dot{\Psi}_{A,B})/2\pi$ at $t=0$) mainly because the on board oscillator frequency (transmitted angular frequency ω_0) is not known with a sufficient accuracy (in the order of some kHz). This error causes therefore an offset, expressed by the first residual frequency term $\Omega_{A,B}/2\pi = (\omega_0 - \hat{\omega}_0)/2\pi$. Moreover, it affects the removal of the dynamic ($\dot{\Psi}_{A,B}/2\pi \neq 0$), which is directly proportional to the transmitted frequency. Another minor contribution is the error on a priori range rate model used to set the down-conversion (DC) chain[4]. The residual frequency in the recorded signal, at $t=0$, is however much smaller than the recorded bandwidth and the frequency drift ($t>0$) should not be more than few hundreds Hertz in typical acquisition session of $600s$ (Iess et al., 2006). The constant phase terms ϕ_{A_0} and ϕ_{B_0} account for the phase introduced by the local oscillators[5] . The correlation process consists in computing, for each channel, the differential phase delay ambiguous to multiples of 2π and then, combining all the measurements together, in removing the ambiguity and providing the spacecraft time delay (DOR).

The correlation process is carried out by means of the following steps:

1. Estimation of the transmitted frequency.
2. Signal reconstruction.
3. Phasor rotation removal.
4. Phasors cross multiplication.

[4] A priori uncertainties of $1Hz$ can be easily attained (Iess et al., 2006)

[5] The phase generated by the oscillators used in the DC chain is composed in a generic time t by two terms:

- a phase term due to the phase accumulated by the oscillator starting from its reset time t_0: $\omega_{LO}(t-t_0)$
- a phase term, intrinsic of the oscillator, introduced at the reset time: Φ_0

The first phase term is known while the second, different between the two stations but in common among the channels, is unknown. For simplicity the local oscillator reset time is assumed to be equal at the starting acquisition time ($t=0$), and only the second term is considered.

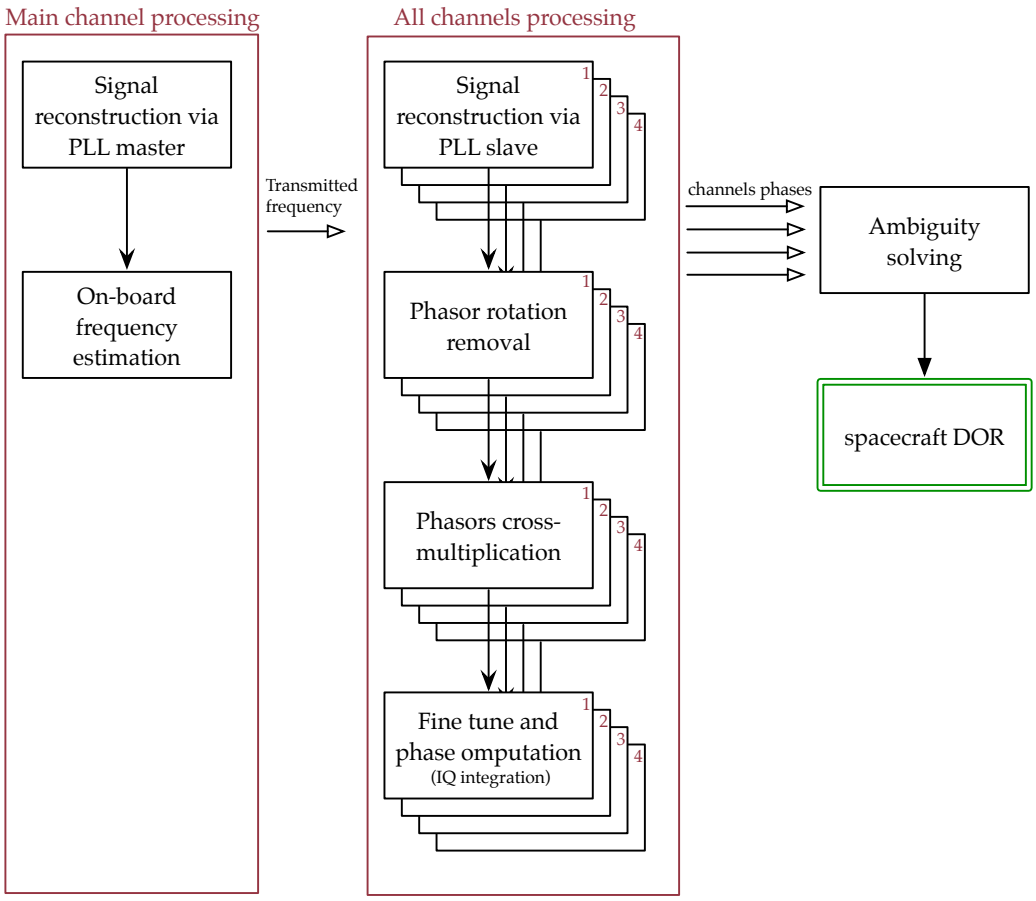

Figure 2.6: Top level diagram of the standard spacecraft correlation method.

5. Fine tune and phase computation.

6. Ambiguity removal.

The inaccuracy on the a priori knowledge of the transmitted frequency, due to the use of on board oscillator in one-way link configuration, requires an initial step, necessary to provide a better estimate of it. The signal of the primary channel is firstly reconstructed by means of a digital phase-locked loop (PLL) . The reconstructed signal, interpolated with a simple mathematical model for the signal dynamics (polynomials), permits to reconstruct the received frequency

$$\hat{f}_{sky} = f_{pll} + f_{lo} \tag{2.9}$$

and to compare it with the frequency of a received signal model computed using the dynamic model $\dot{\rho}_m$ (range and range-rate) provided by Flight Dynamics Group (FD)

$$f_{sky} = \hat{\omega}_0/2\pi(1 - \frac{\dot{\rho}_m}{c}) \tag{2.10}$$

The offset between the reconstructed and the predicted sky frequencies permits to estimate the transmitted frequency and to adjust the frequency prediction ($\hat{\omega}_0$). This initial step, carried out processing the carrier signal (or any other channel strong enough to be tracked by means of a PLL), provides a new and adjusted model necessary not only to stop the phasor rotation (step 3), but also to carry on the signal reconstruction (step 2). The predicted frequency drives indeed an heterodyne integrator, called PLL-slave, to filters out the undesired noise outside a selectable bandwidth (typically $10 - 20Hz$) around the SC signal, channel by channel. Once the the filtering step has been done, the phasors must be stopped. Signals characterized by counterrotating phasors are therefore computed using the a priori model (dynamic prediction plus estimated transmitted frequency)

$$\begin{aligned} &\exp\left[i\left(-\Omega_A t - \Psi_{mA}\right)\right] \\ &\exp\left[i\left(-\Omega_B t - \Psi_{mB}\right)\right] \end{aligned} \tag{2.11}$$

where

The angular frequency terms $\Omega_{A,B} = (\omega_0 - \hat{\omega}_0)$ account for the constant offset between the a priori and the predicted transmitted frequency.

The time variant phase terms $\Psi_{mA,B}$ account for the predicted residual frequency, into the recorded signal, due to dynamic.

Multiplying the recorded and reconstructed complex data streams (step 3) with this computed signal, we obtain

$$\begin{aligned} X_A(t) &= S_{0A} \cdot \exp\left[i\left(-\Omega_A t - \Psi_{mA}\right)\right] = S_{0A} \exp\left[i\left(\phi_{A_0} + \Psi_A - \Psi_{mA}\right)\right] \\ X_B(t) &= S_{0B} \cdot \exp\left[i\left(-\Omega_B t - \Psi_{mB}\right)\right] = S_{0B} \exp\left[i\left(\phi_{B_0} + \Psi_B - \Psi_{mB}\right)\right] \end{aligned} \tag{2.12}$$

The resulting beat signals $X_A(t)$ and $X_B(t)$ are at zero frequency, except for the on board jitter $\Delta\omega$ and a possible small residual frequency offset and drift due to the small uncer-

tainty on the frequency prediction, accounted by the derivative of phase terms $\Psi_A - \Psi_{mA}$ and $\Psi_B - \Psi_{mB}$. The signal of the station A is then multiplied with the conjugated one from station B (step 4)

$$X_{AB}(t) = X_A(t)X_B^*(t) = S_{0A}S_{0B}\exp\left[i\left(\phi_{A_0} - \phi_{B_0} + (\Psi_A - \Psi_{mA}) - (\Psi_B - \Psi_{mB})\right)\right] \quad (2.13)$$

Since the errors affecting the signal at the two stations (X_A and X_B) are strongly correlated, the cross multiplication permits to reduce them largely. However the resulting phasor has still a small constant rotation that has to be removed to provide a phase measurement accurate enough. This residual frequency is firstly searched in the frequency domain, using a FFT and looking for the spectrum peak. The research is ulteriorly refined performing several correlation with signals having frequencies around that rough estimated frequency and looking to the amplitude of the correlated signal. The phasor of $X_{AB}(t)$ after the fine tune step becomes

$$X_{AB}(t) \approx S_{0A}S_{0B}\exp\left[i\left(\phi_{A_0} - \phi_{B_0} + \psi_{A_0} - \psi_{B_0}\right)\right] \approx S_{0A}S_{0B}\exp\left[i\Delta\Phi\right] \quad (2.14)$$

where $\psi_{A_0} - \psi_{B_0}$ is the differential phase delay[6] at time $t = 0$ due to SC position. The integration, channel by channel, of the in-phase (I) and quadrature (Q) phasor components provides finally the total differential phase delay, containing the geometric delay as well as the L.O. contributions

$$\begin{aligned} Z = \int_0^T X_{AB}(t)\,dt = S_{0A}S_{0B}T\exp\left[i\Delta\Phi\right] \\ \Delta\Phi = \arctan\left[\frac{\mathbf{Im}(Z)}{\mathbf{Re}(Z)}\right] \end{aligned} \quad (2.15)$$

The computed $\Delta\Phi_i$ (with $i = 1, n_{channels}$) are then combined together to remove the ambiguity (and the oscillator phases) and compute the spacecraft DOR. A linear interpolation (fig. 2.7) in the phase-frequency plan easily provides the desired spacecraft delay (DOR) being equal to the slope $\Delta\Phi/2\pi\Delta f$ of the interpolating line.

[6] If in step 3, the signal used to remove the rotation accounts also for the range delay at time t=0, the differential phase delay is not an absolute value but it is the difference with the a priori predicted differential phase delay at time t=0

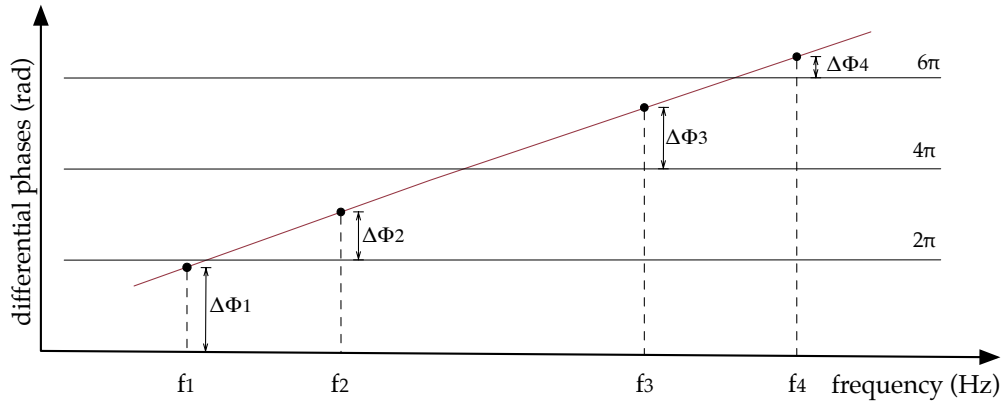

Figure 2.7: Ambiguity removal process. The differential phase delays, coming from all channels, are interpolated with a straight line whose slope is equal to the time delay.

2.2 Quasar correlation

The delay determination of the quasar signal (fig.2.8), acquired at the ESA deep space ground stations, is accomplished through two separate processing steps:

1. Correlation
2. Fringe search

The first step consists in a fringe rotation and delay compensation, driven by the model, to remove as much as possible the known geometric delay between the two stations. The two resulting data streams are then cross-correlated for a range of delays around zero accounting for the unknown clock offset. The integration (of about 1 second) of the discrete correlation function produces a three dimensional complex correlation matrix, function of time, residual delay and beat frequency. This matrix is analyzed, in the second step, to derive an estimate of the residual geometric delay and of its derivative. The process is schematically depicted in fig. 2.9 and is deeply analyzed in the following two subsections.

Correlation process

The signal $s(t)$ emitted by the quasar, is band limited and can be represented as a Fourier integral

$$s(t) = \int_{\omega_2}^{\omega_1} S(\omega) \exp\left[-i\omega t\right] \, d\omega \tag{2.16}$$

That signal, is received at the two antennae, with a certain time delay. Assuming as reference point one antenna (conventionally antenna B), and expressing the corresponding

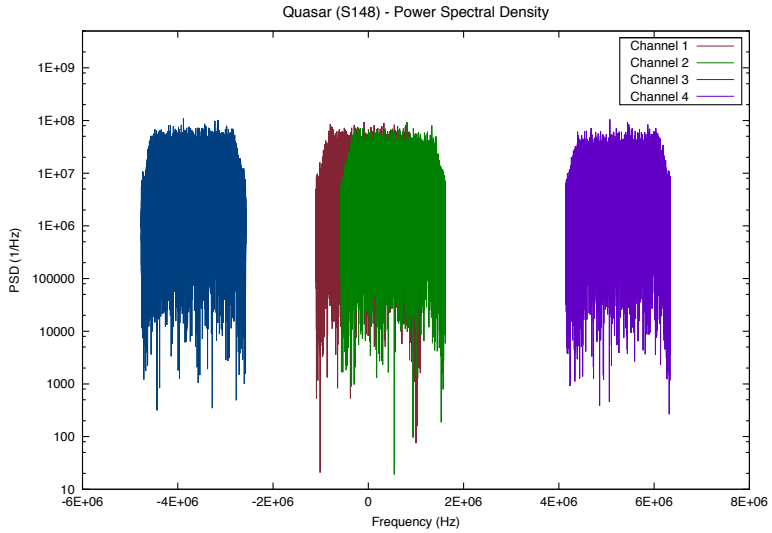

Figure 2.8: Quasar S148 spectra (over 1 second data) of the four 2MHz channels recorded during VEX 2012-214 acquisition. (Frequency relative to the DC applied to the carrier).

geometric delay as $\tau_g(t)$, the signal received by the other antenna (here referred as A) is

$$s_A = s(t - \tau_g) = \int_{\omega_2}^{\omega_1} S(\omega) \exp\left[-i\omega t\right] \exp\left[i\omega\tau_g(t)\right] \, d\omega \tag{2.17}$$

This delay term includes the geometric delay and all the spurious delays, as those due to clock offsets, receivers, antenna misalignments. Such delays must be determined at the end of the process. At each antenna the signal is down converted to nearly zero frequency using several local oscillators. The cumulative effect of them, is to multiply the input signal by a complex exponential

$$\exp\left[i\left(\omega_{lo}t + \phi_{lo}\right)\right] \tag{2.18}$$

We assume that ω_{lo} is exactly what expected and ϕ_{lo} is a slowly varying function. The resulting signal is then filtered by a low pass filter of total band B and sampled at a rate of $B/2\pi$ complex samples per second. Expressing the Fourier integral for $s_A(t)$ in terms of the down converted frequency, instead of the original sky frequency, we have

$$s1_A(t) = \exp\left[i\left(\omega_{lo}\tau_g\left(t\right) + \phi_{lo}\left(t\right)\right)\right] \int_{-B/2}^{+B/2} S(\omega + \omega_{lo}) \exp\left[-i\omega t\right] \exp\left[i\omega\tau_g\left(t\right)\right] \, d\omega \tag{2.19}$$

For very small time intervals, the time delay can be expanded linearly around certain time t_0

$$\tau_g = \tau_{g_0} + \dot{\tau}_g(t - t_0) \tag{2.20}$$

Modeling the true delay τ_g with a suitable function τ_m accounting for the earth rotation (very well known) and tropospheric optical path, we can remove most of the delay effects.

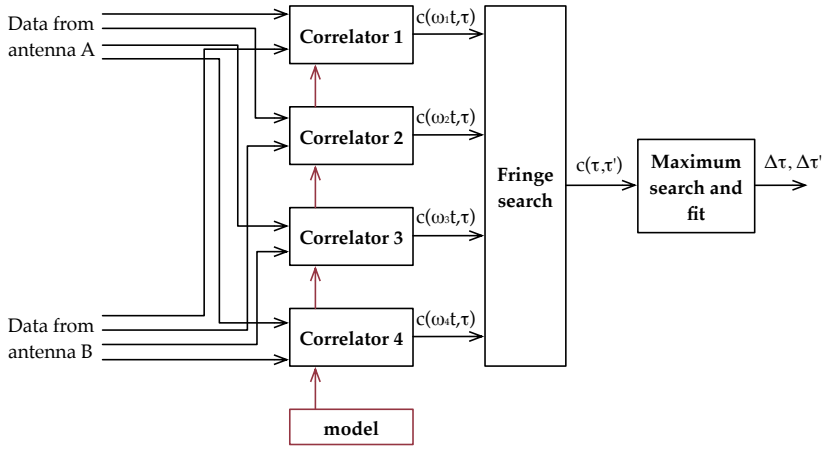

Figure 2.9: Top level diagram of the quasar correlation process.

Also that function is expanded linearly over small time intervals

$$\tau_m = \tau_{m_0} + \dot{\tau}_m(t - t_0) \tag{2.21}$$

and the reference time t_0 are taken corresponding to instants when τ_m is exactly a multiple of the sampling rate. The constraining condition for time segment length is

$$|\dot{\tau}_m(t - t_0)| \leq \pi/B \tag{2.22}$$

and assuming a recording bandwidth $\approx 2MHz$ and $\dot{\tau}_m \approx 1 - 2\mu s/s$, determined by the Earth rotational velocity, follows τ_{m_0} need to be adjusted at most every $200ms$. The removal of the effects due to geometric delay is carried out in two steps:

1. Compensating the Earth rotation introducing a Doppler shift at a frequency $\omega_f = \omega_{lo}\dot{\tau}_m$. That process is called fringe rotation and it is carried out multiplying the data stream by a signal computed using the a priori model.

2. Delaying the data stream of a quantity $-\tau_{m_0}$ accounting for the fixed geometric delay.

After the fringe rotation the beat signal is

$$\begin{aligned} s2_A(t) &= s1_A \exp\left[-i\left(\tau_{m_0}\omega_{lo} + \dot{\tau}_m\omega_{lo}(t - t_0)\right)\right] \\ &= \exp\left[i\left(\omega_{lo}\Delta\tau + \phi_{lo_B}\right)\right] \int_{-B/2}^{+B/2} S\left(\omega + \omega_{lo}\right) \cdot \mathrm{ABC}\, d\omega \end{aligned} \tag{2.23}$$

where $\Delta\tau = \tau_{g_0} - \tau_{m_0}$ represents the residual delay, the quantity we want to determine at the end of the process, and A,B,C are three exponential terms accounting for different contributions:

$\mathrm{A} = \exp\left[-i\omega\left(t - \tau_{m_0}\right)\right]$ corresponds to the time delay τ_{g_0}.

B $= \exp[i\omega\Delta\tau]$, almost constant in time but variable across the bandwidth, accounts for the residual delay. [7]

C $= \exp[i\dot{\tau}_g(t-t_0)]$, variable both in time and in frequency, is called fractional bit shifting. If integrated, it produces a partial decorrelation of the signal. As $|\dot{\tau}_g(t-t_0| \leq \pi/B$, and $|\omega| \leq B/2$ the maximum phase in the exponential is $\pi/2$, at the band edges, and decreases toward the band centre. This corresponds to a decorrelation of $sinc(\pi/2) = 2/\pi$ at the edges, that cannot be neglected. Correlation in the frequency domain may solve the problem, as a fractional bit shift correction may be applied. Alternatively, a short integration time (of the order of a few ms) must be used, and the correction applied to these sub-integrations before summing them together.

Once fringe rotation has been applied, a certain delay has to be added. The maximum usable delay must fall within the frequency and time resolutions for the instrument. The frequency resolution is limited by the correlator size. For a reasonable size of ± 16 samples, the delay range must fall well within this time span, i.e. $\pm 8\mu$ s at $\approx 2MHz$ bandwidth. This can be achieved by performing a preliminary correlation with a much larger time span, and adjusting the model accordingly. The dynamic part of the model is usually much more accurate, and residual fringe rates of more than a few tens of Hertz can be easily obtained, or, in other words, $\omega_{lo}\Delta\tau$ varies slowly, with timescales of several seconds. A final integration time of 1 second is thus realistic for the correlator output. It is better to keep the residual delay and fringe rate well within the usable limits, as the sensitivity of the correlator degrades towards these limits. After this second step the signal becomes

$$\begin{aligned} & s3_A(t) = s2_A(t+\tau_{m0}) \\ & = \exp[i(\omega_{lo}\Delta\tau + \phi_{lo_B})] \int_{-B/2}^{+B/2} S(\omega_{DC}) \exp[-i\omega t] \exp[i\omega(\Delta\tau + \dot{\tau}_{g_0}(t-t_0))]\, d\omega \end{aligned} \tag{2.24}$$

where $\omega_{DC} = \omega + \omega_{lo}$.

The correlator computes the cross correlation of the signals coming from the two antennae

$$c_{AB}(\tau) = \int s3_B s3_A^*\, dt \tag{2.25}$$

and, assuming the fractional fringe correction has been applied, it provides for each integration period t, the function

$$\begin{aligned} & c(\tau, t) = \\ & \exp[i\omega_{lo}(\Delta\tau_B - \Delta\tau_A) + i\Delta\phi_{lo}] \int |S(\omega_{DC})|^2 \exp[-i\omega t] \exp[i\omega(\Delta\tau_B - \Delta\tau_A)]\, d\omega \end{aligned} \tag{2.26}$$

where $\Delta\phi_{lo} = \phi_{lo,B} - \phi_{loA}$

[7] An unmodelled delay has two effects:

- Produce a phase slope across the bandwidth $\exp[i\omega\Delta\tau]$
- Produce a residual fringe frequency $\exp[i\omega_{lo}(\dot{\tau}_g - \dot{\tau}_m)]$

In equation 2.23 the phase term due to residual fringe frequency of order $(\dot{\tau}_g - \dot{\tau}_m)(t-t_0)$ has been implicitly ignored as the model is considered accurate enough to follow the phase over the short time interval $(t-t_0)$.

Fringe search

The correlator output is a function of the delay, time and frequency channel (identified by the different values of the local oscillator angular frequency ω_{lo}). The goal of this operation is finding the final residual delay with the required accuracy. We assume that the local oscillators are built in order to have the same phase among the channels at the same UT time, but different for the two antennae. This is in general not true for the local oscillator (L.O.) in the receiver front-end, but if all frequency channels share the same local oscillator, this L.O. contributes with a constant unknown phase on all the channels. If each frequency channel is provided with a digital local oscillator (typically a direct digital synthesizer, or DDS), their phase can be aligned among different antennae by resetting them at a common UT time. This is true in particular for the digital receiver used at ESA. It is also assumed that the local oscillators are set to the same frequency at the two antennae. If this is not true, a frequency difference term, with the correct initial phase, must be added to the Doppler correction of one of the two data streams. Thus either the L.O. phases must remain constant between stations, or enough information (reset time, exact frequency) must be provided for each L.O. in order to reconstruct its phase at a generic time. A common phase offset or (small) time offset common to all frequency channels is not a problem, as it is part of the quantities calibrated by the EGRS observation. With this assumption we set $(\phi_{lo_B} - \phi_{lo_A}) = 0$. We also define

$$\Delta\tau_{AB} = \Delta\tau_B - \Delta\tau_A \tag{2.27}$$

and expand it

$$\Delta\tau_{AB} = \Delta\tau_{AB,0} + (t - t_0)\,\Delta\dot{\tau}_{AB} \tag{2.28}$$

with t_0 now set around the center of the total integration period (assuming that the residual delay is sufficiently well modeled by a linear approximation). The correlator output, as a function of the frequency channel, time and delay is

$$\begin{aligned} c\left(\omega_{lo}, t, \tau\right) &= \exp\left[i\omega_{lo}\Delta\tau_{AB,0}\right] \exp\left[i\omega_{lo}\left(t - t_0\right)\Delta\dot{\tau}_{AB}\right] D\left(\tau - \Delta\tau_{AB}\right) \\ D\left(\tau\right) &= \int_{-B/2}^{+B/2} S^2\left(\omega + \omega_{lo}\right) \exp\left[-i\omega\tau\right]\, d\omega \end{aligned} \tag{2.29}$$

where $D(\tau)$ is the so called single band delay function. If $S(\omega)$ is reasonable flat in the spectral range of interest, $D(\tau)$ is with good approximation a $sinc()$ function. The function $c(\omega_{lo}, t, \tau)$, representing a three-dimensional matrix, is sampled on a grid in three variables, with typically 4 points for ω_{lo}, one point per second for t, and 16-32 points in τ. The first step is a to transform c on the time axis obtaining

$$\begin{aligned} c_1\left(\omega_{lo}, \omega_f, \tau\right) &= \int_{-T/2}^{+T/2} c\left(\omega_{lo}, t, \tau\right) \exp\left[-i\omega_f t\right]\, dt = \\ &= \exp\left[i\omega_{lo}\Delta\tau_{AB,0}\right] F\left(\omega_f - \omega_{lo}\Delta\dot{\tau}_{AB}\right) D\left(\tau - \Delta\tau_{AB}\right) \end{aligned} \tag{2.30}$$

where

T is the total integration period

$F(\omega)$ is the fringe spectrum, that is usually close to a $sinc$ function of its argument.

We can define a new variable, called residual delay rate, $l = \omega_f/\omega_{lo}$ and regridding the function $c_1(\omega_{lo}, \omega_f, \tau)$ through a linear interpolation (spline interpolator), we obtain

$$c_2\left(\omega_{lo}, l, \tau\right) = \exp\left[i\omega_{lo}\Delta\tau_{AB,0}\right] F'\left(l - \Delta\dot{\tau}_{AB}\right) D\left(\tau - \Delta\tau_{AB}\right) \tag{2.31}$$

where F' is just the resampled version of F[8]. The information from the different frequency bands can be combined together by transforming along the ω_{lo} axis. A direct transform is more easily used, as the number of frequency points is usually very limited. We obtain thus the function

$$\begin{aligned} c_3(\tau_m, l, \tau) &= \sum \exp\left[-i\omega_{lo}\tau_m\right] c_2\left(\omega_{lo}, l, \tau\right) = \\ &= D_m\left(\tau_m - \Delta\tau_{AB,0}\right) F'\left(l - \Delta\dot{\tau}_{AB}\right) D\left(\tau - \Delta\tau_{AB}\right) \end{aligned} \tag{2.32}$$

where $D_m(\tau_m) = \sum \exp\left[-i\omega_{lo}\tau_m\right]$ is called the multiband delay function. D_m has a maximum at zero, and a width roughly equal to the reciprocal of the maximum spacing among the frequency channels. It is periodic, with a period equal to the reciprocal of the maximum common denominator among the frequency spacings, and usually has a lot of strong secondary maxima.

D_m must be computed on a discrete grid wide enough to cover all the region where the singleband delay function $D(\tau)$ is not negligible, and with a resolution step much finer than the reciprocal frequency span of the frequency channels: $\Delta\tau_m < 1/(\omega_+ - \omega_-)$, where ω_- and ω_+ are the lower and higher frequency channels. Ambiguity can be reduced combining the information from the singleband and multiband delays. This can be done choosing the delay element with the appropriate delay in computing $c_3(\omega_{lo}, l, \tau)$. In this way, computational time is also reduce, since c_3 is computed on a bidimensional grid of limited size. This is equivalent to transform the four correlation functions $c_2(\omega_{lo}, l, \tau)$ on the τ axis, combine the four resulting functions on a common frequency axis, and transform back to the multiband delay domain. This final function $c_4(\tau, l) = c_2(\tau, l, \tau)$, computed on a bidimensional grid in (l, τ) has a strong peak for $\tau = \Delta\tau_0$ and $l = \Delta\dot{\tau}$. This peak can be better identified if function $D(\tau)$ and $F'(l)$ are computed using oversized FFT's. The final value can be computed by fitting a paraboloid or truncated $sinc$ around the maximum. The procedure will give also formal error for derived quantities $\Delta\tau_0$ and $\Delta\dot{\tau}$.

2.3 ΔDOR system accuracy

Evaluating the performance of the ΔDOR system, in terms of observables accuracy, is fundamental. Many errors affects, indeed, the ΔDOR observables and in general any radio-

[8]Regridding the correlation functions is important in VLBI operations, where the relative bandwidth $\Delta\omega_{lo}$ is a significant fraction of the sky frequency, and where the residual delay rate may be high. In our case the fractional bandwidth is of the order of 0.2%, that corresponds to a decorrelation of ± 13 degrees for a residual fringe frequency of $0.1Hz$ and an integration time of 300 seconds.

metric data. The main errors source have been already discussed in the par. 1.2, however the effect of thermal noise in the phase measurements is here investigated and provided quantitatively. After having discussed also the quasar positioning error, an error budget can be computed, showing the overall performance of the system. Furthermore, is here explained the, so called, fragmented correlation. This approach is commonly used and consists in dividing the entire batch of data in fragments.

2.3.1 Thermal Noise effect

The thermal noise due to the receiver, strongly affects the correlation used to measure the phase delay of the signals. To compute an overall accuracy of the ΔDOR system is therefore necessary to quantitatively determine the measurements precision achievable in case of spacecraft signal as well as for quasar signal.

Quasar correlation

The measurement precision (standard deviation) in seconds achievable with a quasar signal is given by (Kinman, 2004)

$$\sigma_\tau = \frac{1}{0.7 \cdot 2\pi\Delta f}\sqrt{\frac{2T_{s1}T_{s2}}{T_{q1}T_{q2}BT_{obs}}} \tag{2.33}$$

where

T_{obs} is the observation (and correlation) time

B is the passband bandwidth for each component of measured quasar signal

Δf is the spanned bandwidth

T_{s1} and T_{s2} are the system noise temperature

T_{q1} and T_{q2} are the equivalent temperature at the two antennae due to radiation from the quasar. They are related to the flux S_c as

$$T_{qi} = 0.0003\pi\eta_i r_i^2 S_c \tag{2.34}$$

where r_i and η_i are the aperture radius and efficiency of the antenna

Spacecraft correlation

The spacecraft delay measurement error (standard deviation) due to the thermal noise is (Kinman, 2004)

$$\sigma_\tau = \frac{\sqrt{2}}{2\pi\Delta f\sqrt{T_{obs} \cdot P/N_0}} \tag{2.35}$$

where

T_{obs} is the observation time

Δf is the total spanned bandwidth

P/N_0 is the signal over noise density ratio

This expression is found assuming the same SNR for the two antennae (the factor $\sqrt{2}$ reflects that assumption).

2.3.2 Quasar positioning error

The angle measured by the ΔDOR measurements is referred to the position of the quasar. An error on it obviously reflects on the spacecraft positioning. This error is (Border and Koukos, 1993):

$$\Delta\tau_{ddor} = \frac{B_p}{c}\epsilon_\theta \tag{2.36}$$

where

ϵ_θ is the angular position error in radians

c is the speed of electromagnetic wave in vacuum (m/s)

B_p is the projection of the baseline onto a line that is perpendicular to the line-of-sight direction to the quasar

2.3.3 Error budget

Taking in account what reported in this paragraph, what explained in par. 1.2 and referring to Border and Koukos (1993) and Kinman (2004), an indicative error budget for the current ΔDOR systems can be evaluated. Considering the general parameters reported in tab. 2.1, the total error (tab. 2.2,fig. 2.10) is of about $0.4ns$, strongly dominated by thermal noise.

Parameter	Value	Comments
SC SNR P/N	$15dBHz$	Typical value when using telemetry
QS flux S_c	$0.7jansky$	Generally between 0.3 and 1.5
AntennaA efficiency η	0.67	
AntennaB efficiency η	0.67	
AntennaA diameter D1	$35m$	ESA antenna
AntennaB diameter D2	$35m$	ESA antenna
System temperature $T_{sys}A$	$45K$	
System temperature $T_{sys}B$	$45K$	
T_{obs} SC	$300s$	Typical ESA operative acquisition
T_{obs} QS	$600s$	Typical ESA operative acquisition
Spanned bandwidth Δf	$9MHz$	ESA mission VEX
Baseline	$11621km$	CEB-NNO
Clock Instability	$3 \cdot 10^{-15}$	
Instrumental phase ripple ϵ_{phi}	$0.2rad$	
Separation time T_{sep}	$600s$	
Separation angle $\Delta\theta$	$5deg$	Up to 10 deg
SEP angle γ_{SEP}	$50deg$	
Carrier frequency f_c	$8.4GHz$	X-band
Baseline positioning error ϵ_θ	$1nrad$	
QuasarA positioning error ϵ_θ	$1nrad$	
QuasarB positioning error ϵ_θ	$1nrad$	
SCA elevation angle γ_{SC}	$45deg$	
SCB elevation angle γ_{SC}	$45deg$	
QSA elevation angle γ_{QS}	$40deg$	
QSB elevation angle γ_{QS}	$40deg$	
Solar wind velocity ν_{SW}	$400km/s$	
Earth spin axis uncertainty ϵ_{UTPM}	$10cm$	
Zenith path delay uncertainty	$5cm$	

Table 2.1: Parameters used for ΔDOR error budget.

Error source	Value (ns)
Quasar Thermal noise	0.242
Spacecraft Thermal noise	0.257
Quasar positioning	0.039
Clock Instability	0.003
Phase ripple	0.124
Station location	0.008
Earth orientation	0.029
Ionosphere	0.058
Solar plasma	0.004
Troposphere	0.034
Total error	**0.384**

Table 2.2: ΔDOR Error budget

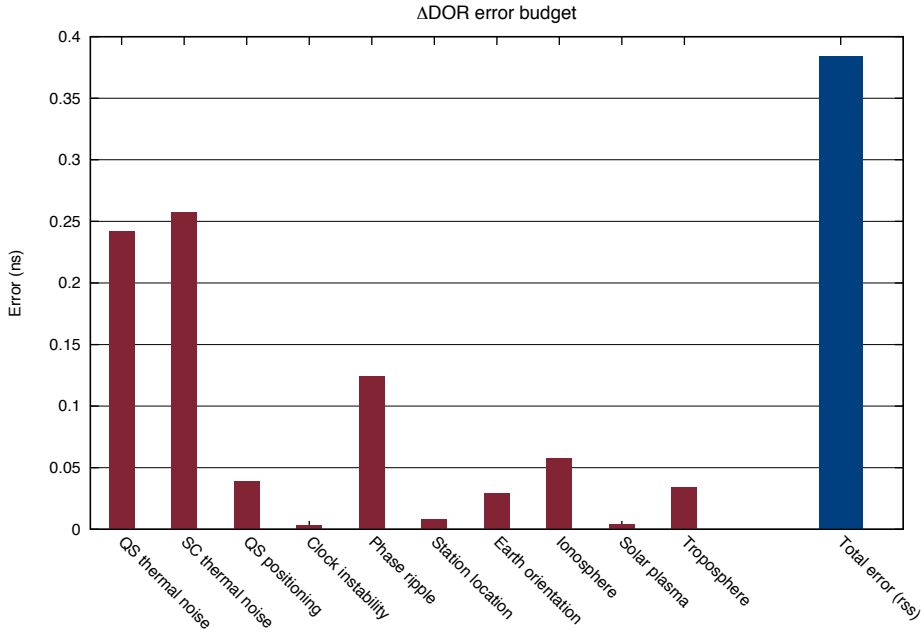

Figure 2.10: ΔDOR error budget.

2.3.4 Fragmented correlation

Although the correlation is based on some minutes of data, the process is carried out dividing the entire batch of data in several fragments of a certain number of seconds, generally 20 or 30. The correlation is performed therefore for each chunk of data, providing a number of observables equals to the fragments number. All these observables are then fitted and the mean value is taken as the ΔDOR observables of the acquisition and the sigma as the error associated to the measurement, containing therefore the random errors due to thermal noise (the systematic errors are not included). This approach, called fragmented correlation, is needed because the fit of the phases, needed to provide the initial phase of each channel, is strongly affected by troposphere. Over a long integration time, the signatures of the troposphere become dominant and invalidate the fit.

Chapter 3

△DOR enhancement: Wideband and Low-SNR

3.1 Wideband functionality

As in any interferometric measurement the total spanned bandwidth, which is the frequency difference between the external channels used in the correlation, is a crucial parameter because the accuracy is determined by its inverse. Currently at ESA station the achievable total spanned bandwidth is limited by the hardware used into the downconversion chain, which consists in an X-band (or Ka-band) downconverter, an L-band downconverter (LDC) and the Intermediate Frequency Modem System (IFMS). The LDC used has the capability to output a portion of spectrum wide at most $28MHz$. This problem can be overcome implementing a new configuration (fig. 3.1). Using several (up to three) LDC to acquire

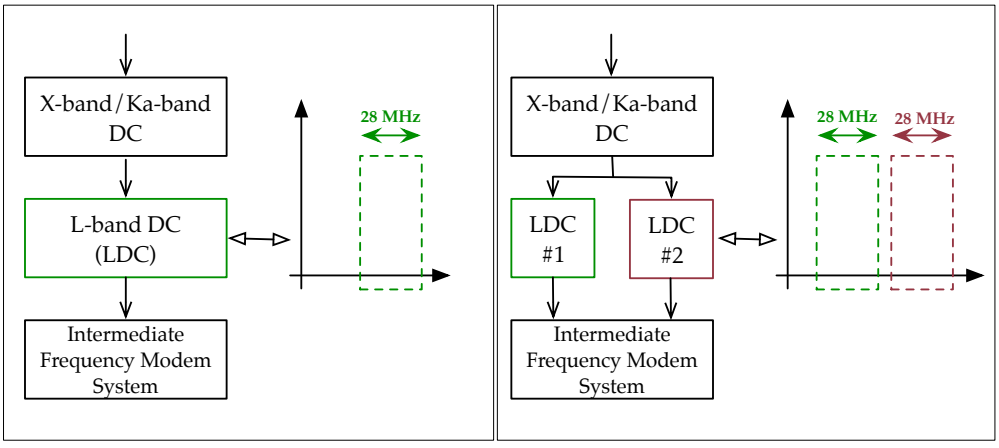

Figure 3.1: GS hardware configuration for standard (left) and wideband (right) acquisition.

different portion of the signal spectrum, and several back end receivers (IFMS) is possible indeed to increase the spanned bandwidth and therefore increase the achievable measurement accuracy. This configuration is not compliant with the algorithm used actually into the correlator. The initial phase of the signal coming from different LDC and recorded by different IFMS is different for all the channels (or different portions of the spectrum); this is due to:

- Different LDC used in the down-conversion stage
- Non perfect UTC synchronization of the IFMS
- Different delay of the cables used

These initial phases, not common to all channels, avoid the ambiguity resolution. A new method, called phase subtraction method, has been therefore implemented in order to make the correlator capable to process data acquired in this new wideband configuration.

Mathematical formulation

The following mathematical formulation does not describe, again, in details the correlation process, which has been explained in the previous chapter. Some mathematical operations are indeed neglected in favor of a more conceptual explanation. It is shown how the standard correlation mode cannot work with acquisitions carried out using different LDC and IFMS (wideband configuration); moreover, it is shown how to overcome the initial phases issue with the method that implies the subtraction of the quasar correlation phases from the spacecraft correlation phases. This formulation applies to a general QS and SC acquisition; of course, the same can be said about second QS or SC acquisition.

The phase of the signal at a generic time t can be written as

$$\Phi_{SIG_{A,B}}^{i^{S,Q}} = \Phi_{0_{A,B}}^{i^{S,Q}} + 2\pi \cdot f_{LO}^{i} \cdot (t - t_0)_{A,B}^{S,Q} + \Phi_{CLK}^{i} + \Phi_{\tau}^{i^{S,Q}} \tag{3.1}$$

where

$\Phi_{SIG_{A,B}}^{i^{S,Q}}$ is the phase of the signal for the i-th channel, at stations A and B, for spacecraft and quasar.

$\Phi_{0_{A,B}}^{i^{S,Q}}$ is the unknown phase of the signal when the local oscillator is reset, at time t_0. This may be different for SC and QS, as in general the oscillators are reset between two acquisitions; it is also different for station A and B.

$2\pi \cdot f_{LO}^{i} \cdot (t - t_0)_{A,B}^{S,Q}$ is the phase advance from the reset time to the generic time t (f_{LO} is the frequency of the local oscillator).

Φ_{CLK}^{i} is the clock offset between the ground stations, and it is considered as constant throughout the session. It is a differential contribution between stations A and B.

$\Phi_\tau^{i^{S,Q}}$ is the phase due to the delay in arrival time of the signal at the two stations; as the clock offset, it is a differential contribution, but varies in time and is different between SC and QS.

The reset times and local oscillator frequencies are known. Moreover, Flight dynamics Group provides a model of the differential one way ranging for SC and QS. The correlator applies to the signal a model of the phase associated to the differential delay that can be expressed as

$$\Phi_{m_{A,B}}^{i^{S,Q}} = 2\pi \cdot f_{LO}^i \cdot (t - t_0)_{A,B}^{S,Q} + \Phi_{\tau,m}^{i^{S,Q}} \tag{3.2}$$

where the last term on the right is the phase computed using the dynamic predictions. Note that the quasar is considered as fixed with respect to the Earth; therefore the dynamics of the differential delay is identified with the Earth rotation. For this reason, this formulation assumes that the correlator is able to remove exactly the contribution of the delay of the QS signal. Rather, the model for the spacecraft is imperfect, and the difference between the model and the actual phase is the SC residual differential one-way ranging. By applying the model, and thus by subtracting eq. 3.2 from eq. 3.1 we have, for QS and SC respectively,

$$\Phi_{A,B}^{i,Q} = \Phi_{0_{A,B}}^{i,Q} + \Phi_{CLK}^i \tag{3.3}$$

$$\Phi_{A,B}^{i,S} = \Phi_{0_{A,B}}^{i,S} + \Phi_{CLK}^i + \Delta\Phi_\tau^i \tag{3.4}$$

where the $\Delta\Phi_\tau^i$ term accounts for the difference between the actual phase and the model. By multiplying the data stream at station A by the complex conjugate of the data stream at station B, and thus subtracting the phases at station B from the phases at station A, we have

$$\Delta\Phi^{i,Q} = \Delta\Phi_0^{i,Q} + \Phi_{CLK}^i \tag{3.5}$$

$$\Delta\Phi^{i,S} = \Delta\Phi_0^{i,S} + \Phi_{CLK}^i + \Delta\Phi_\tau^i \tag{3.6}$$

where the clock offset and the delay contributions do not cancel out, as they were already considered as differential contributions.

So far, no assumptions have been made on the reset phases. They may, in principle, be different for SC and QS and for all the channels. The current correlation process assumes that the initial unknown phases can be different between spacecraft and quasar, but they are the same for all the channels. This is possible because the operational acquisition of the signal for ΔDOR processing has involved only one IFMS and one LDC, limiting the available spanned bandwidth to $28MHz$, but consequently not introducing differential phases among the channels. The ambiguity resolution, that is the fit of the phases $\Delta\Phi$ in eq. 3.5 and eq. 3.6, is possible in this configuration, as the phases $\Delta\Phi_0$, being the same for all the channels, cancel out completely. Thus, the ambiguity resolution of the quasar phases provides the clock offset, and the spacecraft correlator can take advantage of the knowledge of the clock offset to compute the residual ΔDOR. Rather, in the wide-band configuration, not only are the phases unknown, but they are also different for all channels. As a conse-

quence, the phases $\Delta\Phi$ cannot be removed neither from eq. 3.5 nor from eq. 3.6, leading to the impossibility to compute a clock offset through the ambiguity resolution of the quasar correlator; in this case, the computed clock offset contains also the contribution of the different initial phases, and it is not possible to separate the two components.

The solution proposed requires the local oscillators not to be reset between different acquisitions; this way, the initial phases, channel by channel, are the same between SC and QS, and so is the delta between the two stations

$$\Delta\Phi_0^{i,Q} = \Delta\Phi_0^{i,S} \tag{3.7}$$

The contribution of the clock offset is the same for the two different radio sources; thus, subtracting the phases obtained correlating the quasar data (eq. 3.5) from the phases coming from the SC correlation (eq. 3.6), and applying eq. 3.7, we have

$$\Delta\Phi^{i,S} - \Delta\Phi^{i,Q} = \Delta\Phi_\tau^i \tag{3.8}$$

By solving the ambiguity resolution of the phases in eq. 3.8, it is possible to solve directly for the residual delta differential one-way ranging (ΔDOR); in fact, the clock offset has already been removed by the subtraction of the phases. As a consequence, it is not possible to solve for the clock offset and for the quasar DOR, but only for the ΔDOR.

Summarizing, the principal characteristics of this approach are the following:

- It is required that the local oscillators not be reset between different acquisitions.
- The clock offset contribution is taken into account by subtracting the quasar correlation function phases from the SC ones, and not by solving for it in the QS correlation process; therefore the correlator solves for the ΔDOR directly.

Referring to the error budget reported in the previous chapter (tab. 2.10) a new one can be computed considering the updating due to wideband functionality:

- A spanned bandwidth of $38MHz$.
- A power to noise spectral density of the external channels of about $35dBHz$[1].

The thermal noise of the spacecraft signal is drastically reduced as it is affected by both the upgrades while the thermal noise in the quasar signal is reduced only due to the increased spanned bandwidth. The total error decrease of a factor (tab. 3.1) of about 4.

[1]The wideband approach requires the use of dedicated ΔDOR tones leading to an higher power to noise spectral density of the external channels.

Error source	Value (ns)	
	Standard	Wideband
Quasar Thermal noise	0.242	**0.057**
Spacecraft Thermal noise	0.257	**0.006**
Quasar positioning	0.039	0.039
Clock Instability	0.003	0.003
Phase ripple	0.124	**0.029**
Station location	0.008	0.008
Earth orientation	0.029	0.029
Ionosphere	0.058	0.058
Solar plasma	0.004	0.004
Troposphere	0.034	0.034
Total error (rss)	**0.384**	**0.106**

Table 3.1: ΔDOR Error budget with standard (left) and wideband (right) configuration.

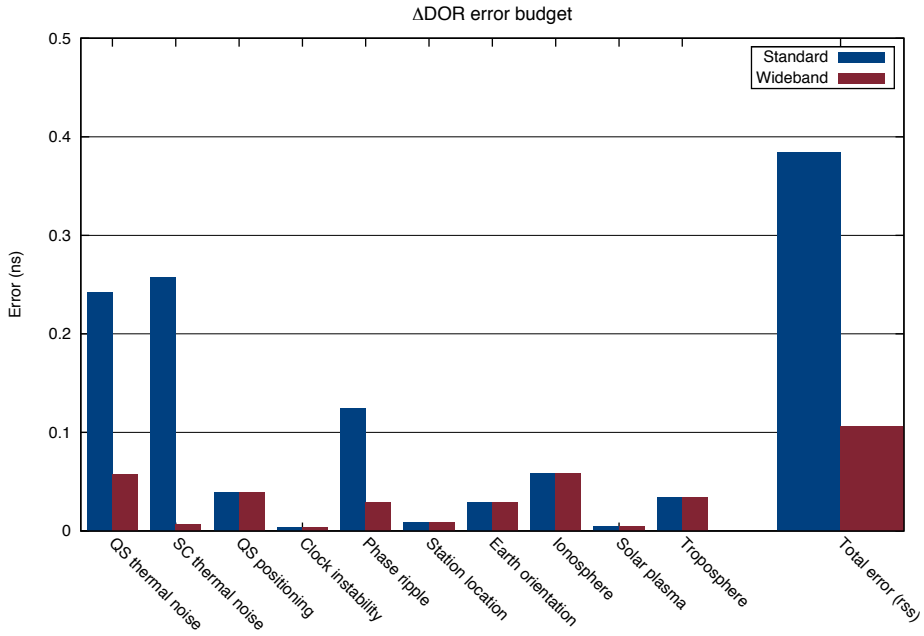

Figure 3.2: ESA ΔDOR error budget with standard and wideband configuration.

3.2 Low-SNR functionality

The current correlation algorithm uses a digital phase locked loop on the main channel to estimate the on board transmitted frequency. The signal tracking is however reliable only if (at least) one channel has a signal over noise density ratio value larger than $13dBHz$. For such weak signal, the estimate of the frequency could be not sufficiently accurate using a digital PLL. Since the following signal reconstruction of the other channels is carried out by means of a heterodyne integrator (PLL slave) driven by frequency predictions, it is therefore strongly affected by the error on the on board frequency estimate. An alternative way of correlating the spacecraft data, called Low-SNR mode, has been therefore implemented. This new method is suitable for every kind of signal, in terms of SNR, permitting to correlate signal having very low signal to noise density ratio values. The ESA operational requirement consists in the possibility to correlate one channel having at least $13dBHz$ and the others having $1dBHz$.

Mathematical formulation

Since the new algorithm must be suitable for very weak signals, the Low-SNR method is a PLL-free architecture[2]. The implementation differs from the standard correlation in the initial processing phases. The initial step, used to estimate the transmitted frequency, and the following step, which consists in the signals reconstruction and filtering, are carried out indeed without the use, respectively, of a PLL and heterodyne integrator (PLL-slave). In particular, the transmitted frequency estimation is carried out, processing the signal of the trust channel (signal with SNR $\geq 13dbHz$), following two steps:

- Removal of the Doppler rate contribution from the trust channel[3] using dynamical prediction and a priori frequency estimate.
- Frequency estimation by means of FFT and peak search.

Once the transmitted frequency has been estimated and the frequency predictions have been adjusted, the signal of each channel is ready to be reconstructed and filtered. With the Low-SNR method, the process consists in:

- Removal of the dynamic contribution from all channels[4].
- Decimation (filtering and resampling).

At the end of these four steps, the signal of each channel has been reconstructed and the phasors rotation has been largely removed. The correlation method follows as for the standard one.

[2]Non coherent methods are generally preferable in case of low SNR.
[3]Note that DC chain also compensate for the Doppler shift
[4]In the standard correlation, the phasor rotation stoppage is carried out once the signal has been reconstructed/filtered

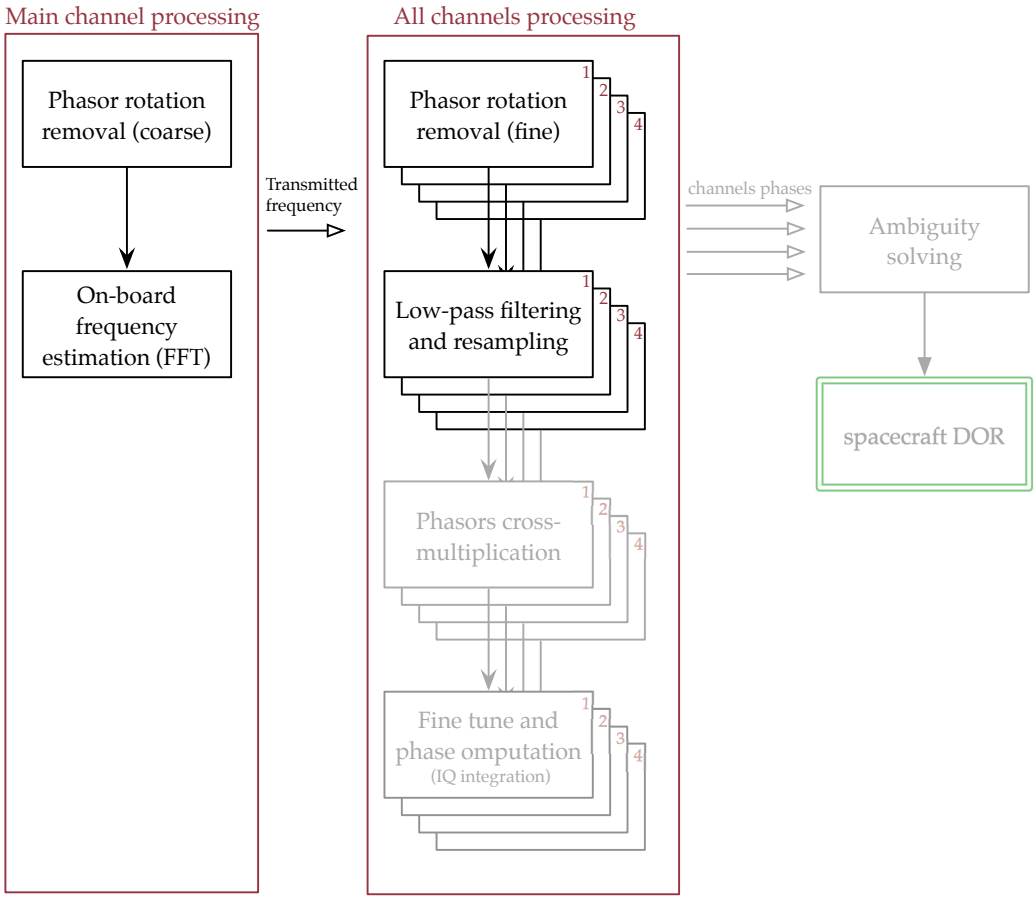

Figure 3.3: Top level diagram of low-SNR spacecraft correlation algorithm. The grey blocks remains unchanged with respect to standard algorithm.

The following detailed mathematical description of the new algorithm often refers to par. 2.1, however many fundamental things are repeated, sometimes in a little difference way.

The signal received, down converted and recorded at one station is

$$\begin{aligned} S_A &= S_{0_A} \exp\left[i\left(\omega_{SC}t - \omega_{LO_A}t - \frac{\omega_{SC}}{c}\rho_A(t) + \phi_{A_0}\right)\right] \\ S_B &= S_{0_B} \exp\left[i\left(\omega_{SC}t - \omega_{LO_B}t - \frac{\omega_{SC}}{c}\rho_B(t) + \phi_{B_0}\right)\right] \end{aligned} \tag{3.9}$$

where

ω_{SC} is the transmitted angular frequency.

ω_{LO_A} and ω_{LO_B} are the total local oscillator (L.O.) angular frequencies used in the two down-conversion chains. They account for the a priori transmitted frequency and for the Doppler shift due to SC dynamic.

$\frac{\omega_{SC}}{c}\rho_{A,B}(t)$ are the phase dynamic contributions, with $\rho_{A,B}(t)$ equal to the SC ranges with respect to the two stations.

$\phi_{A,B}$ are the oscillators initial phases.

The range term $\rho(t)$ can be modeled as a second degree polynomial

$$\rho_{A,B}(t) = c_{0_{A,B}} + c_{1_{A,B}}t + c_{2_{A,B}}t^2 \tag{3.10}$$

and the L.O. angular frequency ($\omega_{LO_{A,B}}$), depending from the first guess of estimated frequency ($\hat{\omega}_{SC}$) and accounting only for the Doppler shift (the first derivative of range), can be expressed as

$$\omega_{LO_{A,B}} = \hat{\omega}_{SC} - \frac{\hat{\omega}_{SC}}{c}c_{1_{A,B}} \tag{3.11}$$

With the last assumptions eq 3.9 becomes, neglecting the station suffixes,

$$S = S_0 \exp\left[i\left(\left(\omega_{SC} - \hat{\omega}_{SC}\right)t - \frac{\omega_{SC}}{c}\left(c_1 t + c_2 t^2\right) + \frac{\hat{\omega}_{SC}}{c}c_1 t + \hat{\phi}_0\right)\right] \tag{3.12}$$

The recorded signal has four phase terms:

- a phase term accounting for the offset on the on board oscillator.
- a phase term due to the predicted dynamic contribution (only frequency shift).
- a phase term accounting for the time variant dynamic contribution (Doppler shift and Doppler rate)[5].
- a phase constant term accounting for the initial phase of the local oscillator and the phase delay at time $t = 0$ ($\frac{\omega_{SC}}{c}c_0$).

[5]Note that the real dynamic has been approximated with a second degree polynomials which means to consider only the first two derivatives of range.

The Doppler-rate contribution can be removed[6] multiplying the recorded signal with a model signal having phase

$$DR(t) = \exp\left[i\left(-\frac{\hat{\omega}_{SC}}{c}c_2t^2\right)\right] \tag{3.13}$$

The resulting beat signal

$$SS(t) = S(t)DR(t) = S_0\exp\left[i\left(\left(\omega_{SC}-\hat{\omega}_{SC}\right)t - \frac{\omega_{SC}-\hat{\omega}_{SC}}{c}\left(c_1t+c_2t^2\right)+\hat{\phi}_0\right)\right] \tag{3.14}$$

has in terms of frequency:

- a constant frequency term $\omega_{SC}-\hat{\omega}_{SC}$ which directly reflects the error on the a priori knowledge of the transmitted frequency.
- a constant frequency term $\frac{\omega_{SC}-\hat{\omega}_{SC}}{c}c_1$ accounting for the not compensated doppler shift because of the error on the predicted transmitted frequency.
- a frequency drift term ($2\frac{\omega_{SC}-\hat{\omega}_{SC}}{c}c_2t$) accounting for the not compensated doppler rate because of the error on the predicted transmitted frequency.

Computing an FFT on signal $SS(t)$ and looking for its maximum is possible to estimate[7] the constant frequency term

$$\omega_{FFT_{max}} = \left(\omega_{SC}-\hat{\omega}_{SC}\right) - \frac{\omega_{SC}-\hat{\omega}_{SC}}{c}c_1 \tag{3.15}$$

An approximated on board transmitted frequency can be finally computed neglecting the second term (residual dynamic)

$$\omega_{est} = \omega_{FFT_{max}} - \hat{\omega}_{SC} = \omega_{FFT_{max}} + \omega_{LO}/\left(1-\frac{c_1}{c}\right) \tag{3.16}$$

The largest error committed with this approximation

$$\omega_{error} = \omega_{SC} - \omega_{est} = \frac{\omega_{SC}-\hat{\omega}_{SC}}{c}c_1 \tag{3.17}$$

is of the order of $0.8Hz$ having assumed a maximum error on a priori estimated frequency of $25kHz$ and a c_1 coefficient (range-rate) equal to $10km/s$.
This processing, which substitute the PLL(master) in the standard mode, allows the frequency estimate also from low-SNR signals, as far as the signal peak in the FFT is detectable. Such condition is guaranteed by the ESA requirement that at least one channel shall have a $SNR > 13dBHz$.

[6] The dynamic prediction for what regard the higher derivative terms are generally very accurate. Furthermore, the time span of data used in the initial processing is generally small (20 or 30s). The derivative of range rate c_2 could be considered therefore perfectly known and the error in the removal of Doppler rate is only due to the error on a priori transmitted frequency.

[7] The residual frequency drift in the typical time span on which the FFT is computed (about 20s/30s), is small and can be neglected.

At the end of this step, a new model for predicted received signal is ready (transmitted frequency plus dynamic prediction) and the signal of each channel should be reconstructed. The recorded signal is firstly multiplied, in order to stop the phasors rotation, by a complex signal

$$X_m(t) = \exp\left[i\left(\omega_{est}t - \frac{\omega_{est}}{c}(\rho_{m_{A,B}}(t) - \rho_{m_{A,B}}(0)) - \omega_{LO_{A,B}}t\right)\right] \tag{3.18}$$

Assuming $\omega_{est} = \omega_0$, the resulting signals (equivalent to the signals in eq. 2.12) are

$$X_A(t) = S_{0A}\exp\left[i\left(\phi_{A_0} + \Psi_A - \Psi_{mA}\right)\right]$$
$$X_B(t) = S_{0B}\exp\left[i\left(\phi_{B_0} + \Psi_B - \Psi_{mB}\right)\right]$$

where

ϕ_{A_0} and ϕ_{B_0} are the oscillators unknown phases

$\Psi_A - \Psi_{mA}$ and $\Psi_A - \Psi_{mA}$ are the phase terms accounting for the residuals dynamic due to its mismodeling.

The signals, are then filtered in frequency domain, narrowing the bandwidth to a value such that the beaten signal falls comfortably inside, and resampled at the corresponding Nyquist frequency. Typical bandwidths of the low- pass filter are in the range $50 - 100Hz$ for common signals. For weak signals is necessary to filter with bandwidth much smaller, up to $1Hz$ for signal having power over noise density ratio of $1dBHz$. That is very trivial and hugely stress the requirements in terms of dynamic a priori knowledge. Reducing the bandwidth to $1Hz$ means that the residual dynamic into the signal has not to be greater than $0.5Hz$ to avoid aliasing. Considering only the first term of dynamic, the range-rate must be known at the level[8] of cm/s.

The correlation process continues as in the standard mode (from step 3):

- Computing the phasor product for each channel $X_{AB}(t) = X_A(t)X_B^*(t)$ (see eq. 2.13)
- Fine tune, integration of the phasor over the desired time and phase delay computation $\Delta\Phi = \arctan\left[\mathbf{Im}(Z)/\mathbf{Re}(Z)\right]$ (see eq. 2.15)
- Ambiguity solving by interpolating phase points in the phase frequency plane.

[8]The frequency error introduced by doppler shift modeling error is:

$$\Delta f = f_0\frac{\Delta c_1}{c} \approx 8.2\cdot 10^9 Hz\frac{1.8cm/s}{2.99\cdot 10^8 m/s} \approx 0.5Hz$$

The transmitted frequency introduces an error negligible because it is is generally estimated, after the first step, at the level of 0.01Hz.

Chapter 4

$\triangle$DOR enhancement: Tests and results

Several tests have been performed to validate, in terms of functionality and performance, the two enhancements.

The two additional capabilities refer to two different aspects of the ΔDOR computational process. In particular the wide-band capability is an alternative way to combine the phases obtained correlating spacecraft and quasar data streams. The Low-SNR functionality is, on the other hand, an alternative way to correlate the narrow band signal coming from the spacecraft, and is therefore a different way to obtain the spacecraft phases. As referred in fig. 4.1, the ΔDOR observables can be computed using four different configurations:

- Narrow band / PLL
- Wide band / PLL
- Narrow band / Low-SNR
- Wide band / Low-SNR

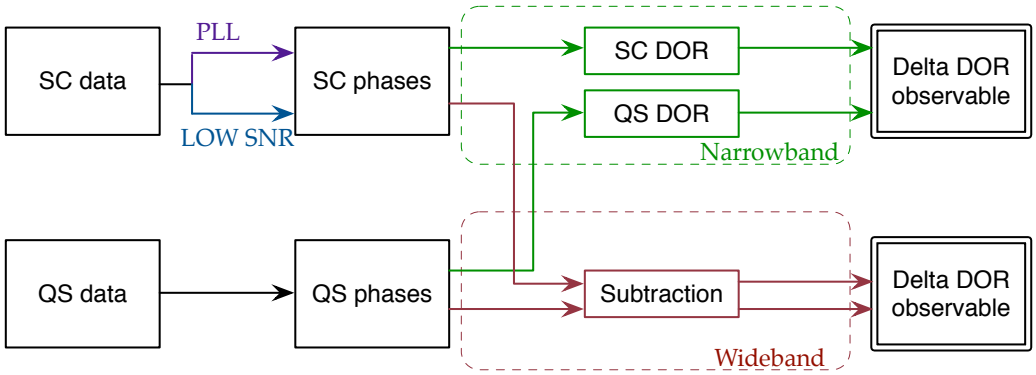

Figure 4.1: Different funtionalities for ΔDOR computation.

The wideband capability has been tested by processing real data acquired in different configuration and reprocessing data already acquired and correlated in the previous years. The Low-SNR functionality has been not only tested with real data, but in terms of performance, by means of Montecarlo simulations.

4.1 Wideband functionality

To asses the functionality and performance of the wideband capability the following tests have been carried out:

1. Quasar only wideband-like acquisition
2. Venus EXpress (VEX) wideband-like acquisition
3. Juno wideband acquisition (ESA-NASA)

4.1.1 Quasar only: wideband-like acquisition

On June 21, 2012 (2012-173), from the Deep Space stations Cebreros (Spain) and New Norcia (Australia), ESA has carried out a ΔDOR acquisition consisting in a quasar only sequence Q1-Q2-Q1. The received signal has been driven (fig. 4.2) through two different down-conversion chains in order to simulate a wideband configuration. Two LDC have been used, outputting the same portion of spectrum to the back end receiver (IFMS). The recorded signal consists, in the end, in three channels coming from one LDC and the other channel coming from the second LDC. This configuration has been called wideband-like because, even if it simulates a wideband approach, using multiple LDC, it doesn't actually increase the spanned bandwidth. Correlating the three scans, one reconstructs three sets of phases (one for each channel). Then, wideband processing is simulated computing the phase difference of ACQ1-ACQ2 and ACQ1-ACQ3. The time delay (ΔDOR residual) computed resolving the ambiguity from these four differential phase, has to be zero within the

sigma associated to the measurement. We are dealing indeed with only quasars, whose position is known. The two quasars, S651 and S696, have respectively a flux of about 0.5 and $0.3Jy$, and for each scan $8s$ have been correlated.

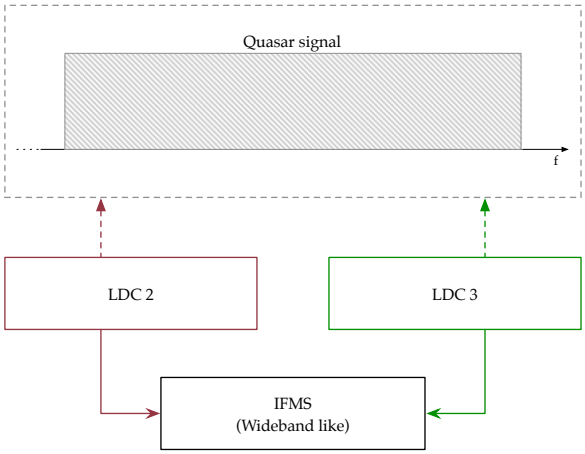

Figure 4.2: QUASAR 2012-173: Acquisition configuration.

The results, reported in table 4.1, show a full agreement with the expected results. The ΔDOR residuals are fully compatible with the zero value below the 1 sigma level. Moreover, the four phases, one for each channel, are aligned as we expected. The phase subtraction method, here applied in a quasar only test, permits to cancel out possible unknown initial phases among the channels and it is therefore verified.

	Ch 1 phase	Ch 2 phase	Ch 3 phase	Ch 4 phase	Theoretical Sigma (ns)	DDOR residual (ns)
Q1-Q2	0.83	0.92	0.87	0.98	2.8	-2.26
Q2-Q3	5.31	-0.98	-1.02	-1.06	2.8	0.76

Table 4.1: QUASAR 2012-173: Correlation results.

4.1.2 Venus EXpress: wideband-like acquisition

On August 1, 2012 (2012-214), a Venus Express (VEX) acquisition has been carried out to test the wideband functionality. The tracking, from ESA Deep Space stations Cebreros (Spain) and New Norcia (Australia), has been carried out acquiring data with two distinctive configurations, a standard (or narrow) configuration and a wideband configuration. Two distinctive L-band down converters (LDC) and two distinctive receivers (IFMS) have been used (fig 4.3).

The two LDC were configured in the same way, acquiring and outputting the same portion of spectrum. The IFMS were, on the other hand, configured that IFMS2 received

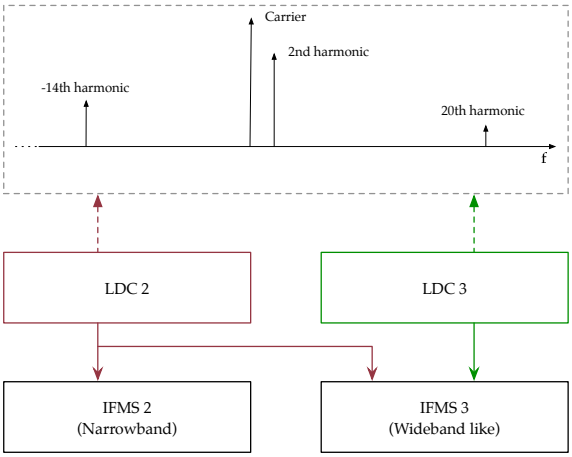

Figure 4.3: VEX 2012-214: Acquisition configuration.

the signal only from one LDC, and therefore recorded all four channels from LDC2, while IFMS3 received the signal from both LDC and it recorded three channels from LDC3 and one channel from LDC2. The four channels frequency plan (table 4.2) adopted provided a spanned bandwidth of approximately 9MHz [1].

Channel	Signal	Frequency (Hz)	Sub channel Freq (Hz)
1	Carrier	8419084073	0
2	2nd Harmonic telemetry	841960836	524288
3	-14th Harmonic telemetry	8415414057	-3670016
4	20th Harmonic telemetry	8424326953	5242880

Table 4.2: VEX 2012-214: Frequency plan.

The wideband-like configuration of IFMS3, using two LDC outputting the same portion of spectrum, doesn't actually increase the spanned bandwidth. However, it permits to compare the two algorithms, standard/narrowband and wideband, correlating the same signal acquired in a standard (IFMS2) and in a wideband-like (IFMS3) configuration. Moreover, it permits to investigate the effect of the use of multiple LDC.

The acquisition consisted of a S-Q-S sequence, with a quasar (S148) of about $0.5Jy$. The general correlation parameters used for the tests are reported in table 4.3.

The two first tests were consequently:

- Narrowband (NB) correlation of data coming from IFMS2
- Wideband (WB) correlation of data coming from IFMS3

[1] The exact spanned bandwidth is 8912896 Hz.

Acquisition type	S-Q-S
Correlation time (s)	300/300/300
Fragmentation scheme (s)	20/60/20
BW master	20Hz
BW slave	10Hz

Table 4.3: VEX 2012-214: Correlation settings.

Data	Corr. type	Channel configuration	DDOR (ns)	Sigma (ns)
IFMS2	NB	4ch. from LDC2	1.05	0.52
IFMS3	WB	3ch. from LDC3 1ch. from LDC2	0.45	0.50

Table 4.4: VEX 2012-214: Correlation results in wideband-like (IFMS3) and narrowband (IFMS2) configuration.

The results[2] (Barbaglio et al., 2012) show a compatibility at 1 sigma-level (tab.4.4). To fully investigate the small discrepancy of one sigma another test has been carried out: standard/narrowband correlation of data from IFMS3 (wideband like configuration) using only the channels coming from LDC3. The comparison (table 4.5) with result obtained by means of a wideband correlation of all channels of IFMS3 shows a full agreement, well below the 1 sigma level. That comparison, and the following agreement, is possible because the missing

Data	Corr. type	Channel config.	DDOR (ns)	Sigma (ns)
IFMS3	WB	3ch. from LDC3 1ch. from LDC2	0.45	0.50
IFMS3	NB	3ch. from LDC3	0.55	0.54

Table 4.5: VEX 2012-214: Correlation results in wideband-like configuration (IFMS3).

channel (coming from the LDC2) is the closest to the carrier, thus not significantly affecting the ambiguity resolution. The correlation of IFMS3 data (4 ch. or 3 ch.) shows that when standard and wideband correlation are compared using data coming from the same down conversion chain, the ΔDOR observables are in very good agreement. Introducing a different component (LDC2) in the chain affects the correlation to a level of $0.5ns$. More tests are therefore needed to statistically characterize the behavior of different LDC in the down-conversion chain. All results are also reported in fig.4.4.

[2]The ΔDOR measurement and its associated error (sigma) are computed from the statistics of the DOR provided by each correlated data fragment.

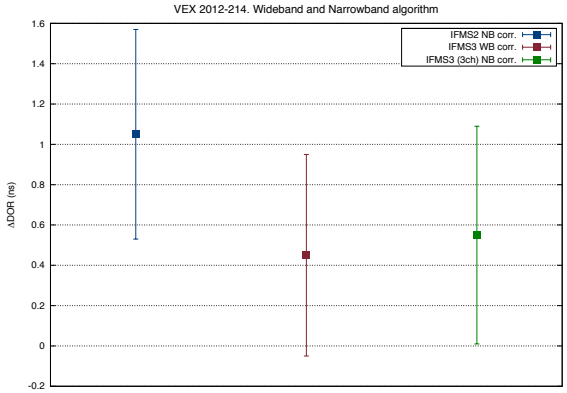

Figure 4.4: VEX 2012-214: Results obtained with two different configurations, standard-narrowband (IFMS2) and wideband-like (IFMS3). Different algorithms used.

4.1.3 Juno: wideband acquisition

On 23rd September 2012 (2012-267) the first wideband ΔDOR pass in in the history of European Space Agency has been carried out. The new ESA Deep Space station in Malargue (Argentina), has tracked simultaneously with the Deep Space Network (DSN) station of Goldstone (California), the NASA spacecraft Juno, during its journey to Jupiter. Since Juno has the capability to use ΔDOR tone, the frequency plan implemented (table 4.6) provided a spanned bandwidth of $38.2MHz$, more than four times the bandwidth usually spanned in the typical ESA acquisitions.

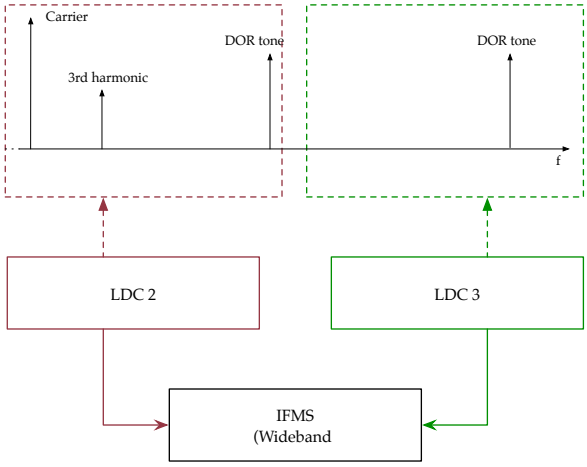

Figure 4.5: Juno 2012-267: Acquisition configuration.

The ΔDOR pass consisted in two consecutive S-Q-S sequences, the acquired quasar (S279) had an approximately flux power of $1.42Jy$ and the used correlations setup, de-

Channel	Signal	Frequency (Hz)	Sub channel Freq (Hz)
1	Carrier	8404131917	0
2	Tone	8442332512	38200595
3	Telemetry Harmonic	8404975664	843747
4	Tone	84323232214	19100297

Table 4.6: Juno 2012-267: Frequency plan.

cided by Jet Propulsion Laboratory (JPL) and European Space Operations Center (ESOC), is reported in tab. 4.7.

Acquisition type	S-Q-S
Correlation time (s)	400/300/400
Fragmentation scheme (s)	20/30/20
BW master	50Hz
BW slave	50Hz

Table 4.7: Juno 2012-267: Correlation settings.

The results (table 4.8) obtained show an accuracy never reached before in an ESA correlation. The errors (sigma) associated to the measured ΔDOR[3] are indeed in the order of 40 picoseconds[4], a factor of about 13 lower than the sigma computed in the previous VEX acquisition (2012-214) and, generally, in all VEX acquisitions. Furthermore, these results are compatible with those obtained by JPL correlating the same data.

Several aspects contribute to this extraordinary accuracy. As already explained, the use of dedicated tones permitted to increase the spanned bandwidth which directly affects the ΔDOR measurements error. In addition, the dedicated tones are characterize by higher power over noise density ratios with respect to telemetry harmonics. In this particular case, the benefit amounted to 20dB on the external channels[5], removing essentially the contribution of the spacecraft thermal noise to the overall error[6].

	DDOR (ns)	Sigma (ns)
First sequence	1.043	0.040
Second sequence	1.004	0.035

Table 4.8: Juno 2012-267: Correlation results.

[3]The ΔDOR measurement and its associated error (sigma) are computed from the statistics of the DOR provided by each correlated data fragment.

[4]Note that the sigma associated to the measurement reflects only the random errors contribution.

[5]The tones P/N_0 has been measured to be of $35dBHz$, while $15dBHz$ is the typical value for the VEX external channels.

[6]The difference of $20dB$ results in a factor of 10 in the error associated to the thermal noise of spacecraft signal.

4.2 LOW-SNR functionality

The Low-SNR functionality has been tested in two different ways:

1. Using real data with added noise
2. Using simulated data (Montecarlo)

4.2.1 Real data with added noise

A test to investigate the Low-SNR capability has been carried out taking a real acquisition, the VEX 2012-214 already discussed in par. 4.1.2, and adding white noise in the fourth channel to lead it to 3dBHz.

The acquisition consisted in a S-Q-S sequence, with a quasar (S148) having a flux of about $0.5Jy$. The data[7], both the original and modified one (added noise), have been correlated using Low-SNR algorithm and the general correlation settings reported in tab. 4.9.

Acquisition type	S-Q-S
Correlation time (s)	300/300/300
Fragmentation scheme (s)	20/60/20
BW master	20Hz
BW slave	10Hz

Table 4.9: Low-SNR VEX 2012-214: Correlation settings.

The correlation results, reported in tab. 4.10 and fig. 4.6, show a full compatibility, confirming the correctness of the Low-SNR functionality.

	DDOR (ns)	Sigma (ns)
Data with noise (3dBHz)	0.43	3.3
Original Data	0.53	0.45

Table 4.10: Low-SNR VEX 2012-214: Correlation results. Comparison between correlation results using data with added noise on fourth channel (3dBHz) and results using the original data.

[7]The data used are that of IFMS3. Here it is not discussed again the particular configuration used in the VEX 2012-214 acquisition. Refers to par 4.1.2.

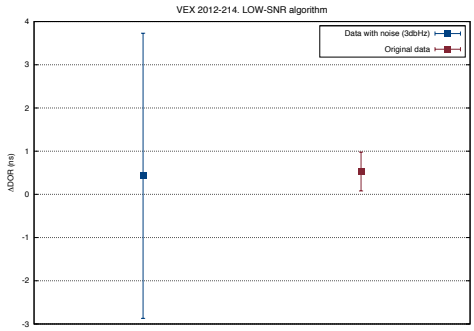

Figure 4.6: Low-SNR VEX 2012-214: Correlation results. Comparison between correlation results using data with added noise on fourth channel (3dBHz) and results using the original data.

4.2.2 Simulated data

Montecarlo simulations are very useful to characterize the behavior of the SC correlation algorithms under very different conditions of noise. By collecting results obtained with several realization of noise is possible to extract a reliable statistic to be compared with the theoretical expectations, and to provide also a useful analysis of the system performance.

Three tests have been carried out:

TEST A. Four different Montecarlo with four different levels of noise. Correlation carried out using Low-SNR and PLL (standard) algorithms.

TEST B. Two different Montecarlo with data at very high level of noise.

TEST C. A Montecarlo of simulated data at the worst condition of noise stated by the requirement (a channel at $13dBHz$, and the others at $1dBHz$).

TEST A

This test aims to characterize the Low-SNR algorithm in terms of performance, also with respect to the standard (PLL) one. The data ($20s$) have been therefore simulated considering different noise levels (P/N_0), equal for all four channels, and the frequency plan (tab. 4.11) has been chosen to provide a $8912896Hz$ spanned bandwidth (VEX typical frequency plan). The level of noise has been varied from 10 to $40dBHz$ with a step size of $10dBHz$. For each

Channel	Signal	Frequency (Hz)	Sub channel Freq (Hz)
1	Carrier	8400000000	0
2	2nd Harmonic telemetry	84000524288	524288
3	-14th Harmonic telemetry	8396329984	-3670016
4	20th Harmonic telemetry	8405242880	5242880

Table 4.11: LOW-SNR TEST A: Frequency plan.

level one hundred sets of SC data have been simulated (random realization of noise) and

then correlated to obtain the four phases, one for each channel, and the resulting DOR measurement. The Low-SNR algorithm has been used for each noise condition while the PLL one has been used only for the two highest P/N_0, $40dBHz$ and $30dBHz$.

(a) DOR error

P/N_0	Theoretical DOR error (s)	PLL DOR error (s)	LOW-SNR DOR error (s)
10	1.79E-09	N/A	3.90E-09
20	5.65E-10	N/A	1.16E-09
30	1.79E-10	3.39E-10	3.53E-10
40	5.65E-11	1.05E-10	1.04E-10

(b) Phase error

P/N_0	Theoretical phase error (rad)	PLL phase error (rad)	LOW-SNR phase error (rad)
10	7.07E-02	N/A	1.50E-01
20	2.24E-02	N/A	4.67E-02
30	7.07E-03	1.32E-02	1.33E-02
40	2.24E-03	4.59E-03	4.47E-03

Table 4.12: Low-SNR TEST A: Montecarlo results. Comparison between PLL algorithm and Low-SNR algorithm.

The DOR and channel phase error standard deviation[8] , coming from Montecarlo simulations, show(tab.4.12 and fig.4.7) a compatibility with the theoretical values below the 3-sigma level[9].

Moreover, for $40dBHz$ and $30dBHz$, the results obtained with the two algorithms show a full agreement.

[8]The mean values, not reported, are well below the standard deviation, indicating the absence of biases.

[9]The factor of two between the computed sigma and the theoretical one is due to the simultaneous estimate of unknown frequency and phase. In fact, only if the frequency is known, the Cramer-rao (CR) lower bound for the phase estimation error is independent from the initial time t_0 and equal to the reported theoretical sigma. Otherwise, as in this case, it is function of the initial time t_0 with a minimum equal to the bound corresponding to the frequency known case(Rife and Boorstyn, 1974). According to Rife and Boorstyn (1974), the CR lower bound reaches this minimum when the samples timetags are symmetrical around zero. Mathematically, it means that the initial time of the signal has to be

$$t_0 = -(n-1)/2 * \delta t \tag{4.1}$$

where n is the number of samples and δt is the sampling time. The correlator, which is implemented using the initial time equal to 0, will be modified accordingly, permitting therefore to remove that factor of two.

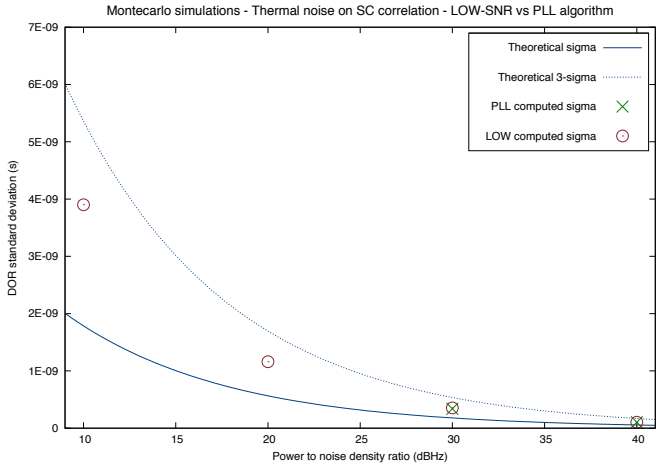

(a) DOR error

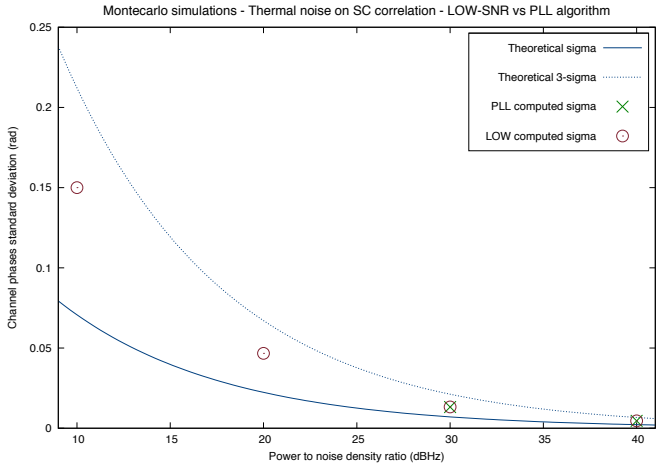

(b) Phase error

Figure 4.7: Low-SNR TEST A: Montecarlo results. DOR(a)/Phase(b) error (std. dev.) with PLL algorithm (green x) and Low-SNR algorithm (red circles).

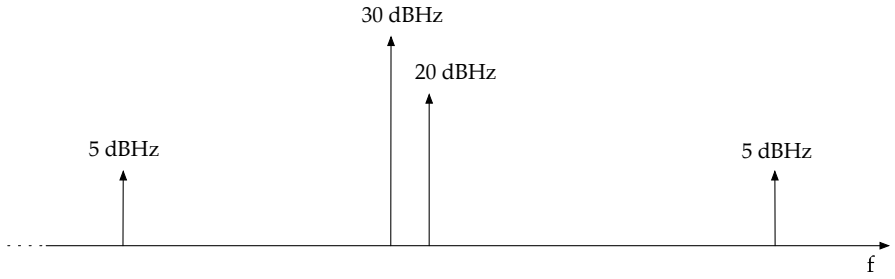

(a) B1

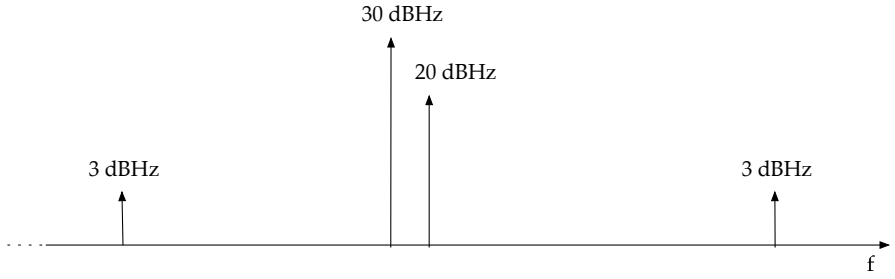

(b) B2

Figure 4.8: Low-SNR TEST B: Noise configuration.

TEST B

Two Montecarlo, of hundred points each, have been carried out, simulating a realistic high noise condition. The four channels have been simulated having a frequency plan providing a spanned bandwidth of $8912896Hz$ with a carrier of $30dBHz$, a subcarrier of $20dBHz$ and the two external channels of $5dBHz$ for the first Montecarlo (B1) and $3dBHz$ for the second one (B2).

Channel	Signal	Frequency (Hz)	Sub channel Freq (Hz)
1	Carrier	8400000000	0
2	2nd Harmonic telemetry	84000524288	524288
3	-14th Harmonic telemetry	8396329984	-3670016
4	20th Harmonic telemetry	8405242880	5242880

Table 4.13: Low-SNR TEST B: Frequency plan.

The correlation of $20s$ data has been performed with the Low-SNR algorithm and a bandwidth of $1Hz$. The Montecarlo results[10] (table 4.14) show a compatibility with the theoretical ones below the 3-sigma level (fig. 4.9).

[10]The mean values, not reported, are well below the standard deviation, indicating the absence of biases.

	Number of points	Theoretical DOR error (ns)	Computed DOR error (ns)
B1. (5 dBHz)	80	3.16	6.74
B2. (3 dBHz)	132	3.99	9.3

Table 4.14: Low-SNR TEST B: Montecarlo (simulation and correlation) results. Low-SNR performance with signal at very high level of noise.

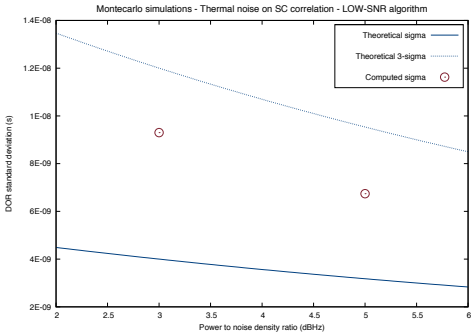

Figure 4.9: Low-SNR TEST B: Montecarlo (simulation and correlation) results. Low-SNR performance with signal at very high level of noise.

TEST C

The ESA requirement for Low-SNR signal consists in the capability to correlate a signal having on a channel (master) at least $13dBHz$ and on the others $1dBHz$.

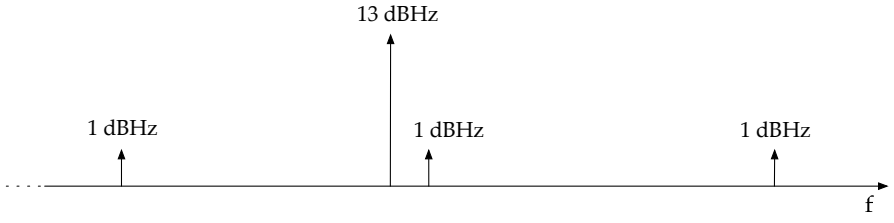

Figure 4.10: Low-SNR TEST C: Noise configuration.

A Montecarlo of one hundred points each, using SC simulated data having the four channels with that level of noise has been therefore carried out. The frequency plan used provided a spanned bandwidth of $8912896Hz$ and 60s of data for each correlation have been used. The results[11] (Barbaglio et al., 2012) show a compatibility (tab.4.16) once again below the theoretical 3-sigma level.

[11]The mean values, not reported, are well below the standard deviation, indicating the absence of biases.

Channel	Signal	Frequency (Hz)	Sub channel Freq (Hz)
1	Carrier	8400000000	0
2	2nd Harmonic telemetry	84000524288	524288
3	-14th Harmonic telemetry	8396329984	-3670016
4	20th Harmonic telemetry	8405242880	5242880

Table 4.15: Low-SNR TEST C: Frequency plan.

Theoretical DOR error (ns)	Theoretical phase error (rad)	Computed DOR error (ns)	Computed phase error (rad)
2.91E-09	0.16	7.5E-09	0.24

Table 4.16: Low-SNR TEST C: Montecarlo results. Low-SNR algorithm validation on the worst condition of noise possible (ESA requirement).

Part II

Pseudo noise ranging system

Chapter 5

Ranging systems overview

The range measurement is based on the principle of the finite light time and consists in measuring the time τ necessary for a wave[1] to propagate from a source to a target

$$\rho = \tau c \tag{5.1}$$

Deep space ranging systems generally provides the round trip phase delay measurement of a ranging signal transmitted by a station, received by the spacecraft and sent back toward Earth. Using ground station clocks permits to have indeed a reference frequency with better performance, in terms of frequency stability, and to avoid or reduce some errors (see par. 1.2). If the transmitting station and the receiving one are the same, the configuration is called two-way, provides the best achievable performances on tracking accuracies and is therefore the most used for deep space missions[2].

A two-way ranging measurement could be schematically presented with the following three steps:

1. A ground station transmits an uplink carrier modulated, in phase, by a ranging signal.
2. The spacecraft receives the signal, locks to the carrier and demodulates the ranging signal. Before being remodulated onto a downlink carrier, the ranging signal processing can follow two different approaches:
   - **Turnaround/transparent approach:** The demodulated ranging signal is filtered with a certain bandwidth, typically of about $1.50MHz$ (Kinman and Berner, 2003).
   - **Regenerative approach:** The ranging signal is acquired and regenerated.
3. The ground station receives the signal, locks into the downlink carrier, demodulates the ranging signal and correlates it against a copy of what was sent. The result of the

[1] In our case we consider the case of radio signal, even if also exists range measurement carried on using optical waves.

[2] For some outer planet missions, the light time between Earth and spacecraft is large enough that the measurement must be carried out using different station for uplink and downlink. This is known as three-way ranging

correlation is the round-trip light time (RTLT) between the ground equipment and the spacecraft, related to range as

$$\tau_{RTLT} = \frac{2\rho}{c} \tag{5.2}$$

Since the time delay is inferred from the a phase delay, the range measurement has a certain ambiguity (2π in terms of phase) which has to be resolved using an a priori estimate. Because the uplink carrier may be tuned in frequency, the ranging measurement is provided in units that are directly related to the period of the carrier, called Range Units (RU). By convention, 1 RU is the length of 2 cycles of the uplink carrier frequency (Berner, 2001).

The three fundamental parameters characterizing a ranging measurement are:

- Measurement resolution
- Ambiguity resolution
- Accuracy

The resolution of the measurement is determined by the highest frequency of the ranging signal, called clock component. The correlation permits indeed to resolve the signal a fraction of one cycle of the signal being measured. An higher frequency means shorter cycle and therefore increases the ranging measurement resolution. On the other hand, shorter cycle means an higher ambiguity, being the measurement modulo one cycle. To increase the ambiguity of the measurement, the ranging signal contains other components with lower frequencies. The lowest one determines the unambiguous range. The last aspect, is the accuracy achievable in the ranging measurement. Numerous error sources affect indeed the accuracy, introducing random or systematic errors (see par. 5.3).

Ranging systems can be divided in two main groups, depending on the structure of the ranging signal used:

- Sequential ranging systems
- Pseudo-noise (PN) ranging systems

Currently in deep space tracking the first kind of ranging systems is widely used. It roughly consists in sending, sequentially, tones characterized by different frequencies[3]. The highest frequency tone is called clock component and determines the measurement precision achievable while the others are used for ambiguity resolution. This system allows a simple correlator, which only looks for one frequency at a time, but, on the other hand, the starting epoch of the ranging signal must be known (Berner et al., 1999) and only a turn-around/transparent channel could be used. The second kind of ranging system is based on using pseudo-random noise codes (different types) rather than a sequence of tones. The ranging signal is built from a logical combination of a clock component (sequence of ± 1) with a certain number of components having different length, resulting in a unique sequence of length equal to the multiplication of the lengths of all components. The chip rate of the code, that is the clock component, determines therefore the measurement resolution

[3]Even if in ESA system, actually, a code is sequentially built with different tones, the concept remains the same.

while the entire code length is the ambiguity limit. The correlator becomes more complex due to the necessity to acquire in parallel multiple components. However the transponder can reconstruct the position of the code and, having removed the requirement to know when the sequence started, the PN ranging systems allow the regenerative approach as well as the transparent one. The net result of the regeneration would be an increase in the effective return ranging power-to-noise spectral density up to 30dB (Berner et al. (1999)). For this reason, regenerative PN ranging is currently being developed and implemented in the transponders of future deep space missions.

5.1 Sequential ranging

The sequential ranging signal consists in a sequence of tones (separate tones for NASA or combined sequentially in a code for ESA), which are all coherently related to each other and to the uplink carrier. The first tone to be transmitted is the one with the highest frequency f_o . It is called clock tone and determines the resolution of the ranging measurement achievable. However, as the correlation can resolve to one period of the tone, the measurement has a large ambiguity. Only the fractional part of the phase delay can be measured and the integer number of cycles is unknown. The ambiguity is reduced combining the correlations of the subsequent tones which are at lower frequencies. The last transmitted component, having the the lowest frequency, determines the ambiguity resolution of the code, which, in meter, can be expressed as

$$U = \frac{c}{2f} \tag{5.3}$$

The range measurement is performed sequentially, acquiring a component once a time. The first tone to be correlated is the main tone, or clock component, and once it has been acquired the receiver starts to correlate the other components. The major advantage of that sequential approach is that one-correlation operation is needed at a time, and therefore the receiver/demodulator is easy. However, the starting time must be known to perform the correlation and an accurate estimate of round trip light time (RTLT) is therefore necessary. Consequently, the on board regenerative approach is not possible, and the ranging signal, at the spacecraft is demodulated, filtered and remodulated in a turn-around channel.

NASA and ESA uses two different schemes for their sequential ranging systems. In both cases, each signal component is a factor of two lower in frequency than the previous one. While NASA transmit once component at time, maximizing the ranging power, ESA combines the ambiguity components (from the second one to the last) in a code, and modulates it onto the clock component.

5.1.1 NASA tone ranging: signal structure

The ranging scheme used by Deep Space Network (DSN)[4] consists in 21 tones (tab. 5.1) having frequencies (Kinman, 2009)

$$f_n = 2^{-n} f_0 \tag{5.4}$$

where n goes from 4 to 24 and f_0 is the frequency of the theoretical component 0, related to the uplink carrier as

$$f_0 = \begin{cases} 2^{-7} f_S, & S - band \\ 2^{-7} \frac{221}{749} f_X, & X - band \end{cases} \tag{5.5}$$

Component Number	Frequency (Hz)
4	1032556.981
5	516278.490
6	258139.245
7	129069.623
8	64534.811
9	32267.406
10	16133.703
11	8066.851
12	4033.426
13	2016.713
14	1008.356
15	504.178
16	252.089
17	126.045
18	63.022
19	31.511
20	15.756
21	7.878
22	3.939
23	1.969
24	0.985

Table 5.1: Tones frequencies used in NASA-DSN sequential ranging.

The ranging signal is composed in a sequence of tones chosen between these 21. The clock component (highest frequency) is generally chosen to be one of the first 7 ones (from 4 to 10) and the number of the following (decreasing frequency) tones to be transmitted is determined by the required ambiguity solving capability. Some ambiguity-solving components may be multiplied by a higher-frequency component (chopping) to enforce spectral isolation between the ranging signal and command on the uplink or telemetry on the downlink (Kinman, 2009).

[4]Nasa ground stations network

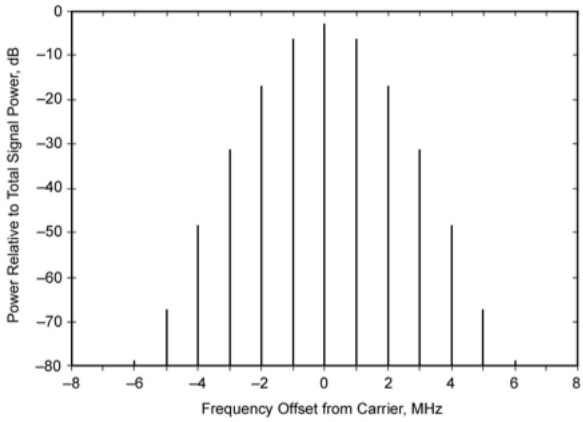

(a) Spectrum for Sinewave Range Component; 1 MHz, $\phi_r = 0.80$ rad rms

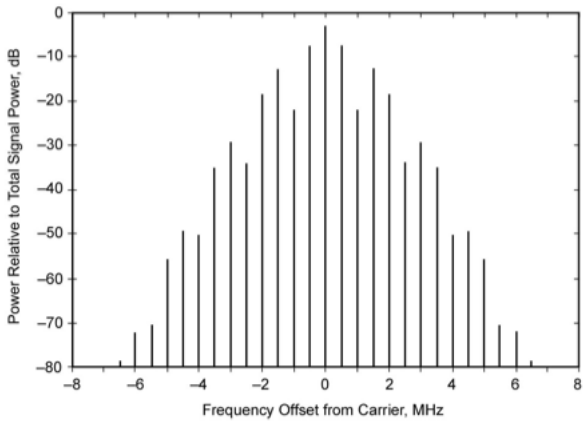

(b) Spectrum with chopping; 1 MHz, m=2, $\phi_r = 0.80$ rad rms

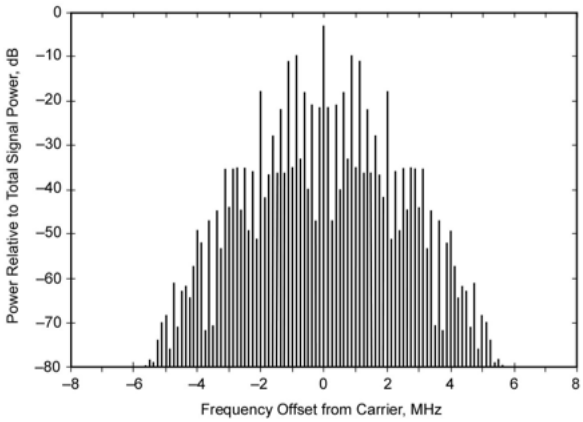

(c) Spectrum with chopping; 1 MHz, m=8, $\phi_r = 0.80$ rad rms

Figure 5.1: NASA-DSN sequential ranging spectrum (Kinman, 2009). m is the ratio between the chop component frequency and the squarewave range component.

5.1.2 ESA code ranging: signal structure

The sequential ranging signal used by European Space Agency (ESA) consists of a sine wave (tone), which is phase modulated by a sequential series of codes, used for ambiguity resolution

$$C_n = Q_1 \oplus Q_2 \oplus Q_3 ... \oplus Q_n \tag{5.6}$$

where

C_n is the n-th code

$\oplus$ stands for exclusive or

Q_i are squarewaves at frequencies $2^{-i} f_t$

Each code is synchronized to the tone such that phase transitions occur when the unmodulated tone phase is 90 deg and, as for ranging signal used at DSN, is transmitted for a fixed period of time to perform correlation and phase alignment. The nominal tone f_t, which is the clock component, is selected within the range (ESA-ESTEC (2005)) 100kHz-1,5MHz and in a region of the transponder bandwidth where the group delay is stable.

The ranging signal spectrum changes during the ambiguity resolution process, because the time variance of transmitted codes. During the acquisition, the code number increases and the code power is spread over an increasing number of lines (fig. 5.2). When the last step of the ambiguity resolution is completed, the code has created a quasi-continuous baseband spectrum, which extends (between first nulls) from $2^{-N} f_t$ to $(2 - 2^{-N}) f_t$ where f_t is the tone frequency, and N is the longest code length (ESA-ESTEC, 2005).

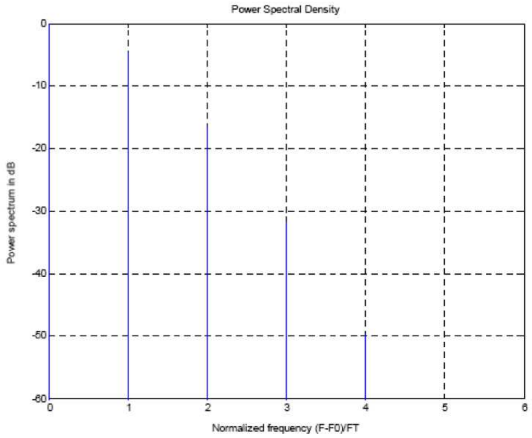

(a) Ranging signal spectrum for code length = 2^0

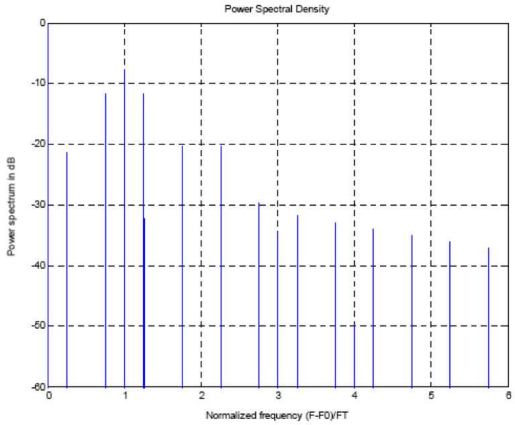

(b) Ranging signal spectrum for code length 2= 2^2

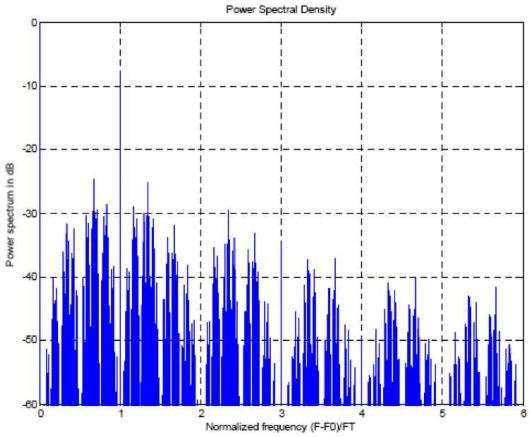

(c) Ranging signal spectrum for code length = 2^{12}

Figure 5.2: ESA code sequential ranging spectrum (ESA-ESTEC, 2005). Carrier modulation index of $1.0rad$ and tone modulation index of 45deg. Power relative to the modulated carrier power.

5.1.3 Power allocation in a transparent channel

The sequential ranging, as already explained, allows only a transparent approach in the spacecraft transponder instead of a regenerative one. The different signal processing onboard results in a different contribution of the uplink noise and consequently in a different power allocation in the ranging downlink signal. This aspect is important to be investigated because is fundamental in the assessment of the downlink ranging power to noise spectral density ratio, parameteter which determines the ranging jitter. Follows, therefore, a detailed formulation, according to Berner et al. (1999), Kinman (2009) and Kinman and Berner (2003), about the signal power and its distribution on all modulating signals (telemetry, commands, ranging) for what regard a transparent/turnaround channel. The case of a regenerative one will be exploited in par. 5.2.3. To have a general expression some relations, reported in tab. 5.2 are used.

Range Clock	Command/Telemetry	$\alpha(\psi)$	$\beta(\psi)$
sinewave	sinewave subcarrier	$J_0\left(\sqrt{2}\psi\right)$	$\sqrt{2}J_1(\sqrt{2}\psi)$
squarewave	squarewave subcarrier or direct mod.	$\cos(\psi)$	$\sin(\psi)$

Table 5.2: Definition for the modulation scheme.

We consider an uplink signal containing simultaneously either command (subcarrier) and ranging (sinewave or squarewave)

$$s_{ul}(t) = \sqrt{2}\sin\left[\omega_0 t + \phi_c c(t) + \phi_r r(t)\right] \tag{5.7}$$

where

ω_0 is the angular frequency of uplink carrier

$c(t)$ is the command signal (binary data on a sinewave or squarewave subcarrier)

$r(t)$ is the ranging signal (sinewave $\sqrt{2}\sin(\omega t)$, squarewave $S(\omega) = sign[\sin(\omega t)]$)

ϕ_c is the command modulation index, rad rms

ϕ_r is the uplink ranging modulation index, rad rms

That signal may be expanded by means of trigonometry and Jacoby-Anger identities into three fundamental [5] terms:

- The residual carrier $\sqrt{2}\alpha(\phi_r)\alpha(\phi_c)\sin\omega_0 t$
- The fundamental command sidebands $\sqrt{2}\alpha(\phi_r)\beta(\phi_c)c(t)\cos\omega_0 t$
- The fundamental ranging sidebands $\sqrt{2}\beta(\phi_r)\alpha(\phi_c)r(t)\cos\omega_0 t$

[5] There are also higher order sidebands and intermodulation products that are ignored in the analysis. That is possible because are generally quite small and many of the intermodulation products are in phase quadrature to the ranging signal (Kinman and Berner, 2003).

The uplink signal power allocation can be expressed by means of these three relations:

The ratio of the residual carrier to total signal power (carrier suppression)

$$\left|\frac{P_C}{P_T}\right|_{UL} = \alpha^2(\phi_r)\alpha^2(\phi_c) \tag{5.8}$$

The ratio of ranging signal power (P_R) to total signal power (P_T)

$$\left|\frac{P_R}{P_T}\right|_{UL} = \beta^2(\phi_r)\alpha^2(\phi_c) \tag{5.9}$$

The ratio of command(data) signal power(P_D) to total signal power

$$\left|\frac{P_D}{P_T}\right|_{UL} = \alpha^2(\phi_r)\beta^2(\phi_c) \tag{5.10}$$

Once the signal is received by the spacecraft, the turn-around (transparent) ranging channel of the transponder demodulates the uplink carrier (coherent demodulation by means of $\sqrt{2}\cos(\omega_0 t)$) and filters the baseband ranging signal (with a typical bandwidth of $1.5Mhz$). That signal, before being remodulated onto the downlink carrier, is adjusted to maintain a constant total power by the automatic gain control (AGC) circuit. The phase modulation of the downlink carrier due to ranging signal plus command feedthrough and noise in the turn-around ranging channel is

$$\psi(t) = \theta_r r(t) + \theta_c c(t) + \theta_n u(t) \tag{5.11}$$

where

θ_r is the downlink ranging modulation index, rad rms

θ_c is the downlink command modulation index, rad rms

θ_n is the downlink modulation index of uplink noise, rad rms

$u(t)$ is the unity-variance, zero-mean Gaussian random process

The modulated downlink carrier is then modeled as

$$s_{dl}(t) = \sqrt{2}\sin\left[G\omega_0 t + \psi(t) + \theta_b b(t)\right] \tag{5.12}$$

where

G is the transponding ratio

θ_b is the telemetry modulation index, rad rms

$b(t)$ is the telemetry signal (binary data on a squarewave subcarrier or just binary data).

Expanding the expression of the downlink signal, as already done with the uplink one, the three terms are found:

- The residual carrier $\sqrt{2}\alpha(\theta_r)\alpha(\theta_c)e^{-\theta_n^2/2}\alpha(\theta_b)\sin(G\omega_0 t)$
- The telemetry sidebands $\sqrt{2}\alpha(\theta_r)\alpha(\theta_c)e^{-\theta_n^2/2}\beta(\theta_b)b(t)\cos(G\omega_0 t)$
- The ranging sidebands $\sqrt{2}\beta(\theta_r)\alpha(\theta_c)e^{-\theta_n^2/2}\alpha(\theta_b)r(t)\cos(G\omega_0 t)$

The downlink signal power allocation can be defined with the following three relations:

The ratio of the residual carrier to total signal power

$$\left|\frac{P_C}{P_T}\right|_{DL} = \alpha^2(\theta_r)\alpha^2(\theta_c)e^{-\theta_n^2}\alpha^2(\theta_b) \tag{5.13}$$

The ratio of ranging signal power (P_R) to total signal power (P_T)

$$\left|\frac{P_R}{P_T}\right|_{DL} = \beta^2(\theta_r)\alpha^2(\theta_c)e^{-\theta_n^2}\alpha^2(\theta_b) \tag{5.14}$$

The ratio of telemetry(data) signal power(P_D) to signal total power

$$\left|\frac{P_D}{P_T}\right|_{DL} = \alpha^2(\theta_r)\alpha^2(\theta_c)e^{-\theta_n^2}\beta^2(\theta_b) \tag{5.15}$$

Some considerations are now necessary about the downlink modulation indices. They are indeed, effective modulation indeces, never equal to the design value θ_d of the downlink modulation index. As already said, the AGC controls the signal level in order to maintain the total power in the turn-around ranging channel to be a constant value. The modulation indeces follows therefore

$$\theta_r^2 + \theta_c^2 + \theta_n^2 = \theta_d^2 \tag{5.16}$$

and they can be expressed as

$$\begin{aligned} \theta_r &= \theta_d\Lambda \cdot \beta(\phi_r)\alpha(\phi_c) \\ \theta_c &= \theta_d\Lambda \cdot \alpha(\phi_r)\beta(\phi_c) \\ \theta_n &= \theta_d\Lambda \cdot \sigma_u \end{aligned} \tag{5.17}$$

The square of σ_u is

$$\sigma_u^2 = B_R\left(\left|\frac{P_T}{N_0}\right|_{UL}\right)^{-1} \tag{5.18}$$

where B_R is the turn-around ranging channel bandwidth and $\left|\frac{P_T}{N_0}\right|_{UL}$ is the uplink total signal power to noise spectral density ratio. The normalization factor Λ is

$$\Lambda = \frac{1}{\sqrt{\beta^2(\phi_r)\alpha^2(\phi_c) + \alpha^2(\phi_r)\beta^2(\phi_c) + \sigma_u^2}} \tag{5.19}$$

Furthermore, the ranging signal to noise ratio out of the ranging channel, G_{rng}, is

$$G_{rng} = \frac{\theta_r^2}{\theta_n^2} = \frac{\beta^2(\phi_r) J_0^2(\sqrt{2}\phi_c)}{\sigma_u^2} \tag{5.20}$$

Substituting the expression 5.18 into 5.20, it becomes

$$G_{rng} = \left|\frac{P_R}{N_0}\right|_{UL} \cdot \frac{1}{B_R} \tag{5.21}$$

where $\left|\frac{P_R}{N_0}\right|_{UL}$ is the ranging signal to noise density ratio

$$\left|\frac{P_R}{N_0}\right|_{UL} = \left|\frac{P_R}{P_T}\right|_{UL} \cdot \left|\frac{P_T}{N_0}\right|_{UL} \tag{5.22}$$

If command is not sent or the command feedthrough is small enough to be neglected, eq. 5.16 is modified in

$$\theta_r^2 + \theta_n^2 = \theta_d^2 \tag{5.23}$$

and, combining it with eq. 5.20, the effective modulation indices in the turn-around ranging channel become

$$\begin{aligned} \theta_r &= \theta_d \cdot \sqrt{\frac{G_{rng}}{1+G_{rng}}} \\ \theta_n &= \theta_d \cdot \frac{1}{\sqrt{1+G_{rng}}} \end{aligned} \tag{5.24}$$

Using these new definitions in eq. 5.13 and 5.14, we can write for the power distribution in absence of command signal:

The ratio of ranging signal power to total power

$$\left|\frac{P_R}{P_T}\right|_{DL} = \beta^2(\theta_d \cdot \sqrt{\frac{G_{rng}}{1+G_{rng}}}) \cdot e^{-\frac{\theta_d^2}{1+G_{rng}}} \cdot \alpha^2(\theta_b) \tag{5.25}$$

The ratio of residual carrier power to total power

$$\left|\frac{P_C}{P_T}\right|_{DL} = \alpha^2(\theta_d \cdot \sqrt{\frac{G_{rng}}{1+G_{rng}}}) \cdot e^{-\frac{\theta_d^2}{1+G_{rng}}} \cdot \alpha^2(\theta_b) \tag{5.26}$$

The latter equations (or from the more general 5.13, 5.14, 5.15) clearly show how the presence of uplink noise feeding through to the downlink affects the valuable downlink power. Moreover, the uplink noise and noisy intermodulation products are themselves a source of interference, increasing the effective noise floor. This last effect is not here discussed but can be found on Kinman and Berner (2003).

Finally, having defined the power allocation in the downlink signal, is possible to derive

the ranging signal over noise spectral density ratio as

$$\left|\frac{P_R}{N_0}\right|_{DL} = \left|\frac{P_R}{P_T}\right|_{DL} \cdot \left|\frac{P_T}{N_0}\right|_{DL} \tag{5.27}$$

This crucial parameter expresses quantitatively the presence of thermal noise with respect to the signal, and is therefore a key parameter in the evaluation of the range system accuracy.

5.1.4 Acquisition performance

The range measurement is complete once the intrinsic ambiguity in the measured phase delay of the clock component has been removed. This is done through a sequence of correlations against the ambiguity-resolving components. The random noise introduced by the electronics of the receiver affects not only the range accuracy, but also the acquisition of the that other tones, in terms of acquisition probability. A certain integration, or, acquisition time is therefore necessary to minimize the failure in acquiring a certain component or the overall ranging sequence.

Acquisition probability

A tone is successfully acquired if the received signal plus noise is greater than zero. Given a gaussian channel, with noise $n(t)$, the probability of acquiring a component n is[6] (Berner and Bryant, 2002)

$$\begin{aligned} P_n &= Prob\left(\left(\sqrt{P_r} + n(t)\right) > 0\right) = \\ &= Prob\left(\left(\frac{n(t)}{\sigma_n}\right) > -\frac{\sqrt{P_r}}{\sigma_n}\right) = \\ &= \frac{1}{\sqrt{2\pi}} \int_{-\infty}^{\frac{\sqrt{P_r}}{\sigma_n}} e^{-\frac{x^2}{2}}\, dx \end{aligned} \tag{5.29}$$

and considering $\sigma_n = \sqrt{\frac{N_o}{2T}}$,

$$\begin{aligned} P_n &= \frac{1}{2\pi} \int_{-\infty}^{\frac{\sqrt{P_r}}{\sqrt{\frac{N_0}{2T}}}} e^{-\frac{x^2}{2}}\, dx = \\ &= \frac{1}{2}\left(1 + erf\left(\sqrt{\frac{P_r}{N_0}T}\right)\right) \end{aligned} \tag{5.30}$$

[6]The term $erf(\cdot)$ stands for the error function

$$erf(y) = \frac{2}{\pi} \int_0^y e^{-t^2}\, dt \tag{5.28}$$

For a sequential ranging system, the probability of acquiring all $n-1$ components, starting from the first component n_1 to the last one N, is the product of individual component probabilities of acquisition (Kinman, 2009; Berner and Bryant, 2002)

$$P_{acq} = \prod_{n=n1}^{N} P_n = P_n^{n-1} = \left[\frac{1 + erf\left(\sqrt{\frac{P_r}{N_0} T}\right)}{2} \right]^{n-1} \tag{5.31}$$

While for tone ranging approach used at DSN the total ranging power is entirely put into the component that is being correlated, for ESA code system, the power is distributed all over the code. The term $\frac{P_R}{N_0}$, taking in account this aspect, is therefore not constant and the above expression has to be modified accordingly.

Acquisition time

Using the formulation of the acquisition probability reported before is possible to evaluate the acquisition time necessary to carried out a range measurement. For sequential ranging system, the process consists in sending a clock component, for T_1 seconds, and a certain number n of lower frequency tones, transmitted for T_2 seconds each. Considering dead times before, at the end and between the components/tones, the overall cycle time of a sequence can be expressed as (Berner and Bryant, 2002)

$$T_{cyc}|_{seq} = (2 + T_1) + (n-1)(1 + T_2) + 1 \tag{5.32}$$

For a downlink available signal power to noise density ratio $P_R/N_0$and given an accuracy σ_s, the integration time T_1 for the clock component is (inverting eq. 5.75 and 5.76)

$$T_1 = \begin{cases} (8\pi^2 \sigma_s^2 f_{RC}^2 \frac{P_r}{N_0})^{-1}, & \text{sinewave range clock} \\ (64 \sigma_s^2 f_{RC}^2 \frac{P_r}{N_0})^{-1}, & \text{squarewave range clock} \end{cases} \tag{5.33}$$

Moreover, given a certain requested acquisition probability, the integration time T_2 of the other tones (ambiguity resolution) is (inverting Eq. 5.31)

$$T_2 = \left[erf^{-1}\left(2\left(P_{acq}\right)^{\frac{1}{n-1}} - 1\right)\right]^2 \left(\frac{P_r}{N_0}\right)^{-1} \tag{5.34}$$

Using eq. 5.33 and 5.34 in eq. 5.32, the total cycle time, for a sequential ranging, can be finally expressed as (Berner and Bryant (2002))

$$T_{cyc} = \left(\frac{P_R}{N_0}\right)^{-1} \left[(n+2)\frac{P_R}{N_0} + \frac{1}{K f_{RC}^2 \sigma_s} + (n-1)\left\{ erf^{-1}\left(2\left(P_{acq}\right)^{\frac{1}{n-1}} - 1\right)\right\}^2 \right]^{-1} \tag{5.35}$$

where K is equal to 64 for squarewave and $8\pi^2$ for a sinewave. The expression found is valid when considering the NASA tone scheme, while for ESA is an approximation[7].

[7]The time T_2 requested for the acquisition of the ambiguity solving tones (for a fixed probability) is indeed not constant, due to the sequential decrease of the tone power.

5.2 Pseudo noise (PN) ranging

The term Pseudo-Noise refers in a strict sense to the use of a ranging-sequence system in which the ranging sequence is a logical combination of the so-called range clock-sequence and several PN sequences. A Pseudo-Noise sequence is a binary ± 1 sequence of period L whose periodic autocorrelation function has peak value +L and all (L-1) off-peak values equal to -1 (Massey et al., 2007).

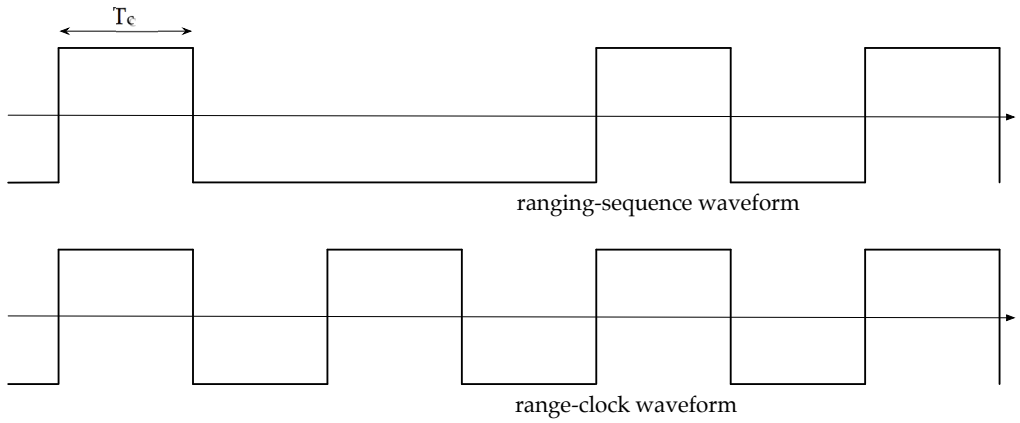

Figure 5.3: PN Ranging-Sequence waveform.

The range clock component, whose frequency equals half of the code chip-rate, has the most of the total ranging power and determines the resolution of the measurement. On the other hand, the intrinsic ambiguity of the phase delay measurement is removed using the PN sequences, called probing sequences, whose periods are divisors of the ranging sequence period. The ranging sequence, acquired by the receiver, is correlated separately against models of these probing sequences and their distinct cyclic shifts. The probing sequences must have the property that, when all these in-phase decisions are correctly made, they determine the delay (modulo the ranging sequence period L_{PN}) in chips of the received ranging sequence relative to its corresponding model (local replica). This particular property of the PN codes allows the code position reconstruction by means of a number of correlations smaller than the number of correlations needed if the entire code has to be compared with its all cyclic shifts.[8]. On the other hand, the (one-way) ambiguity resolution of the system is directly related to the length of the entire ranging sequence and is, in meters,

$$U = \frac{1}{2} c \cdot L_{PN} \cdot T_c = \frac{c \cdot L_{PN}}{4 f_{RC}} \tag{5.37}$$

[8]The length of the entire ranging sequence is equal to the product of the PN code components lengths, which are relatively prime

$$L_{PN} = L_1 \cdot L_2 \cdot L_3 ... \cdot L_i \tag{5.36}$$

Using the probing sequences to recover the code position requires $\sum(L_i - 1)$ correlations instead of $L_{PN} - 1$ correlations needed if the entire code is correlated against its cyclic shifts.

The greatest advantage in using Pseudo Noise (PN) ranging systems is the possibility to adopt a regenerative approach on board. It consists in a digital reconstruction, at the spacecraft transponder, of the received ranging signal. This approach, removing the uplink noise, results in an increases of the signal-to-noise density ratio of the downlink signal and therefore in a better accuracy achievable (see 5.2.3). Although this kind of codes have been used in the past[9], regenerative PN ranging systems for interplanetary missions, where thermal noise plays a fundamental role in the system performance, started to be developed and implemented only in the last years. In 2000's NASA enhanced with this purpose its Deep Space Network facilities and implemented the regenerative channel in the Spacecraft Transponding Modem (STM) (Berner et al., 2004, 2000; Bryant, 2001); and on 2011, with New Horizons mission, the first flight demonstration of a regenerative ranging system (Haskins et al., 2012; DeBoy et al., 2004) has been carried out. ESA, on the other hand, will provide its stations with receiver capable to support the future mission BepiColombo which will use this novel ranging technique.

5.2.1 PN code structure and properties

Consultative Committee for Space Data Systems (CCSDS) (CCSDS 414.0-G-1 (2010)) recommends two codes to be used for long-range deep space missions where a low signal-to-noise environment exists. Both codes have similar structure and come from the same family of PN codes, the balanced weighted-voting Tausworthe codes. They differ for the strength (voting factor) of the ranging clock component. A voting factor of 2, code T2B, is recommended for range measurements where acquisition time is the key aspect while a voting factor of 4, code T4B, is suitable when the range precision is the priority.

They consist in a logical combination of six binary sequences, called PN components, of length 2, 7, 11, 15, 19 and 23:

C_1:	+1	-1													
C_2:	+1	+1	+1	-1	-1	+1	-1								
C_3:	+1	+1	+1	-1	-1	-1	+1	-1	+1	+1	-1				
C_4:	+1	+1	+1	+1	-1	-1	-1	+1	-1	-1	+1	+1	-1	+1	-1
C_5:	+1	+1	+1	+1	-1	+1	-1	+1	-1	-1	-1	-1	+1	+1	-1
	+1	+1	-1	-1											
C_6:	+1	+1	+1	+1	+1	-1	+1	-1	+1	+1	-1	-1	+1	+1	-1
	-1	+1	-1	+1	-1	-1	-1	-1							

Each component is placed in a circular shift register with length equal to the component length and clocked at the chip rate. The first component, C_1, is the clock component, and therefore define the precision resolution of the ranging sequence, while the others are used for ambiguity resolution. The ranging sequence is built by AND'ing components C_2 through C_6 and OR'ing the result with the clock component, C_1, multiplied by a weighting/voting factor ν. The resulting sequence length is the product of the six sequence

[9] Suboptimal and optimal processing started in the early 1970's (Tausworthe, 1987; Tausworthe and Smith, 1987; Berner et al., 1999).

lengths, 1009470 bits (Berner et al., 1999)

$$Seq(i) = \nu C_1(i) \cup (C_2(i) \cap -C_3(i) \cap -C_4(i) \cap C_5(i) \cap -C_6(i)) \text{ for } i = 0 \text{ to } 1009469 \quad (5.38)$$

A code property of interest is the balance between the number of 1s and -1s in the composite sequence. An imbalance will result in a DC component in the PN code spectrum. It is best to minimize the code imbalance, since energy in the DC component cannot be used for ranging[10].

	Sequence length	Number of 1s	Number of -1s	Longest run of 1s	Longest run of -1s	DC value
T4B	1009470	504583	504887	7	5	3.01E-4
T2B	1009470	504033	505437	9	9	1.39E-3

Table 5.3: T2B/T4B PN codes: DC properties.

The correlation properties (Tab. 5.4) of the code are an important aspect in the chosen of the codes. They indeed directly affects both the acquisition performance and the measurement accuracy. The two parameters defining the code behavior in terms of correlation are:

- The in-phase correlation value. It occurs when the component sequence is aligned with its respective component in the composite PN code.
- The out-of-phase correlation value. It occurs when the component sequence is delayed by 1 to L-1 chips (where L is the length of the component sequence) relative to its respective component in the composite PN code.

	T4B In-phase Correlation	T4B out-of-phase Correlation	T2B In-phase Correlation	T2B Out-of-phase Correlation
C_1	947566	-947566	633306	-633306
C_2	61904	-10368	247020	-41404
C_3 (inv.)	61940	-6160	250404	-24900
C_4 (inv.)	61940	-4400	251332	-17852
C_5	61940	-3456	251604	-14056
C_6 (inv.)	61904	-2800	251940	-11388

Table 5.4: T2B/T4B PN codes: Correlation properties.

Applying an higher weight t results in an increase of the clock component power with respect to the total ranging power. The clock attenuation (tab. 5.5) depends by the in-phase fractional correlation values of the clock component as (CCSDS 414.0-G-1, 2010)

$$\text{range clock attenuation} = -20\log(C_1\text{in-phase correlation/sequence length}) \quad (5.39)$$

[10]For this reason the component C_3, C_4 and C_6 are inverted in the balanced Tausworthe (TB) codes.

	In-phase cor.	Normalized In-phase cor.	Range clock attenuation
T4B	947566	0.9387	0.550 dB
T2B	633306	0.6273	4.049 dB

Table 5.5: T2B/T4B PN codes: Range clock attenuation.

The spectrum (5.4) of a simulated PN ranging signal clearly shows the strong clock component at half of the chip rate and the continuos spectrum ($\sin(x)/x$ shape) due to effect of the longer repetition components that determine the pseudo-randomness of the code.

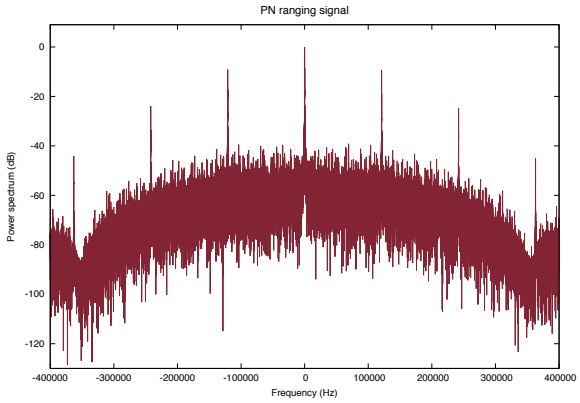

Figure 5.4: PN ranging signal spectrum: T4B, sinewave, $24.2Mchip/s$ and $0.7rad - pk$. The central line is the residual carrier while the side lines are the clock components. Power relative to the modulated carrier power.

5.2.2 PN acquisition, tracking and measurement approaches

Due to flight hardware limitations and the mass and power constraints the on board architecture could differ from that suitable for ground station. In particular two kind of architectures are considered, referring to BepiColombo mission and its Deep Space Transponder (DST)(fig. 5.5) (Boscagli et al., 2007a):

- A mixed serial/parallel architecture suitable for on board applications
- A full parallel approach for station implementations

On board architecture

The transponder ranging functions, if a regenerative approach is used, consist in

- Ranging clock acquisition and tracking
- Ranging sequence acquisition and tracking
- Coherent retransmission of the recovered code

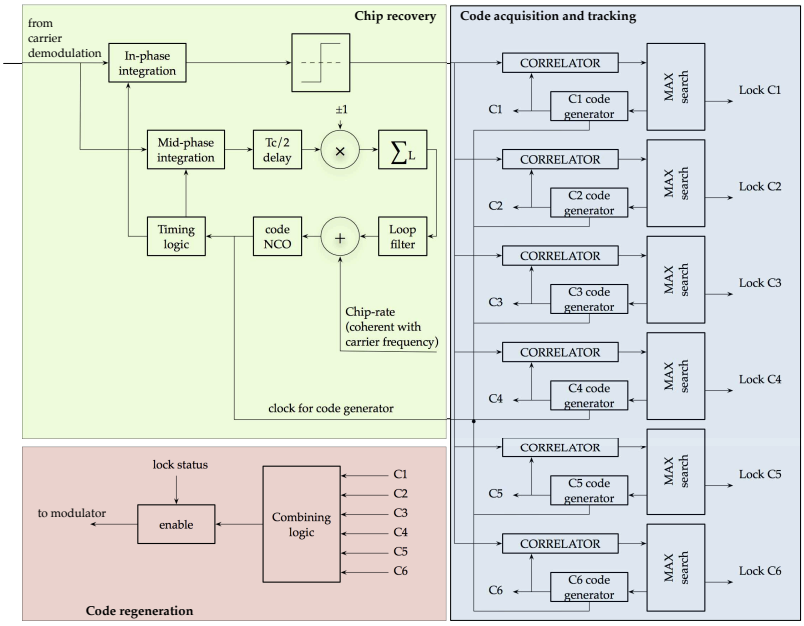

Figure 5.5: Functional block diagram of regenerative ranging channel as implemented in the BepiColombo X/X/Ka DST (Boscagli et al., 2007b).

After the coherent demodulation, accomplished by means of a phase locked loop (PLL), the receiver has to recover the chip-rate and phase of the code in order to drive with a proper timing signal the matching filter (in-phase integrator) necessary to reconstruct it. Since the PN code has a strong clock component, a squarewave tracking loop can be used as a Chip Tracking Loop (CTL). In BepiColombo Deep Space Transponder (DST) , the CTL is implemented modifying a data transition tracking loop, removing the in-phase arm and replacing it with a ± 1 multiplication to match the fact that the PN sequence resembles a squarewave (Boscagli et al., 2007b). After locking to the range clock, the receiver needs to acquire the ranging sequence. Driven by the CTL, an in-phase integrator (matched filter) reconstructs the received code, chip by chip. That received sequence $r(n)$ is then correlated against a local model of each probing sequence C_i and its k cyclic shift in order to find the correct phase of the probing sequences and recover the code position.

$$y_i^k = \sum_n r(n) \cdot C_i(n-k) \tag{5.40}$$

The ranging acquisition is carried out using six parallel correlators. Each correlator implements a serial search over the L_i possible phase shifts of the related probe sequence C_i. The correlations values are finally compared with a maximum search strategy and, once the phases of all $6C_i$ have been recovered, the position of the received entire ranging sequence is detected. The reconstructed sequence, synchronized to the received one, finally modulates the coherent downlink signal.

Ground station architecture

The ground station can use, on the other hand, a full parallel approach. 76 correlators could run in parallel, correlating the code with the overall 76 cyclic shifts needed for the 6 components[11]. The accurate range measurement, obtained comparing the received and the transmitted range clock phases, can be carried out in two different ways. In case of closed loop approach a CTL can be still used, while for an open loop approach, the range clock phase measurement can be provided by means of an I/Q correlation. The round trip delay can be finally evaluated as (Boscagli et al., 2007a)

$$T_{RT} = \sum_{i=1}^{6} d_i \alpha_i T_c + \tau \tag{5.41}$$

where

τ is the output of the I/Q correlator ($0 \leq \tau \leq T_c$)

d_i is the estimated phase for code C_i ($0 \leq d_i \leq L_i - 1$)

α_i are coefficient evaluated using the Chinese remainder theorem

α_1	504735
α_2	721050
α_3	642390
α_4	134596
α_5	850080
α_6	175560

5.2.3 Power allocation in a regenerative channel

In par. 5.1.3 has been analyzed the power allocation in a downlink signal in case of transparent/turnaround approach used at the spacecraft. In particular the ranging power to total power ratio on the down-link, has been found to be expressed by (eq. 5.14)

$$\left|\frac{P_R}{P_T}\right|_{TA} = \beta^2(\theta_r)\alpha^2(\theta_c)e^{-\theta_n^2}\alpha^2(\theta_b) \tag{5.42}$$

where

θ_r is the downlink ranging modulation index, rad rms

θ_c is the downlink command modulation index, rad rms

θ_n is the downlink modulation index of uplink noise, rad rms

θ_b is the telemetry modulation index, rad rms

α and β refers to the following table

Range Clock	Command/Telemetry	$\alpha(\psi)$	$\beta(\psi)$
sinewave	sinewave subcarrier	$J_0\left(\sqrt{2}\psi\right)$	$\sqrt{2}J_1(\sqrt{2}\psi)$
squarewave	squarewave subcarrier or direct mod.	$\cos(\psi)$	$\sin(\psi)$

Table 5.6: Definition for the modulation scheme.

In case of a regenerative channel, the signal received by the transponder has a different treatment and some changes to this expression are necessary. The transponder demodulates indeed the ranging signal, recovers and regenerates the received code, and remodulates it onto the downlink carrier. The ranging signal, phase modulated onto the downlink carrier, can be assumed to be free[12] of the uplink thermal noise and command feedthrough (Ruggier, 2004). The noise modulation index θ_n and the command modulation index θ_c can be considered equal to zero and the downlink ranging modulation index θ_r equals the design value θ_d of the downlink ranging modulation. The noise robbing effect vanishes and the ranging power to total power ratio on the down-link, in case of regenerative channel, becomes

$$\left|\frac{P_R}{P_T}\right|_{REG} = \beta^2(\theta_d)\alpha^2(\theta_b) \tag{5.43}$$

From eq. 5.43 is evident how the uplink noise, using a regenerative approach, not affects the downlink power to noise spectral density ratio. However it introduces a phase jitter on the downlink ranging signal which has to be taken in account when evaluating the ranging measurement accuracy. Dividing eq. 5.43 by eq. 5.42 is possible to define the gain G_{reg} obtainable in the downlink ranging signal using regenerative channel instead of the classical transparent channel at the spacecraft

$$G_{reg} = \frac{\beta^2(\theta_d)}{\beta^2(\theta_r)\alpha^2(\theta_c)e^{-\theta_n^2}} \tag{5.44}$$

Neglecting the command feedthrough and using eq. 5.25 (par 5.1.3) instead of eq. 5.42, the gain expression becomes

$$G_{reg} = \frac{\beta^2(\theta_d)}{\beta^2\left(\theta_d \cdot \sqrt{\frac{G_{rng}}{1+G_{rng}}}\right) \cdot e^{-\frac{\theta_d^2}{1+G_{rng}}}} \tag{5.45}$$

[11]The total length components is 77 but the range clock is an antipodal sequence.

[12]The regeneration circuitry's tracking loop has a much more narrow bandwidth. Typical value of some Hz instead of a turn-around ranging channel of about $1.5MHz$ (Simone et al., 2004). This permits to cut off the uplink noise and the command signal. The downlink ranging signal could be therefore considered as a simple phase modulation of the received ranging signal/code.

where the term G_{rng} represents the signal to noise ratio (SNR) of the uplink signal in the turnaround channel and is given (eq. 5.21) by

$$G_{rng} = \left|\frac{P_R}{N_0}\right|_{UL} \cdot \frac{1}{B_R} \tag{5.46}$$

Figure 5.6 shows quantitatively the gain G_{reg}, provided by the regenerative approach, as function of different uplink signal to noise power spectral density ratios ($\left|\frac{P_R}{N_0}\right|_{UL}$) and for different modulation indices (with a loop bandwidth of $1.5MHz$). For typical deep space mission, the use of regenerative channel results in an increase of the downlink ranging signal power of up to $30dB$. The gain can be used in three ways (Simone et al., 2004):

- To improve the accuracy of the measurement, keeping the same integration time (higher signal over noise density ratio)
- To improve the telemetry (higher modulation index) keeping the same performance on ranging
- To reduce the integration time keeping the same ranging performance

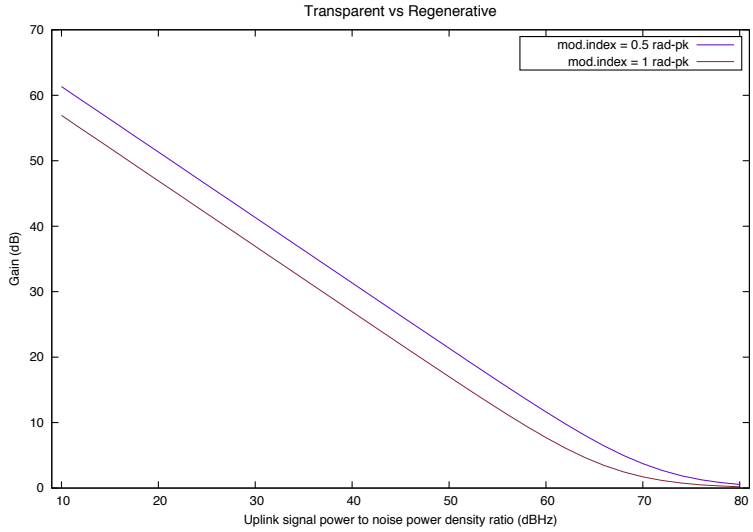

Figure 5.6: Downlink ranging power gain achievable using regenerative approach instead transparent channel. No command in uplink, sinusoidal ranging signal, loop bandwidth (transparent channel) of $1.5MHz$ and uplink/downlink modulation indices of 0.5 rad-pk (blue line) and 1 rad-pk (red line).

5.2.4 Acquisition performance

As already done for sequential ranging, an aspect of a ranging system that has to be investigated is the acquisition performance. The thermal noise, introduced by the receiver,

affects indeed the clock component correlation, in terms of range accuracy, as well as the correlation of the probing sequences used for ambiguity resolution, in terms of acquisition probability. The time necessary to have an acquisition within a certain probability of success is an important parameter which depends from the type of codes and from the acquisition strategy used.

Acquisition probability

Massey et al. (2007) provides the following expression for the error probability in a pair-wise contest of an antipodal sequence [13]

$$P_{e2} = Q\left(\sqrt{\frac{2KE_c}{N_0}}\right) \tag{5.52}$$

where

$$Q(x) = \frac{1}{\sqrt{2\pi}} \int_x^\infty e^{-t^2/2}\, dt \tag{5.53}$$

Using a geometric formulation we can write P_{e2} in terms of the Euclidean distance d and rms noise value σ

$$P_{e2} = Q(d/2\sigma) \tag{5.54}$$

where $d = 2K$ and $\sigma = \sqrt{KN_0/(2E_c)}$. For a generic probing sequence, antipodal or not, the error probability in the decision between the in-phase cyclic shift and one of its out-of-phase cyclic shifts is a function of the in-phase fractional correlation ξ and out-of-phase fractional correlation ψ (fig. 5.7). Applying some geometrical considerations, and introducing the parameter $\lambda = \frac{\xi - \psi}{2\xi}$, called correlation scale factor, we can write the Euclidian distant as:

$$d^2 = 4 \cdot K^2 \cdot \xi^2 \cdot \lambda \tag{5.55}$$

[13] Note that equation is absolutely equivalent to the acquisition probability expression found for a tone in the sequential ranging. With some manipulation we can write the error probability as

$$P_{e2} = Q\left(\sqrt{\frac{2KE_c}{N_0}}\right) = \frac{1}{2} erfc\left(\sqrt{\frac{KE_c}{N_0}}\right) = \frac{1}{2}(1 - erf\left(\sqrt{\frac{KE_c}{N_0}}\right)) \tag{5.47}$$

The resulting acquisition probability is

$$P_a = 1 - P_{e2} = \frac{1}{2}(1 + erf\left(\sqrt{\frac{KE_c}{N_0}}\right)) \tag{5.48}$$

and considering the definition of Energy chip E_c

$$E_C = P_R T_C \tag{5.49}$$

it can be written as

$$P_a = 1 - P_{e2} = \frac{1}{2}(1 + erf\left(\sqrt{KT_C\frac{P_R}{N_0}}\right)) \tag{5.50}$$

The multiplication of the integrated chips by the chip time obviously corresponds to the integration time and the resulting expression

$$P_a = 1 - P_{e2} = \frac{1}{2}(1 + erf\left(\sqrt{T_{int}\frac{P_R}{N_0}}\right)) \tag{5.51}$$

is identical to the one (equation 5.30) obtained for tone acquisition.

Substituting eq. 5.55 in eq. 5.54, is possible to write a general expression[14] of the probability error in a pairwise contest of a generic probing sequence i

$$P_{e2} = Q\left(\sqrt{2K\frac{E_c}{N_0}\xi^2 \cdot \lambda}\right) \tag{5.56}$$

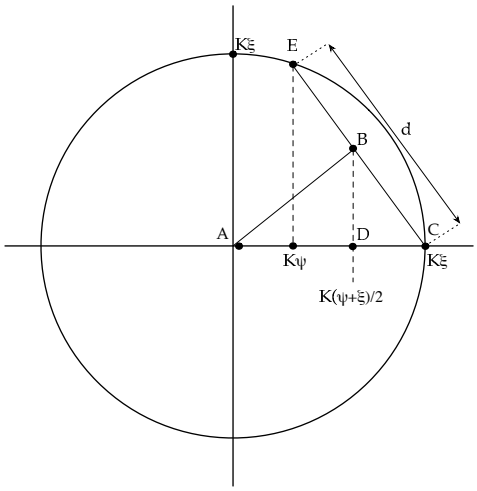

Figure 5.7: Signal-space representation for the decision between the in-phase cyclic shift and one of its out- of-phase cyclic shifts of an arbitrary probing sequence of length K chips, having in-phase fractional correlation ξ and out-of-phase fractional correlation Ψ (Massey et al., 2007).

The acquisition process of the full PN ranging sequence is completed successfully when all of the local generated probing sequences C_i are in-phase with the received ranging sequence

$$P_{ACQ}(C) = \prod_{i=1}^{6} P(C_i) \tag{5.57}$$

Moreover, a generic probing sequence C_i is correctly acquired if and only if its in-phase cyclic shift would win a pairwise contest with each of the $L_i - 1$ out-of-phase cyclic shifts of the sequence. The probability error P_{e_i} in acquiring this sequence can be approximated (Massey et al., 2007), assuming as independent event each correlation, as

$$P_{e_i} \approx (L_i - 1)P_{e2} \tag{5.58}$$

The consequent probability of successfull acquisition for each probing sequence is therefore

$$P(C_i) = 1 - P_{e_i} \approx 1 - (L_i - 1)P_{e2} \tag{5.59}$$

[14]For an antipodal sequence having unity in phase fractional $\lambda = 1$ and $\xi = 1$.

A more accurate analysis in Boscagli et al. (2007a) provides a slightly different formulation for the probability of successfully acquisition of a probing sequence:

$$P(C_i) = \int_{-\infty}^{\infty} \left[1 - \frac{1}{2} erfc(y)\right]^{L_i - 1} \cdot \sqrt{\frac{1}{\pi}} e^{\left[-\left(-y-\sqrt{\gamma}\right)^2\right]} \, dy \tag{5.60}$$

where

$$\begin{aligned} \gamma &= (\xi - \psi)^2 \frac{L_i}{L_i + 1} K \frac{E_c}{N_0} \\ erfc(x) &= 1 - \frac{2}{\pi} \int_0^x e^{-t^2} \, dt \end{aligned} \tag{5.61}$$

These results come from a different approach in evaluating the probability when we are dealing with the probing sequences ($C_i, i > 1$) and not with clock component. In particular the random variables (noise term) are still gaussian with zero mean and variance $\frac{N_0 T}{2}$, but they are no longer independent since $C_{ik}(t) = C_i(t - kT_c)$ is not orthogonal to $C_{ih}(t)$ for $k \neq h$. The noise variance is therefore modified by the term $\frac{L_i+1}{L_i}$ and becomes

$$\sigma^2 = \frac{N_0}{2} T \frac{(L_i + 1)}{L_i} \tag{5.62}$$

In case of on board acquisition, where each probing sequence is acquired serially, the noise component for the L_i different correlations can be assumed statistically independent and the parameter γ is

$$\gamma = (\xi - \psi)^2 K \frac{E_c}{N_0} \tag{5.63}$$

The approximated and accurate formulation provides very similar results in particular for the on-board case. The following analysis on the acquisition time will be mostly based on the approximated formulation both for on board and ground station (GS) architectures, even if a small approximation error is committed. Although the approximated analysis is not fully theoretically correct, it provides a closed expression for the acquisition time showing clearly the dependence from the SNR and the correlation parameters (ξ and ψ).

Acquisition time

In case of PN ranging system, inverting eq. 5.56 is possible to express the correlation time T_i required for a certain sequence C_i given a fixed error probability P_{e2} (on a pairwise contest) and the signal over noise density ratio of the ranging signal (P_R/N_0)

$$T_i = \frac{[Q^{-1}(P_{e2})]^2}{2E_C/N_0} \cdot \frac{1}{\lambda \cdot \xi^2} \cdot T_C = \frac{[Q^{-1}(P_{e2})]^2}{2P_R/N_0} \cdot \frac{1}{\lambda \cdot \xi^2} \tag{5.64}$$

This equation shows that the integration time doesn't depends by the chip rate of the code. Introducing the integration time needed in case of an antipodal sequence having unity in-

phase fractional correlation

$$T_a = \frac{[Q^{-1}(P_{e2})]^2}{2P_R/N_0} \tag{5.65}$$

is possible to normalize the correlation time, giving the possibility to compare in a simple and general way the different codes and components

$$\tau_{cor_i} = T_i/T_a = 1/(\xi_i^2 \cdot \lambda_i) \tag{5.66}$$

Moreover, considering an acquisition strategy based on the maximum search and a single correlator for each probing sequence C_i ($i = 2, 6$)[15] we can define also the normalized acquisition time of an entire probing sequence τ_{acq_i} as

$$\tau_{acq_i} = L_i \tau_{cor_i} \tag{5.67}$$

where L_i is the length of the probing sequence.

T2B	L	ξ	ψ	λ	$\tau_{cor} = 1/(\xi^2 \cdot \lambda)$	$\tau_{acq} = L \cdot \tau_{cor}$
C_1	2	0.6274	-0.6274	1	2.54	2.54
C_2	7	0.2447	-0.0410	0.5838	28.61	200.27
C_3 (inverted)	11	0.2481	-0.0247	0.5498	29.55	325.05
C_4 (inverted)	15	0.2490	-0.0177	0.5355	30.12	451.8
C_5	19	0.2492	-0.0139	0.5279	30.50	579.5
C_6 (inverted)	23	0.2496	-0.0113	0.5226	30.71	706.33
T4B	L	ξ	ψ	λ	$\tau_{cor} = 1/(\xi^2 \cdot \lambda)$	$\tau_{acq} = L \cdot \tau_{cor}$
C_1	2	0.9387	-0.9387	1	1.13	1.13
C_2	7	0.0613	-0.0103	0.5840	455.7	3189.9
C_3 (inverted)	11	0.0613	-0.0061	0.5498	484.0	5324.0
C_4 (inverted)	15	0.0613	-0.0044	0.5359	496.6	7449.0
C_5	19	0.0613	-0.0034	0.5277	504.3	9581.7
C_6 (inverted)	23	0.0613	-0.0028	0.5228	509.0	11707

Table 5.7: T2B/T4B PN codes: Acquisition properties.

The values of tab. 5.7 give an idea about the performance of the two different codes. Giving an higher weight to the range clock the acquisition time is largely increased because of the less power contained in the probing sequences. The longest and weakest component C_6 of the T4B code needs indeed an acquisition time 16 times bigger than the corresponding acquisition time needed if T2B code is used.

$$\frac{|\tau_{cor_6}|_{T4B}}{|\tau_{cor_6}|_{T2B}} \approx 16 \tag{5.68}$$

Given a certain acquisition probability P_{ACQ} and the signal over noise density ratio is possible to quantitatively compute the overall acquisition time. This is carried out firstly

[15] The first component, being antipodal, could be correlated one time only

inverting eq. 5.57, in order to compute the required corresponding error probability P_{e2}, and then using eq. 5.64 (or the normalized value and eq. 5.66). Not only the codes have to be separately analyzed, also the acquisition strategy affects, obviously, the integration time. Therefore we firstly consider the case of on board acquisition, which is led through the use of a mixed serial/parallel correlations, and then the acquisition time corresponding for a full parallel approach.

The on board acquisition architecture developed for BepiColombo is based on a six parallel correlators, one for each probing sequence (see section 5.2.2). The total acquisition time is therefore that needed for the sixth component, which is the longest one (23 cyclic shift). Remembering eq. 5.65,5.64,5.67, it ibecomes

$$|T_{ACQ}|_{SC} = T_a \cdot \tau_{acq_6} = 23 \cdot \frac{[Q^{-1}(P_{e2})]^2}{2P_R/N_0} \cdot \frac{1}{\lambda_6 \cdot \xi_6^2} \tag{5.69}$$

A certain probability of acquisition P_{acq} can be considered in this case, with a good approximation, only affected by the error due to the sixth component acquisition. Since the five other probing sequences are acquired for over their required correlation time (of more than 18%), their probabilities of error are much more smaller and can be neglected. The overall acquisition probability can be therefore determined exclusively by the probability of error in the sixth component and the eq. 5.57 is approximated as

$$P_{ACQ}(C) \approx P(C_6) \approx 1 - (L_6 - 1)P_{e2} \tag{5.70}$$

Given a fixed probability acquisition, the corresponding minimum required probability error P_{e2} is determined inverting that equation.

The ground stations (GS), on the other hand, can be equipped with instrument capable to use a full (76 correlators) parallel approach. All the correlations are therefore evaluated for the same amount of time, determined by the maximum of τ_{cor}, that is the correlation of the sixth component

$$|T_{ACQ}|_{GS} = MAX_i \left\{ \frac{\left[Q^{-1}(P_{e2})\right]}{2 \cdot (P_R/N_0)} \cdot \frac{1}{\xi_i^2 \cdot \lambda_i} \right\} = \frac{[Q^{-1}(P_{e2})]^2}{2P_R/N_0} \cdot \frac{1}{\lambda_6 \cdot \xi_6^2} \tag{5.71}$$

Given a fixed probability acquisition, no approximation should be done and the corresponding minimum required probability error in a pairwise contest P_{e2} is determined inverting the complete eq. 5.57.
Considering an acquisition probability of 99.9%, follows:

- A pairwise error probability P_{e2} equal to $5 \cdot 10^{-5}$ for the on-board acquisition

$$P_{acq} \approx 1 - P_{e23} \approx 1 - (23 - 1)P_{e2} \approx 0.999 \tag{5.72}$$

(a) Partially (6-correlators) parallelized approach (on board)

$\lvert T_{ACQ}\rvert_{SC}$	$\tau_{acq} = \tau_{acq23}$	Acquisition time (seconds)
T2B	706.33	10.7
T4B	11707	177

(b) Fully parallelized approach (GS)

$\lvert T_{ACQ}\rvert_{GS}$	$\tau_{acq} = \tau_{cor23}$	Acquisition time (seconds)
T2B	30.71	0.5
T4B	509.0	8.9

Table 5.8: T2B/T4B PN codes: Acquisition time. Acquisition probability of 99.9% and a signal to noise density ratio of $27dBHz$.

- A pairwise error probability P_{e2} equal to $1.4 \cdot 10^{-5}$ for the full parallelized approach

$$P_{acq} \approx \prod_{i=1}^{6}(1 - (l_i - 1)P_{e2}) \approx 0.999 \tag{5.73}$$

In tab. 5.8 are reported the acquisition time, with different codes and acquisition strategies, computed considering a ranging signal over noise density (P_R/N_0) value of $27dbHz$.

The T2B code needs an acquisition time that is 16 times smaller than that necessary with the other code type, for both the strategies. The full parallelized approach, on the other hand, increases the speed of the acquisition with respect to the semi-parallelized approach, of a factor of 19

$$\frac{\lvert T_{ACQ}\rvert_{SC}}{\lvert T_{ACQ}\rvert_{GS}} \approx 19 \tag{5.74}$$

The single correlation time needed in the fully parallelized acquisition instead of the entire sixth component acquisition time (23 times single correlation) doesn't decrease the overall acquisition time of the predictable factor 23, because of the narrower requirement in terms of error probability on a corresponding antipodal sequence P_{e2} given a fixed acquisition probability. These results, as already said, are an approximation of the acquisition time. However they give an idea of the the ranging system acquisition performances as function of the codes and acquisition strategies used.

5.3 Ranging system accuracy

The evaluation of the observables accuracy achievable with a certain radiometric tracking system is a key point in the evaluation of the system performances. The many errors affecting the ranging observable accuracy are already explained briefly in par. 1.2. This paragraph investigate firstly the ranging jitter due to the thermal noise. The noise introduced by the electronic of the receiver into the signal causes indeed a random error on the ranging measurement, affecting its precision. Then an error budget is evaluated considering systematic as well as random errors.

5.3.1 Ranging jitter

The downlink thermal noise, quantitatively defined by the parameter $\left.\frac{P_R}{N_0}\right|_{DL}$, corrupts the signal correlation introducing a random error in the final phase, and therefore in the range measurement. This error can be easily computed and controlled operating on the integration time (or loop bandwidth) parameter. Considering an open loop case based on I and Q correlation[16], the two-way range measurements error (in meters, one-way) is (Boscagli et al., 2008):

- For a sinewave shaped ranging signal and matched receiver with sine reference at the I/Q branches of the correlator

$$\sigma_{range_{sin-sin}}|_{OL} = \frac{c}{\sqrt{32\pi^2} f_{RC}} \sqrt{\frac{1}{P_{RC}/N_0} \cdot \frac{1}{T}} \tag{5.75}$$

- For a sinewave shaped ranging signal and mismatched receiver with square-wave reference at the I/Q branches of the correlator

$$\sigma_{range_{sin-sq}}|_{OL} = \frac{c}{16 f_{RC}} \sqrt{\frac{1}{P_{RC}/N_0} \cdot \frac{1}{T}} \tag{5.76}$$

- For a squarewave shaped ranging signal and matched receiver with squarewave reference at the I/Q branches of the correlator

$$\frac{c}{16 f_{RC}} \sqrt{\frac{1}{P_{RC}/N_0} \cdot \frac{1}{T}} \leq \sigma_{range_{sq-sq}}|_{OL} \leq \frac{c}{8\sqrt{2} f_{RC}} \sqrt{\frac{1}{P_{RC}/N_0} \cdot \frac{1}{T}} \tag{5.77}$$

where

P_{RC} is the power of the range clock component (W)

N_0 is the one-sided noise power spectral density (W/Hz)

T is the integration time (s)

[16] For a detailed explanation see appendix B.

c is the speed of light (m/s)

f_{RC} is the range clock frequency (Hz)

On the other hand, a closed loop approach[17] based on a chip-tracking-loop (CTL) provides a two-way range measurement error, in meters (one-way), that is (Ruggier, 2004; Boscagli et al., 2008):

- For a squarewave shaped ranging signal and a squarewave shaped reference signal at the CTL (matched case)

$$\sigma_{range_{sq-sq}}|_{CTL} = \frac{c}{8 f_{RC}} \sqrt{\frac{B_L}{P_{RC}/N_0}} \tag{5.78}$$

- For a sinewave shaped ranging signal and a squarewave shaped reference signal at the CTL

$$\sigma_{range_{sin-sq}}|_{CTL} = \frac{1}{\sqrt{2}} \frac{c}{8 f_{RC}} \sqrt{\frac{B_L}{P_{RC}/N_0}} \tag{5.79}$$

where B_L is the one-sided loop bandwidth of CTL.

It is demonstrated, in case of Additive White Gaussian Noise, that the open loop and closed loop show the same estimation error (variance) if (Boscagli et al., 2008)

$$B_L = \frac{1}{2T} \tag{5.80}$$

That is evident for the case sin-sq comparing eq. 5.76 with eq. 5.79. On the other hand, substituting eq. 5.80 in 5.78 and comparing the result with 5.77 follows that for the sq-sq case

$$\frac{1}{\sqrt{2}} \sigma_{range_{sq-sq}}|_{CTL} \leq \sigma_{range_{sq-sq}}|_{OL} \leq \sigma_{range_{sq-sq}}|_{CTL} \tag{5.81}$$

The phase jitter variance for the sq-sq case depends indeed, in the open-loop architecture, to the phase θ to be estimated while not using a closed loop approach. In the lower case bound ($\theta = \pi/4$) the open loop approach performs therefore $3dB$ better with respect to the closed loop based on the CTL. The upper bound for the $\left|\sigma_{range_{sq-sq}}\right|_{OL}$ is related to the delay of θ equal to 0 or $\pi/2$ which is the tracking condition of the CTL. In that condition the variance is the same and in general is possible to write

$$\sigma_{range_{sq-sq}}|_{OL} \leq \sigma_{range_{sq-sq}}|_{CTL} \tag{5.82}$$

End to end ranging jitter performance

As explained in par. 5.1.3, the uplnk noise, when a transparent channel is used on board, directly affects the downlink power to noise density ratio. The end-to-end jitter is therefore easily evaluated using the above equations (OL or CL) with the value of P_R/N_0 of the downlink leg.

[17] For a detailed explanation see appendix C.

For a regenerative channel, the uplink thermal noise doesn't affect the downlink power to noise density ratio but introduces a phase jitter on the regenerated ranging signal which cannot be neglected (see par. 5.2.3). Using only the above equations doesn't provide therefore a reliable estimate of the achievable accuracy. The previous expressions consider indeed only the downlink contribution. The overall end to end ranging jitter performance in case of closed loop (square-sine) both at the SC and GS could be expressed (Boscagli et al., 2006)

$$\sigma^2_{range_{REG}} = \left(\frac{1}{\sqrt{2}}\frac{c}{8f_{RC}}\right)^2 \left\{\frac{N_{01}}{2P_{RC1}}\left[\int_{-\infty}^{+\infty}|H_1(f)H_2(f)|^2\ df\right] + \frac{N_{02}}{2P_{RC2}}\left[\int_{-\infty}^{+\infty}|H_2(f)|^2\ df\right]\right\} \tag{5.83}$$

Knowing the transfer functions $H(f)$ is possible to calculate it. A good simplification can be performed assuming two cases determined by the respective value of bandwidth:

- GS loop bandwidth much bigger than on board loop bandwidth ($B_{L1} << B_{L2}$)

$$\sigma_{range_{REG}} = \sqrt{\left(\frac{1}{\sqrt{2}}\frac{c}{8f_{RC}}\right)^2 \left\{\frac{N_{01}}{P_{RC1}}B_{L1} + \frac{N_{02}}{P_{RC2}}B_{L2}\right\}} \approx \sqrt{\sigma^2_{CTL1} + \sigma^2_{CTL2}} \tag{5.84}$$

- GS loop bandwidth much smaller than on board loop bandwidth ($B_{L1} >> B_{L2}$)

$$\sigma_{range_{REG}} = \left(\frac{1}{\sqrt{2}}\frac{c}{8f_{RC}}\right)\sqrt{B_{L2}\left\{\frac{N_{01}}{P_{RC1}} + \frac{N_{02}}{P_{RC2}}\right\}} \tag{5.85}$$

In case of open-loop architecture, the approximation $B_{L1} >> 1/T$ (being T the integration time) is applicable. Considering the range error on the matched sine case (eq. 5.75), the overall end-to-end standard deviation of the range measurement can be expressed as

$$\sigma_{range_{REG}} = \frac{c}{\sqrt{32\pi^2}f_{RC}}\sqrt{\frac{1}{T}\left\{\frac{N_{01}}{P_{RC1}} + \frac{N_{02}}{P_{RC2}}\right\}} \tag{5.86}$$

5.3.2 Error budget

The evaluation of an error budget for a ranging system is quite complex. The contribution of some error sources have to be indeed analyzed for different timescales and conditions. Here are presented, therefore, two indicative error budgets, referring to two distinctive ranging systems, useful to understand roughly the general ranging system performance and in particular the contribution in using new and advanced techniques. What follows refers on what already explained in par 1.2 and what explained on Iess et al. (2012) and Iess (2007). Two range system configurations have been considered (tab.5.9): a standard system, based on common configuration, and an advanced one, based on the most advanced techniques.

In particular, the first is an X-band standard sequential ranging system based on a transparent approach while the other is a Ka-band ranging system based on PN codes and a regenerative channel on board.

	Standard system	Advanced system
Radio-link	X-band	Ka-band
Ranging system	Sequential tones 1.5MHz	Pseudo noise 24.2Mchip/s
On board approach	Transparent/turn-around	Regenerative
Plasma	Only models prediction	Multi-link calibration
Troposphere	Only models prediction	WVR calibration
Station bias	Current calibration	Advanced calibration

Table 5.9: Range error budget: System configurations.

The plasma has been considered not calibrated in the first case while removed almost completely by means of multi-frequency links in the second one. Moreover, the calibrations of the station biases have been considered at the state of art for the standard ranging system, while a better calibration system has been considered for an advanced ranging system. Currently these group delays are indeed the limiting aspect of the range accuracy being their magnitude on the order of some meters. For the future mission BepiColombo, where the range accuracy requested for the radioscience experiment is on the order of $20cm$ (Iess and Boscagli, 2001), a new and currently not developed calibration system for these station biases is needed. The group delay due to spacecraft segment (transponder and waveguides) strongly depends from the timescales considered. While for short time scales can be considered negligible, over long timescales should be significant. The ranging jitter depends strongly from the radio link configuration and the considered scenario. In table 5.10 are reported the values chosen for the configuration of the two cases. These values are taken from literature and refer to an hypotetic, but realistic, spacecraft and to the ground stations (Martin and Warhaut, 2004) currently used for deep space missions.

Figure 5.8 shows how the dominating error sources for a ranging system are plasma and station biases. Once removed these errors, the use of a regenerative PN ranging system becomes important, permitting to drastically reduce the ranging jitter. In the particular considered case, this error is not so significant but in other scenarios (spacecraft distance) or with different configurations (modulation indices, presence of telemetry) it could be significant. The advantage in using a regenerative approach (see par 5.2.3) and an high clock frequency becomes consequently fundamental.

	Value		Comments
	Standard	Advanced	
Link budget parameters			
Spacecraft distance	2 AU		
Up- and Down-link Freq.	7.2/8.4 GHz	34.4/32.1 GHz	
GS TX power	20.0 kW	0.8 kW	
GS Antenna diameter	35 m		
GS System noise T	90 K		
SC Antenna diameter	1 m		
SC System noise T	300 K		
SC TX power	2 W	30 W	
Uplink P_t/N_0	66.8 dBHz	66.4 dBHz	Loss = 2.5 dB
Downlink P_t/N_0	45.2 dBHz	45.0 dBHz	Loss = 2.5 dB
Downlink P_r/N_0	29.2 dBHz	35.7 dBHz	TC/TM OFF $\theta_r = 0.5$ rad-pk. $B_L = 1.5$ MHz
Clock freq.	1.5 MHz	12.1 MHz	
Integration time	8s		

Table 5.10: Range error budget: Radio link configuration and link budget for standard ranging system (X-band sequential ranging) and advanced ranging system (Ka-band PN ranging).

Error source	Value (cm)	Comments
Thermal noise	14.0	Standard (sequential)
	0.8	Advanced (PN)
S/C contribution	10.0	Medium timescales
G/S bias	150.0	Current calibration
	10.0	New calibration Ka/Ka.
Platform parameters	9.0	Earth orientation, Station locations and Earth tides
Plasma	150.0	No calibration. $SEP > 160$.
	1.40	Multilink calibration.
Troposphere (wet only)	6.50	5cm at zenith, elev. = 50deg
	3.00	WVR calibration.
Total error	**213.4**	Standard ranging system
	17.1	Advanced ranging system

Table 5.11: Range error budget.

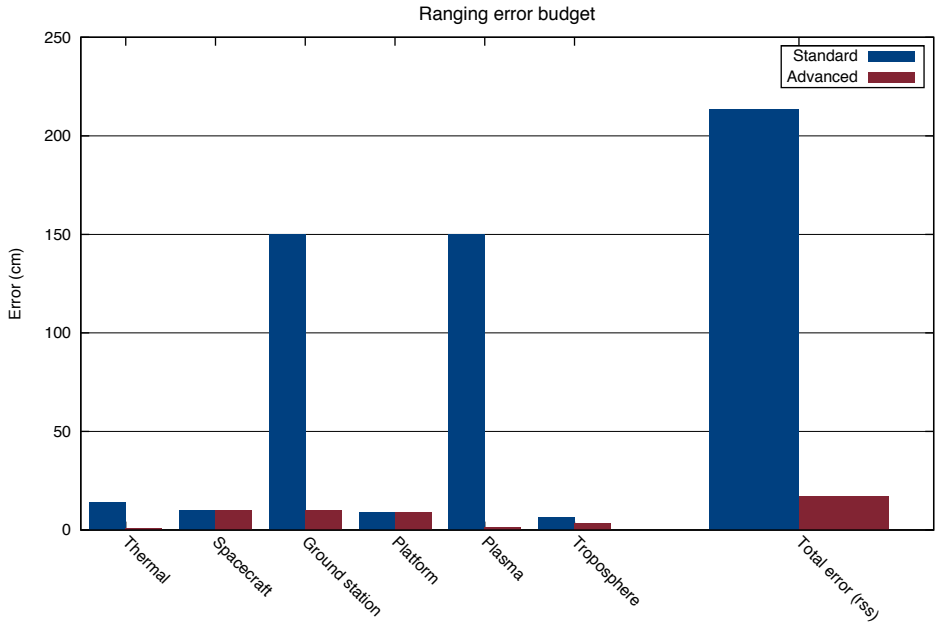

Figure 5.8: Range error budget. In blu a standard transparent sequential ranging system while in red a ranging system based on pseudo noise code and regenerative channel on board.

Chapter 6

Pseudo noise open loop receiver

Ranging systems based on pseudo noise (PN) code, and adopting a regenerative approach on board, have started to be developed in the last years. NASA New Horizons mission, on 2011, has made the first flight demonstration of a regenerative ranging, with a system based on a PN code at $2Mchip/s$ (DeBoy et al., 2004). Also the future cornerstone ESA mission to Mercury, BepiColombo (see appendix A), will be supported by a PN regenerative ranging system, but characterized by higher chip rate ($24Mchip/s$). ESA ground stations don't have, currently, receivers to cope with this new technique and, also the DSN has currently only a partial capability. Furthermore the number of antennae on Earth is quite large while the number of stations equipped with highly expensive receivers for advanced tracking systems is obviously limited. In this scenario, as a support activity to the Mercury Orbiter Radio science Experiment (MORE), the development of an open loop receiver[1] based on a software correlator[2] has began. Although its first task consists in providing support to the BepiColombo Ka translator (KaT) testing activities, its intrinsic flexibility and cheapness make it suitable, indeed, to be used in some of the numerous Earth antennae, for scientific purposes.

Beside of the correlator, also a simulator of the ranging signal (transmitted and received) has been developed, to test the software with end-to-end simulations of the ranging system itself. The following two paragraphs explain in detail the simulator as well as the correlator,

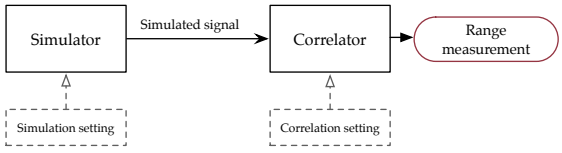

Figure 6.1: Simulator and correlator.

exploiting their software architecture and the mathematical models used.

[1]Note that the work regards the development of the signal correlator, while the signal acquisition system will be developed in future.

[2]A future hardware (FPGA) implementation of the open loop correlator is currently foreseen.

6.1 Simulator

The simulation have to replace ground and space segments involved in the two-way ranging system which is schematically represented in fig 6.2 The ranging signal is generated, modulated onto the uplink carrier, and transmitted towards the spacecraft. During the propagation the uplink signal

- experiences a time variant Doppler shifts, due to relative spacecraft and Earth motion
- is affected by noise due to media (troposphere,ionosphere and solar plasma)
- is attenuated ($\sim \frac{1}{r^2}$).

When received by the SC transponder, the signal is affected also by the thermal noise introduced by the electronic instruments. Then it is processed in a regenerative channel that permits to generate a code locked to the received one except for a certain amount of phase jitter. This code, that is the ranging signal, is remodulated onto the carrier and sent back. During the downlink propagation, as for the uplink, the signal is attenuated and affected by noise. At the ground station the signal is received, corrupted by the receiver thermal noise, down converted and finally quantized and sampled. The simulator takes in account only the thermal noise (random noise) introduced by the electronics and determined quantitatively by the signal power over noise spectral density parameter (P/N_0). Furthermore only the downlink contribution of noise is considered[3]. The simulation outputs are:

- The transmitted signal or the starting code epoch
- The received signal

6.1.1 Mathematical model

The simulator generates a complex or real signal which can be in general modeled as

$$\begin{aligned} s_{complex}(t) &= A_s \exp\left[i\Phi\right] + N(t) \\ s_{real}(t) &= A_s \cos(\Phi) + N(t) \end{aligned} \tag{6.3}$$

where

[3]For a regenerative channel, the uplink noise affects indirectly the range measurements, introducing into the signal an uplink phase jitter due to the regeneration step (Par. 5.3) which is not considered with that assumption. However, n the open-loop approach, the end-to-end jitter is determined by the sum of the reciprocal uplink and downlink signal power to noise density ratios

$$\frac{1}{P/N_0|_{DL}} + \frac{1}{P/N_0|_{UL}} \tag{6.1}$$

and a signal simulated considering a noise determined by a certain $P/N_0|_{SIM}$ can be also seen as a signal containing already the uplink jitter contribution

$$\frac{1}{P/N_0|_{SIM}} = \frac{1}{P/N_0|_{DL}} + \frac{1}{P/N_0|_{UL}} \tag{6.2}$$

Moreover, the uplink P/N_0 is generally larger, by far, than the downlink one, making it negligible in the ranging jitter computation.

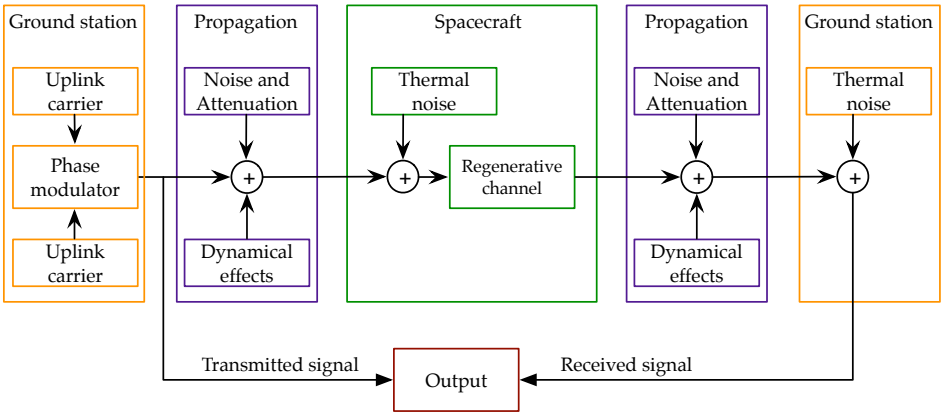

Figure 6.2: Simulator top-level diagram.

Φ is the phase of the signal

A_s is the amplitude of the signal, determined by its power P

$N(t)$ is the noise component

Two models have to be defined:

1. The model of the time variant phase of the two-way signal, modulated in phase by a ranging signal based on a pseudo-noise code
2. The model of noise contribution and signal power

Assume to transmit a constant[4] uplink frequency f_{UL}. The frequency of the signal received by the spacecraft can be modeled as

$$f_{SC_R} = f_{UL} D_u(t) \tag{6.4}$$

where $D_{UL}(t)$ is an unit less factor that accounts for the time-variant Doppler shifts caused by the relative motion between spacecraft (SC) and ground station (GS).

The downlink frequency f_{DL} is coherent with the received uplink frequency by means of a turnaround ratio factor G_t. The signal transmitted by the SC can be expressed therefore as

$$f_{SC_T} = f_{UL} D_u(t) G_t \tag{6.5}$$

The signal received by the station will have the downlink contribution of the orbital motion $D_{DL}(t)$

$$f_{GS} = f_{UL} D_u(t) G_t D_{DL}(t) \tag{6.6}$$

[4]In presence of extremely high Doppler rate , ramps are used to have an a priori compensation of the doppler effects, with the aim to make the acquisition easier or, sometimes, possible

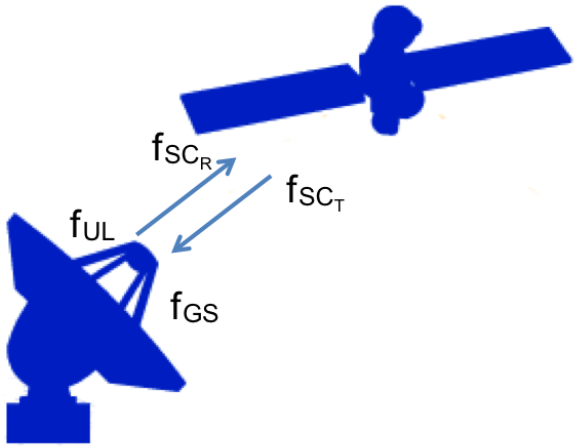

Figure 6.3: Frequencies on a two-way communications.

The ranging signal is also coherent with the carrier by means of a scaling factor β that is the ratio between the range code frequency (the clock component frequency) and the uplink frequency. Considering eq. 6.6, the frequency of the received ranging signal is

$$f_{GS_{RNG}} = f_{UL}\beta D_u(t) G_t D_{DL}(t) \tag{6.7}$$

The Doppler contribution D(t), in uplink and in downlink, can be modeled as

$$\begin{aligned} D_{UL}(t) &= 1 - \frac{1}{c}\dot{\rho}_{UL}(t) \\ D_{DL}(t) &= 1 - \frac{1}{c}\dot{\rho}_{DL}(t) \end{aligned} \tag{6.8}$$

where $\dot{\rho}_{UL}(t)$ and $\dot{\rho}_{DL}(t)$ are the first time derivative of the range between SC and GS and c the speed of an electromagnetic wave in the vacuum. Considering eq. 6.6 and eq. 6.8, the phase of the received carrier, being the time integral of the frequency, is expressed by

$$\begin{aligned} \Phi_{RX_C} &= 2\pi \int_0^t f_{UL} D_u(t) G_t D_{DL}(t)\, dt + \phi_{lo} + \phi_{\rho_0} = \\ &= 2\pi f_{UL} G_t \int_0^t \left(1 - \frac{1}{c}\dot{\rho}_{UL}(t)\right)\left(1 - \frac{1}{c}\dot{\rho}_{DL}(t)\right) dt + \phi_{lo} + \phi_{\rho_0} \end{aligned} \tag{6.9}$$

where

ϕ_{lo} represents a constant phase introduced by the local oscillators (L.O.))[5] and by the turn-around process.

[5]That phase term accounts for an unknown initial phase introduced by the oscillators (uplink and downlink) as well as the phase accumulated by the oscillators between their reset time and the recording starting time. This last term is however well known and can be therefore omitted.

ϕ_{ρ_0} is the phase delay at time $t = 0$

Approximating the integral term

$$\left(1 - \frac{1}{c}\dot{\rho}_{UL}(t)\right)\left(1 - \frac{1}{c}\dot{\rho}_{DL}(t)\right) \approx 1 - \frac{1}{c}\dot{\rho}_{UL}(t) - \frac{1}{c}\dot{\rho}_{DL}(t) \tag{6.10}$$

equation 6.9 becomes

$$\Phi_{RX_C} = 2\pi f_c t + \phi_{lo} - 2\pi\frac{f_c}{c}\rho(t) \tag{6.11}$$

where

$\rho(t)$ is the two way range, defined as the sum of the uplink and downlink range

$$\rho(t) = \rho_{UL}(t) + \rho_{DL}(t) \tag{6.12}$$

$f_c = 2\pi f_{UL} G_t$ is the nominal (without Doppler contribution) received carrier frequency

Similarly, and remembering eq. 6.7, the received ranging signal can be expressed (sinewave shape) as

$$PN_{RX} = A_{PN} \cdot \sin\left(2\pi f_{ck} \cdot (t - \tau) + \phi_{lo_{pn}}\right) = A_{PN} \cdot \sin\left(2\pi f_{UL}\beta \cdot (t - \tau) + \phi_{lo_{pn}}\right) \tag{6.13}$$

where f_{ck} is the clock frequency (half the chip rate), τ is the time delay due to the two way range($\tau = \frac{\rho(t)}{c}$), A_{PN} accounts for the sequence of ± 1 defined by the code and $\phi_{lo_{pn}}$ accounts for the unknown initial phase in the local oscillators generating the clock component.

The phase of the received total signal is the sum of the carrier and the modulating signal phase; thus it can be expressed as

$$\Phi_{RX} = \Phi_{RX_C} + m \cdot PN_{RX} = 2\pi f_c t + \phi_{lo} - 2\pi\frac{f_c}{c}\rho(t) + m \cdot PN_{RX} \tag{6.14}$$

where m is the modulation index. The signal before being acquired in open loop, and therefore sampled and quantized, goes through a down-conversion chain (defined by the total down-conversion frequency f_{DC}) that brings the carrier to an intermediate frequency $f_{IF} = f_c - f_{DC}$. The received, and recorded, signal phase is therefore

$$\Phi_{RX} = 2\pi f_{IF} t + \phi_{lo} - 2\pi\frac{f_c}{c}\rho(t) + m \cdot PN_{RX} \tag{6.15}$$

The transmitted signal phase, considering what already done for the received one and the absence of Doppler contribution, can be easily expressed as

$$\Phi_{TX} = 2\pi f_{IF} t + \phi_{lo} + m \cdot PN_{TX} \tag{6.16}$$

where the ranging signal is

$$PN_{TX} = A_{PN} \cdot \sin\left(2\pi f_{UL}\beta \cdot (t) + \phi_{lo_{pn}}\right) \tag{6.17}$$

Note that the the unknown phase term $\phi_{lo_{pn}}$ in the ranging signal is the same both for the transmitted and the received one, while the unknown initial phase ϕ_{lo} in the transmitted carrier is not the same in the received. That is due to carrier turn-around process which implies the use of a different downlink frequency, by means of a the turn-around ratio G_t. For this reason the carrier cannot be used for range measurement and phase delay is measured comparing the received and transmitted phase of the ranging signal. The range variation in time, that is the dynamic of the signal, is simulated by means of a series of independent third degree polynomials. The time span between each polynomials depends on the dynamic to approximate.

Once obtained the model of the phase (the term Φ in eq. 6.3), a noise and signal power models ($N(t)$ in eq. 6.3) have to be defined. The power of the signal received at the station depends from the geometric configuration and the SC hardware specifications while the noise is due to two different sources: the media and the electronic instruments. The first one is neglected[6] and the phasor accounting the thermal noise at the receiver is modeled as

$$N(t) = A_N \exp\left[i\Phi_N\right] \tag{6.18}$$

where

A_n is a random amplitude having Rayleigh distribution of parameter σ_N^2

Φ_N is a random phase having uniform distribution (values between 0 and π)

In case of a real signal, the noise can be modeled directly[7] as samples of a gaussian distribution with zero mean and variance σ_N^2. Assuming a signal unit power and given a certain signal to noise density ratio (P/N_0), the variance σ_N^2, necessary to simulate the complex or real noise signal, is determined by

$$\sigma_n = \sqrt{\frac{N_0}{P}B} \tag{6.19}$$

where B is the signal bandwidth.

6.1.2 SW architecture

The simulator software has been developed using Fortran as programming language, and the OpenMP libraries to parallelize the process. In particular the parallelization is a fundamental aspect of this development. The high frequency sampling rate necessary to simulate a ranging system based on a nominal chip rate of $24.2Mchip/s$ (ESA mission Bepi-Colombo baseline) means huge amount of data handling and high computational load. Parallelizing the process on multiple threads is therefore really important to make the software functional.

The simulator software consists in a core routine and several subroutine (fig. 6.4). In particular, the simulating process can be divided in 4 steps, each of those carried out by a dedicated subroutine:

[6] It should be taken in account in a error budget computation

[7] The signal can be also simulated as complex and then outputted only the real component.

1. Carrier phase generator
2. PN phase generator
3. Noise generator
4. Quantization

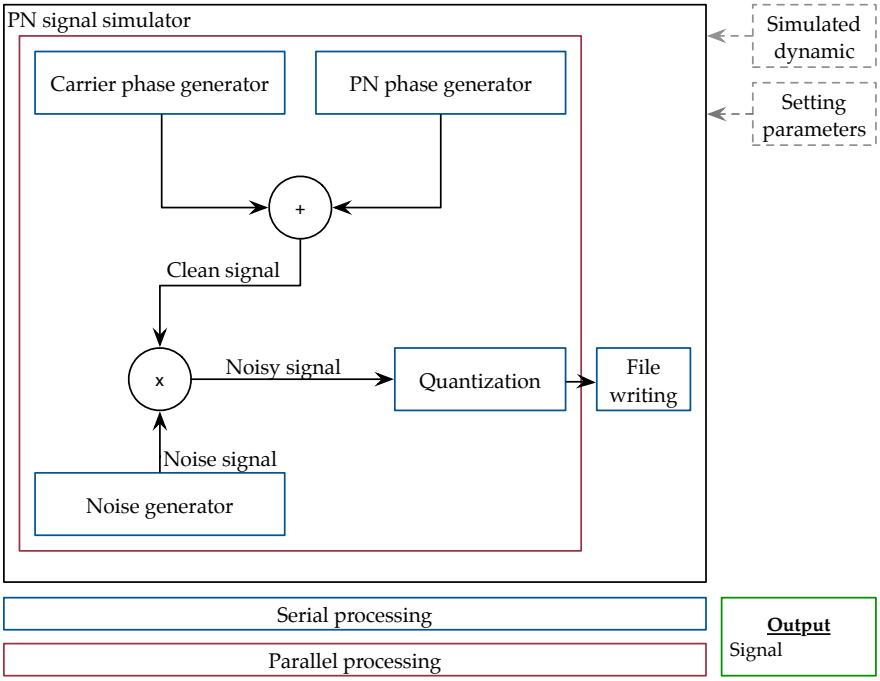

Figure 6.4: Simulator SW diagram.

The first two steps are dedicated to the carrier phase and PN code phase generation. These two are then used to simulate the clean signal (the first term in eq. 6.3). The noise signal $N(t)$ is then generated and summed to the clean one to obtain the noisy signal which is then quantized and written in a binary file. To optimize file dimension, the output samples are packed in a 32 bit word. In case of complex signal simulation, the quadrature-phase (Q) data and the in-phase (I) data for a given time sample are put in the word adjacent[8], going from the Least significant bit (LSB) to the most significative Bit (MSB). The number of samples in each word is determined by how many bits are used for sample. In fig 6.5 different possible configuration are reported. In case of a real signal simulation (only I component), the packaging principle is the same. The samples are put in the word going from the LSB to the MSB. The input parameters for the simulation are a file containing the dynamic to apply, in terms of range variation in time, and a configuration file containing setting parameters. Although the system development has began considering a certain

[8]In case of real signal simulation, only I component is provided

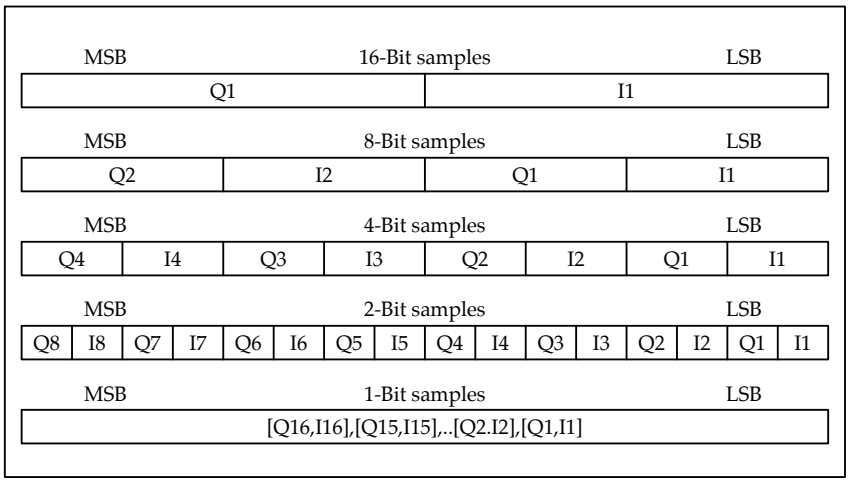

Figure 6.5: Data packaging for complex signal.

nominal baseline based on the ranging system of the ESA future mission BepiColombo, to make the simulator most flexible possible, the all parameters characterizing the system are almost completely settable by the user (tab. 6.1). The frequencies (sampling rate, intermedi-

Simulation setting	
Signal recorded	Real/Complex(I&Q)
Characterizing frequencies	-
PN code	T2B/T4B
PN shapewave	Sinewave/Squarewave
Quantization	Number of bits < 32
Modulation index	-
Noise (dbHz)	-

Table 6.1: Simulation parameters.

ate frequency, code chip rate, carrier frequency) characterizing the signal and the system are completely customizable as well as the the ranging code type (T2B and T4B), the ranging signal shapewave (sinewave or squarewave), the modulation index and the quantization level (number of bits). Moreover, the simulated signal, as already said, can be simulated as a complex or a real signal. Finally the thermal noise affecting the system is determined by the signal to noise density ratio, in terms of dBHz, set by the user.

6.2 Correlator

The correlator's task is to compute, given as input the raw data corresponding to the transmitted and received signal, the range delay. The raw data, simulated or acquired from an antenna, contains a carrier signal, brought to an intermediate frequency, modulated in phase by a ranging signal based on pseudo noise (PN) code. The range measurement is carried out comparing:

- The phase of the received signal with that of the transmitted one, to obtain a fine phase measurement.
- The code position of the received signal with that of the transmitted one, to remove the 2π ambiguity of the fine phase measurements.

The phase and code position of the received signal are unknown and has to be computed by means of a correlation process. On the other hand, the transmitted signal phase should be sometimes very well known, if not, a correlation of the is carried out in the same way as it is done for the received signal.

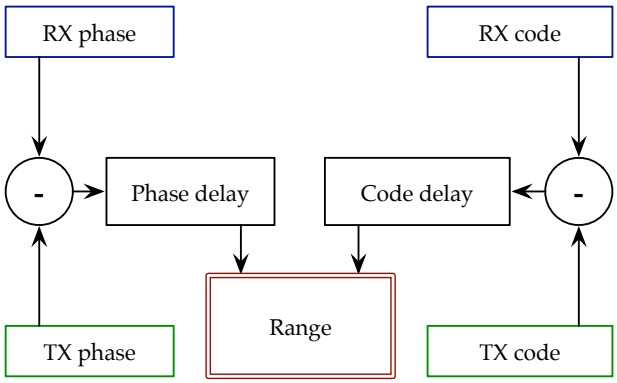

Figure 6.6: Open loop range measurement principle.

6.2.1 Mathematical model

We firstly introduce a general mathematical description of the principle and processing used for the ranging measurements[9] largely taken from Berner et al. (2007). Follows a detailed description of the implemented correlation algorithm.

Starting from a precise epoch, a signal, whose range clock phase is $\psi_{TX}(t)$, is sent from the station. That transmitted (TX) signal is received by the spacecraft and re-transmitted back to the station (2-way ranging). The signal received (RX) and recorded by the station has experienced a time delay $\tau(t)$ due to the finite velocity of propagation and the range

[9] Absolutely general and suitable for sequential ranging as well as for PN ranging system.

clock phase $\psi_{RX}(t)$ could be consequently expressed as

$$\psi_{RX}(t) = \psi_{TX}(t - \tau(t)) \tag{6.20}$$

Since the ranging signal is coherent in frequency to the uplink carrier, the frequency history of the carrier, achievable by means of a phase-locked-loop, is used to synthesize a local model of the received ranging signal whose phase is

$$\psi_M(t) = \psi_{TX}(t - \tau(t)) - \varphi \tag{6.21}$$

The phase of the model local has the same rate of change of $\psi_{RX}(t)$ and an unknown phase term φ. This unknown initial phase φ, and consequently the received signal phase at certain epoch t_{RX}, is measured correlating for a certain integration time the RX ranging signal with the local mode. The received phase at a certain epoch t_{RX} is therefore reconstructed

$$\psi_{RX}(t_{RX}) = \psi_M(t_{RX}) + \varphi = \psi_{TX}(t_{RX} - \tau(t_{RX})) \tag{6.22}$$

The phase of the transmitted signal (TX), if not known a priori, can be measured in the same way at t_{TX} that is not necessary equal to t_{RX}.

Differentiating the received and transmitted phase is finally possible to obtain the delay τ

$$\Delta\psi = \psi_{TX}(t_{TX}) - \psi_{RX}(t_{RX}) = \int_{t_{RX}-\tau(t_{RX})}^{t_{TX}} \frac{d\psi_{TX}}{dt} dt' \tag{6.23}$$

In this equation all the terms except τ, contained in the lower limit on the definite integral, are known.

If the transmitted frequency is not tuned (constant) the above equation is simplified[10] in

$$\begin{aligned} \Delta\psi &= 2\pi f_c k(t_{TX}) \cdot [t_{TX} - t_{RX}] + f_c k(t_{TX}) \cdot \tau(t_{RX}) \\ \tau(t_{RX}) &= \frac{\Delta\psi}{2\pi f_c k(t_{TX})} - [t_{TX} - t_{RX}] \end{aligned} \tag{6.24}$$

The phases provided by the correlation, having an intrinsic ambiguity, provide consequently an ambiguous time delay measurement. The code, reconstructed using a matched filter, is therefore correlated with the six components of the pseudo-noise code. The offsets of all components are used to compute the code position delay (number of chip) which is characterized by a much higher ambiguity resolution (total length of the PN code[11]).

The correlations of the received and, if necessary, the transmitted signals are carried out, in the software developed, independently. The algorithm used to provide phase (ψ_{TX} and/or ψ_{RX}) and code position consists in 4 steps (fig. 6.7):

1. **Carrier demodulation:** The coherent demodulation provides the baseband ranging signal. In case of RX signal, a PLL is necessary to reconstruct the unknown SC dy-

[10] The computation of τ is much more easier with respect to resolve the integral with the unknown τ at the lower integral limit.

[11] The code (T2B or T4B) time length is $\sim$ 40ms, considering a chip rate of 24Mchip/s.

namic contribution, while for the TX signal processing the frequency history is very well known and the demodulation is easier.

2. **Range clock reconstruction:** Knowing the carrier frequency history, an I and Q correlation of the clock component (heterodyne integration) permits to estimate the initial phase and reconstruct the model of the received/transmitted clock component phase.

3. **Code recovery:** A matched filter (Integrate&Dump) recovers the code (± 1).

4. **Code correlation:** The code is correlated against the six PN code components and their cyclic shifts.

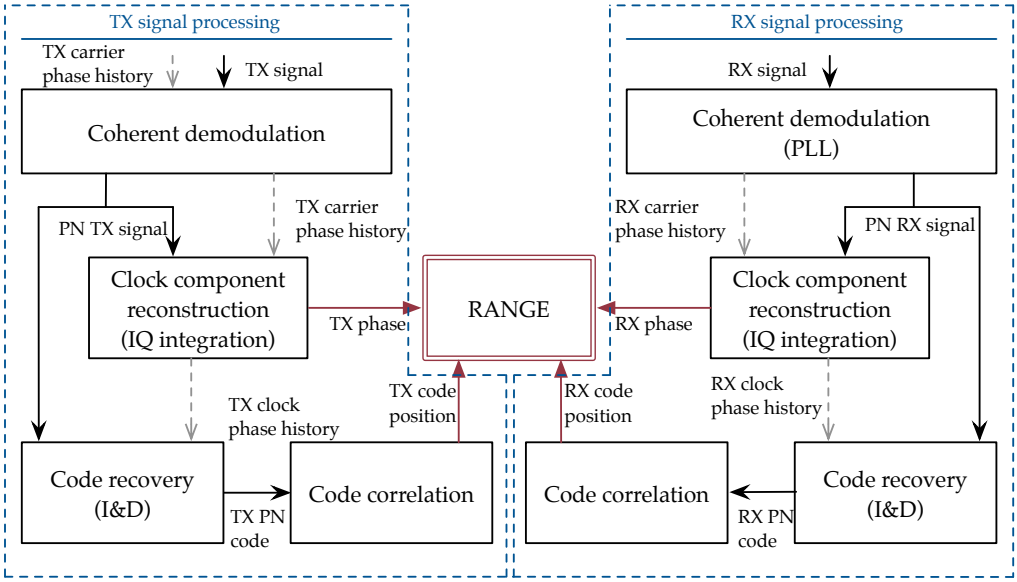

Figure 6.7: Open loop range measurement top level diagram.

The received signal (RX), recorded starting from a certain epoch t_{RX}, for simplicity assumed to be equal to 0, is[12]

$$\begin{aligned} s_{RX,IF}(t) &= A_{sig} \exp[i(2\pi f_{IF} t + \phi_{lo} + mPN(t - r(t)/c) - k \cdot \rho(t))] \\ &= A_{sig} \exp[i(2\pi f_{IF} t + \phi_{lo} + mPN(t + \tau(t)) + \psi_{C_{dyn}}(t))] \end{aligned} \tag{6.25}$$

where

$A_{sig} = \sqrt{2P}$ is the amplitude of the signal and P is the power.

f_{IF} is the intermediate frequency

[12]Neglecting the noise component and considering the acquisition of the two components I and Q (complex signal).

m is the ranging modulation index

ϕ_{lo} is the unknown initial phase due to local oscillators (L.O.)

$\psi_{C_{dyn}}(t) = -k \cdot \rho(t) = -(2\pi f_{carrier}/c) \cdot \rho(t)$ is the phase term accounting for the path delay experienced by the carrier

$\tau(t) = -\rho(t)/c$ is the path delay experienced by the PN signal

The transmitted signal (TX) is expressed by the same equation[13], removing the term due to the dynamic[14] (phase delay):

$$\begin{aligned} s_{TX,IF}(t) &= A_{sig} \exp[i(2\pi(f_{uplink} - f_{lo})t + \phi_{lo} + mPN(t))] \\ &= A_{sig} \exp[i(2\pi f_{IF} t + \phi_{lo} + mPN(t))] \end{aligned} \tag{6.26}$$

The processing of the transmitted signal follows, with some simplification, the processing of the received one. The four steps necessary to compute the received phase and code position are consequently explained in detail for the received signal, reporting only briefly the approach suitable for the transmitted one.

Carrier demodulation

The coherent demodulation of a signal needs a replica of the carrier. The frequency history of the TX signal is very well known while the RX signal has a phase term $\psi_{Cdyn}(t)$ due to dynamical motion (Doppler effect) that is not perfectly known a priori. A phase-locked-loop (PLL) is therefore necessary to reconstruct it in order to have a model of the received carrier. The carrier demodulation process consists in the following four steps:

1. Downconversion and decimation
2. Phase reconstruction by means of a digital PLL
3. Interpolation of the reconstructed phase
4. Beating/mixing of the signal with its replica (coherent demodulation)

The first processing step is necessary to make the recorded signal suitable to be reconstructed using a PLL. The signal is indeed characterized by

- High frequency components[15]
- Strong dynamic (orbital motion) which avoid the use of a narrow PLL bandwidth (common SNR requires maximum bandwidth on the order of tens of Hz)

[13] Once again, the recording time is assumed to be equal to 0 for simplicity.

[14] The range measurement cannot be performed with the carrier signal due to the turnaround ratio applied to the downlink frequency. That effect is here not explicitly modelled; therefore the initial terms ϕ_{lo} have to be considered different between received and transmitted signal.

[15] The residual carrier could be put to an IF frequency on the order of 70 MHz, or in a zero IF-frequency approach to a nominally frequency of 0Hz. In both cases, the ranging signal occupies a bandwidth of about two times the chip rate. For the nominal case of 24Mchip/s, a bandwidth of 50 MHz around the carrier is occupied by the ranging signal.

- High sampling rate[16] that makes the processing hard (high computational load)

A down-conversion permits to bring the residual carrier to a nearly zero frequency and then a decimation (filtering and down-sampling) provides a signal at low sampling rate.

The received and recorded signal is therefore mixed[17] with a not perfect replica of the received carrier whose phase can be expressed as

$$\tilde{\Phi}_{RX,IF}(t) = 2\pi f_{IF} t + \tilde{\psi}_{C_{dyn}}(t) = 2\pi f_{IF} t - k \cdot \tilde{\rho}(t) \tag{6.28}$$

where $\tilde{\rho}(t)$ is the a priori knowledge of the spacecraft dynamic (time variant range).

The signal is then low-pass filtered by means of a simple integrator, in order to remove, almost completely, the modulating ranging signal[18]. This filtering step avoids the aliasing that could be caused by the following down-sampling stage. After these two steps, down-conversion and decimation, the signal is characterized by

- Nearly zero frequency residual carrier and no other components
- Very weak residual dynamic
- Low sampling rate[19]

and its phase can be expressed as the sum of two terms

$$\Phi_{RX,DC,lpf} = \phi_{lo} + \psi_{C_{dynUnk}}(t) \tag{6.29}$$

The first constant term is the unknown phase of the carrier due to L.O. and the second time-variant term ($\psi_{C_{dynUnk}}(t)$) accounts for the uncertainty on the dynamic predictions, being exactly the mismatching between the a priori model and the real trajectory of the spacecraft

$$\psi_{C_{dynUnk}}(t) = \psi_{C_{dyn}}(t) - \tilde{\psi}_{C_{dyn}}(t) = k \cdot (\rho(t) - \tilde{\rho}(t)) \tag{6.30}$$

A digital PLL is then used to lock into the decimated signal,providing reconstructed phases[20]

$$\psi_{RX,pll}(t_i) \approx \phi_{lo} + \psi_{C_{dynUnk}}(t_i) \tag{6.31}$$

which are then interpolated with a simple third degree polynomial[21]

$$\psi_{RX,pll,pol}(t) = a + bt + ct^2 + dt^3 \approx \psi_{rx,pll}(t_i) \approx \psi_{C_{dynUnk}}(t) + \phi_{lo} \tag{6.32}$$

[16]The condition (Nyquist)

$$f_{samp} \geq 2 \cdot (f_{if} + f_{chiprate}) \tag{6.27}$$

set the sampling rate frequency which is at least (zero IF frequency) twice the code chip rate ($24.2MHz$).

[17]If the signal recorded is complex (I and Q), the mixing is a simple multiplications between phasors $exp[i\phi] \cdot exp[-i\phi_{dc}]$. Otherwise the mixing consists in an I and Q multiplication $cos[\phi] \cdot exp[i\phi_{dc}]$.

[18]If only the I component is recorded, the filtering removes also the high frequency component caused by the multiplication of the received signal with the model one.

[19]The sampling rate after the decimation is chosen according to the residual dynamic and the filter performance.

[20]The PLL bandwidth needs to be chosen considering the SNR level and the uncompensated dynamic of the signal.

[21]A series of polynomials can be used as well as other interpolating functions like splines.

The a priori knowledge of the spacecraft trajectory together with the above interpolating polynomial provides a replica of the received carrier phase

$$2\pi f_{IF} + \tilde{\psi}_{C_{dyn}}(t) + \psi_{rx,pll,pol}(t) \approx 2\pi f_{IF} t + \phi_{lo} + \psi_{C_{dyn}}(t) \tag{6.33}$$

The recorded signal, real or complex, is finally multiplied by a counter rotating phasor (coherent demodulation)

$$s_{RX,IF}(t) \cdot \exp[-i(2\pi f_{IF} t + \phi_{lo} + \psi_{C_{dyn}}(t))] \tag{6.34}$$

providing, in the quadrature component of the resulting complex signal, the baseband ranging (PN) signal

$$s_{RX,PN} = A_{pn} PN(t - \rho(t)/c) \tag{6.35}$$

In the case of the transmitted signal, the frequency history is very well known. Instead of a PLL, the unknown initial phase (due to local oscillators) can be reconstructed in two simple steps:

1. Mixing of the recorded signal with the transmitted signal model.
2. I and Q integration

Multiplying the recorded signal for a phasor obtained from the model of the transmitted frequency is possible to remove the frequency term and leave in the signal only the constant initial unknown phase. This phase is finally computed from the I and Q integration of the resulting complex signal

$$\begin{aligned} W_I &= \int_0^T \mathrm{Re}[A_{sig} \exp(\phi_{lo} + mPN(t))]\, dt = A_{sig} T \cos(\phi_{lo}) \\ W_Q &= \int_0^T \mathrm{Im}[A_{sig} \exp(\phi_{lo} + mPN(t))]\, dt = A_{sig} T \sin(\phi_{lo}) \\ \phi_{lo} &= \arctan\left(\frac{W_Q}{W_I}\right) \end{aligned} \tag{6.36}$$

The demodulation follows as for the received signal providing the transmitted baseband ranging signal

$$s_{TX,PN} = A_{pn} PN(t) \tag{6.37}$$

Range clock reconstruction

The phase of the received ranging clock component is

$$\begin{aligned} \phi_{RX_{ck}}(t) &= 2\pi f_{ck} t + \phi_{lo_{pn}} + \psi_{ck_{dyn}}(t) \\ &= 2\pi f_{ck} t + \phi_{lo_{pn}} + \psi_{ck_{dyn_0}} + \int_0^t \dot{\psi}_{ck_{dyn}}(\tau) d\tau \end{aligned} \tag{6.38}$$

where

f_{ck} is the clock component frequency (half the chip rate)

$\phi_{lo_{pn}}$ is an unknown constant initial phase accounting for L.O. oscillators effect

$\psi_{ck_{dyn}}(t) = -k \cdot \rho(t) = \psi_{ck_{dyn_0}} + \int_0^t \dot{\psi}_{ck_{dyn}}(\tau)d\tau$ is the phase term accounting the path delay experienced by the clock component

Since the carrier and the range clock component are coherent, an aided acquisition approach could be used. Once reconstructed with PLL[22], the carrier phase variation in time due to orbital motion can be scaled to have the corresponding phase variation on the ranging signal[23]

$$\int_0^t \dot{\psi}_{ck_{dyn}}(\tau)d\tau = \beta \cdot \int_0^t \dot{\psi}_{C_{dyn}}(\tau)d\tau = \beta \cdot [\psi_{C_{dyn}}(t) - \psi_{C_{dyn}}(0)] \tag{6.39}$$

where β is the scaling factor, equal to the ratio between the clock component frequency and carrier frequency $\beta = f_{ck}/f_{carrier}$. A local signal model that has the same rate of change of phase of the received one is therefore easily computed

$$\Phi_{RX_{PN}}(t) = 2\pi f_{ck} t + \int_0^t \dot{\psi}_{ck_{dyn}}(\tau)d\tau \tag{6.40}$$

This local signal model differs from the received one for the unknown phase at the recording starting time ($t_R = 0$), which is the sum of the unknown initial phase due to L.O. and the range phase delay

$$\psi_{ck_0} = \phi_{lo_{pn}} + \psi_{ck_{dyn_0}} \tag{6.41}$$

An I and Q correlation (beating and integration) between the received ranging signal samples and the local signal model, in a relative long interval of time, permits to compute

[22] Actually the PLL reconstruct the mismatching between prediction and real orbital effect. The sum of the PLL reconstructed phase and the prediction provides, as already explained in the carried demodulation paragraph, the model of the dynamic.

[23] Note that only the time variant term can be considered known, while the phase delay at the time epoch $t = 0$ is unknown.

the unknown initial phase

$$
\begin{aligned}
s_{rx,ck}(t) &= A_{pn} \sin\left(2\pi f_{ck}(t - t_R) + \phi_{lo_{pn}} + \phi_{ck_{dyn_0}} + \int_0^t \dot{\psi}_{ck_{dyn}}(\tau)d\tau\right) \\
W_I &= \int_0^T s_{RX,PN} \cdot \sin(\Phi_{RX_{PN}}(t))dt = \frac{A_{pn}}{2} T \cos(\phi_{lo_{pn}} + \psi_{ck_{dyn_0}}) \\
W_Q &= \int_0^T s_{RX,PN} \cdot \cos(\Phi_{RX_{PN}}(t))dt = \frac{A_{pn}}{2} T \sin(\phi_{lo_{pn}} + \psi_{ck_{dyn_0}}) \\
\phi_{ck_0} &= \phi_{lo_{pn}} + \psi_{ck_{dyn_0}} = \arctan\left(\frac{W_Q}{W_I}\right)
\end{aligned}
\tag{6.42}
$$

This phase term, which provides the fine measure of phase delay after the comparison with the transmitted phase, permits to compute an exhaustive model of the received ranging signal phase, necessary for the following steps. The transmitted signal is processed in the same way, permitting to obtain the transmitted phase of the clock component at time $t = 0$ and therefore the phase history of the transmitted ranging signal. Note that, given a certain accuracy in the phase estimation requested, the integration time needed for the transmitted signal is by far smaller than the integration time needed for the received signal.

Code recovery

With a matched filter, driven by the knowledge of phase history,

$$
\begin{aligned}
\Phi_{RX_{PN}}(t) &= 2\pi f_{ck} t + \int_0^t \dot{\psi}_{ck_{dyn}}(\tau)d\tau + \phi_{lo_{pn}} + \psi_{ck_{dyn_0}} \\
\Phi_{TX_{PN}}(t) &= 2\pi f_{ck} t + \phi_{lo_{pn}}
\end{aligned}
\tag{6.43}
$$

the code is extracted from the demodulated (RX and TX) ranging signal. The process is an integration (sum of the samples) of the signal over a certain time equal to the chip time (time variant for the received code).

Code correlation

The reconstructed code (sequence of ± 1) is correlated (chip by chip multiplication, followed by summation) with the six components of the code and all their cyclic shifts. The comparison of the results provides the code position. This step can be fully parallelized using 76 correlators.

6.2.2 SW architecture

The correlator has been developed using Fortran as programming language and using the OpenMP libraries to parallelize some routines. A detailed block diagram representing the correlation part, which is the core of the software, is shown in fig. 6.8. It consists in four

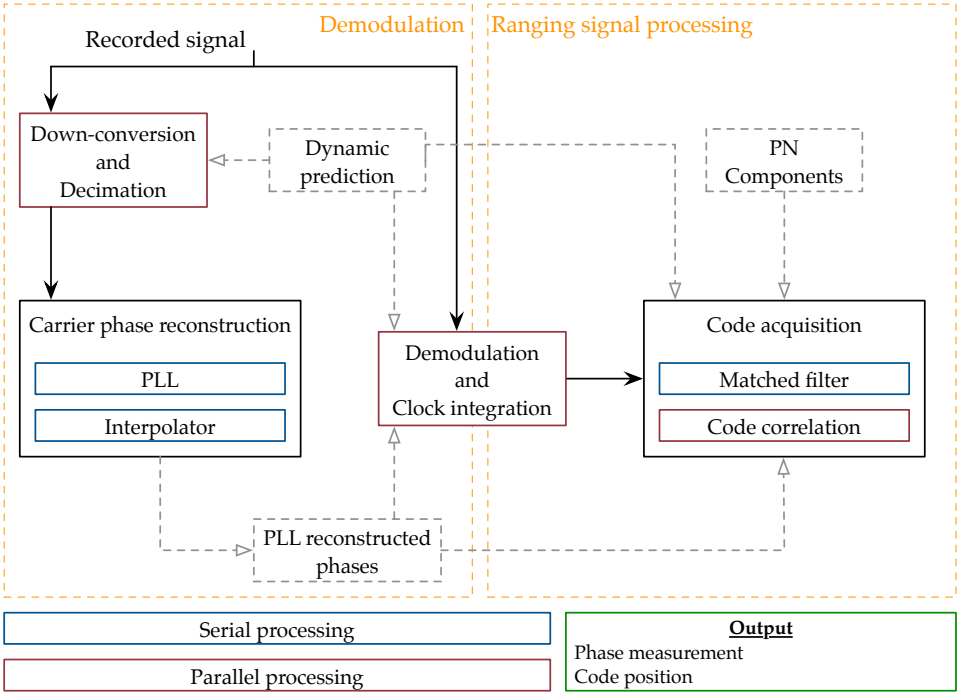

Figure 6.8: Correlator SW diagram. The 4 routines/blocks are designed as a serial (blue) or parallel (red) process.

main routines and several subroutines performing the following steps:

1. Down-conversion and Decimation
2. Carrier phase recovery
3. Demodulation and clock correlation
4. Code acquisition

At the end of the processing, a phase and a code position with a certain timetag are outputted. The range measurement is completed comparing, with a simple routine, phase and code position corresponding to transmitted and received signal (independent processing). All the processing is managed by a bash script.

The input files necessary are two:

- A setting file

- A dynamic prediction file

A certain number of parameters (tab. 6.2), settable by the user, are necessary for the correlation. Many of them are general parameters relative to the features of the signal (real

Correlation setting
Signal recorded (Real/Complex)
Sampling frequency
Carrier frequency
Down conversion frequency
Chip rate
Quantization level (number of bits)
Integration time
LPF bandwidth
PLL bandwidth

Table 6.2: Correlation parameters.

or complex, frequencies, quantization level, number of seconds) while two parameters refer to the carrier recovery step, low pass filter (LPF) and PLL bandwidth. These last two are not standardized since they depend from the a priori knowledge of the spacecraft trajectory and therefore the residual dynamic into the signal to be recovered. The file containing the dynamic prediction consists in a series of third degree polynomials.

Chapter 7

Pseudo noise open loop receiver: Tests and results

To characterize the behavior of the developed open loop receiver, based on a software correlator, several tests have been performed. Three aspects have been investigated with three different tests campaigns:

The correctness of the processing algorithm and its implementation

The performance of the correlator in terms of measurement precision

The performance of the correlator in terms of computational time

The first tests, regarding the correctness of the correlator/receiver, consisted in simulating (Montecarlo) signals without noise and different conditions of quantization and residual dynamic. The error aspected, due to numerical and quantization noise, have to be pretty small to assess the reliability of the process (no systematic errors). The second tests campaign regarded the precision of the measurements in presence of thermal noise (random noise). The signal has been therefore simulated (Montecarlo) with different conditions of noise (SNR) and dynamic in order to evaluate if the measurements error is compatible with that predicted by theory. The last tests regarded the computational optimization, which is obviously a crucial aspect to take in account to characterize the system. In fact, the high frequency of the signal used in this kind of ranging system (PN) results in high computational loads. The processing time is therefore an aspect important to be investigated in order to asses if the open-loop receiver is suitable for operational use.

7.1 No noise

The first campaign tests has been carried out to asses the correctness of the processing algorithm and its implementation. The signal has been therefore simulated without noise to investigate the possible presence of systematic errors introduced by the processing. Three Montecarlo simulations have been carried out:

1. Signal noise free and quantized at 4 bit
2. Signal noise free and quantized at 8 bit
3. Signal noise free and quantized at 16 bit

Different level of quantization have been used also to investigate the sensitivity of the correlation process to that parameter.

Test setup

The setup used for the simulation and correlation is reported in tab. 7.1.

(a) Simulator Setup

PN Code type	BT4
Modulation Index	0.7
Carrier Frequency	32.5 GHz
Signal Type	Complex
Sampling rate	100 MHz
PN shapewave	Sinewave
PN Chip rate	24.2 MHz

(b) Correlator Setup

Integration time	10s
LPF bandwidth	50kHz
PLL Bandwidth	50Hz

Table 7.1: No noise TEST: General parameters setup.

Into the signal has been introduced a residual dynamic, to be tracked by PLL, consisting in a Doppler shift and Doppler rate. Its coefficients, generated randomly, have values up to, respectively $100Hz$ and $0.1Hz/s$ (tab.7.2).

Doppler shift (Hz)	$0 \leq \Delta f \leq 100$
Doppler rate (Hz/s)	$0 \leq \Delta \dot{f} \leq 1$

Table 7.2: No noise TEST: Residual dynamic setup.

Moreover, one hundred points for Montecarlo have been realized to extract a statistic sufficiently reliable.

Test results

In the following table (tab 7.3) and in fig. 7.1 the results obtained are reported. The highest measurement error (standard deviation), with 4 bit quantization, results in a time error of about thirty times under the picosecond. Being well below the achievable accuracy under realistic thermal noise level[1] it is absolutely negligible. Furthermore, also the mean of the phase errors is very small, assessing the substantial absence of systematic errors and the processing correctness[2].

[1] With $30dBHz$ of Clock power over Noise power spectral density and an integration time of $30s$, the theoretical error on phase delay measurements is on the order of mrad, three orders of magnitude higher. See next section.

[2] Actually a little bias for the case of 16bit quantization is present. However, it is absolutely negligible.

	Phase error (rad)	
	Mean	Standard deviation
4 bit	1.94E-07	2.23E-06
8 bit	1.89E-07	2.50E-07
16 bit	2.13E-07	4.30E-08

Table 7.3: No noise TEST: Montecarlo results. Computed phase error mean and standard deviation. Signal without noise and different level of quantizations.

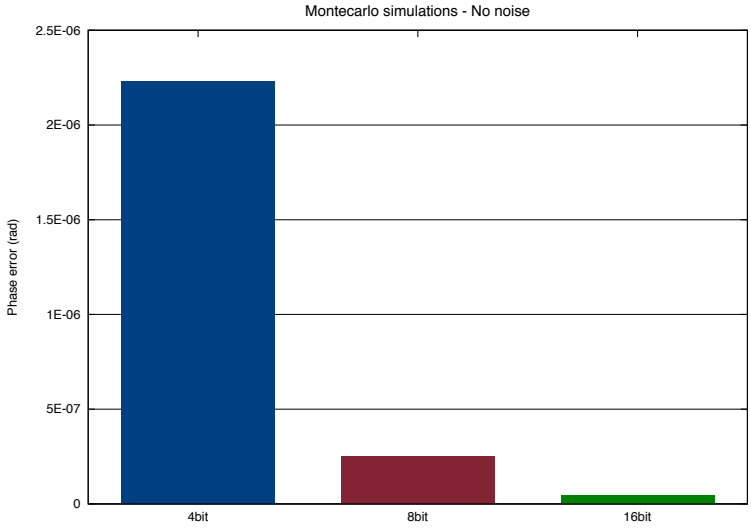

Figure 7.1: No noise TEST: Montecarlo simulations results. Phase error standard deviation. Signal without noise and quantized at 4bits (blue), 8bits (red) and 16bits (green).

7.2 Thermal noise

The presence of thermal noise affects directly the measurements accuracy achievable. Consequently, as already explained in the previous chapters, the measurement is carried out integrating the signal for a certain time in order to reduce the thermal noise effect. The theoretical phase error is[3], in terms of standard deviation

$$\sigma_{phase_{OL}} = \sqrt{\frac{1}{2\left|P_{RC}/N_0\right|_{DL}} \cdot \frac{1}{T}} \tag{7.1}$$

where $\left|P_{RC}/N_0\right|_{DL}$ is the range clock power over noise density ratio in the downlink and T is the integration time.

[3]Here it is only considered the case of Sine-wave matched case.

To test the software in terms of measurements precision several Montecarlo simulations have been carried out with different level of thermal noise.

Test setup

The general setup chosen for the signal simulation and correlation is reported in the tab. 7.4.

(a) Simulator Setup

PN Code type	BT4
Modulation Index	0.7 rad-pk
Carrier Frequency	32.5 GHz
Signal Type	Complex
Sampling rate	100 MHz
Quantization	8 bits
PN shapewave	Sinewave
PN Chip rate	24,2 MHz

(b) Correlator Setup

Integration time	10s
LPF bandwidth	50kHz
PLL Bandwidth	50Hz

Table 7.4: TH. NOISE TEST: General parameters setup.

The simulated dynamics have been chosen to be a single polynomial for the entire simulation/correlation time. Three cases have been considered for the residual dynamic to be recovered by the PLL:

1. Case A. Only a residual Doppler shift
2. Case B. A Doppler shift plus a weak Doppler rate
3. Case C. A Doppler shift plus a strong Doppler rate

The values of the polynomial coefficients have been generated randomly in a certain range of values (tab. 7.5). The residual Doppler shift has been chosen to be no more than $100Hz$

	Case A	Case B	Case C
Doppler shift (Hz)	$0 \leq \Delta f \leq 100$	$0 \leq \Delta f \leq 100$	$0 \leq \Delta f \leq 100$
Doppler rate (Hz/s)	0	$0 \leq \Delta \dot{f} \leq 0.1$	$0 \leq \Delta \dot{f} \leq 1$

Table 7.5: TH. NOISE TEST: Residual dynamic setup.

which corresponds in a Ka-band an error on the probe velocity prediction of about $1m/s$. For the probe acceleration has been considered, on the other hand, a prediction error of $1mm/s^2$ for case B and $1cm/s^2$ for case C, corresponding respectively to $0.1Hz/s$ and $1Hz/s$.

To investigate the performance at very different levels of noise, several Montecarlo have been carried out with different power over noise density ratio. In particular the signal over noise density ratio (S/N_0) has been varied in a range between $33dBHz$ and $48dBHz$, to

have, with the considered link configuration (modulation indices), an available range clock power over noise density ratio into an interval of about $26dBHz$ and $41dBHz$.

S/N_0 (dBHz)	P_R/N_0 (dBHz)
48.59	41.4
45.59	38.4
38.59	31.4
35.59	28.4
33.16	26.0

Table 7.6: TH. NOISE TEST: Noise setup.

One hundred points for each Montecarlo (noise and dynamic combination) have been realized to extract a sufficiently reliable statistic.

Test results

In the following three tables the results obtained with Montecarlo simulations in the three different dynamic cases are reported.

S/N_0 (dBHz)	P_R/N_0 (dBHz)	Phase error (rad)		
		Mean	Theoretical sigma	Computed sigma
33.16	26.0	-1.72E-03	1.12E-02	1.04E-02
35.59	28,4	4.41E-05	8.46E-03	7.40E-03
38.59	31.4	5.27E-04	5.99E-03	5.50E-03
45.59	38.4	-6.04E-05	2.67E-03	2.39E-03
48.59	41.4	-3.36E-04	1.89E-03	1.94E-03

Table 7.7: TH. NOISE TEST: Montecarlo results. Dynamic case A.

S/N_0 (dBHz)	P_R/N_0 (dBHz)	Phase error (rad)		
		Mean	Theoretical sigma	Computed sigma
33.16	26.0	3.28E-04	1.12E-02	1.20E-02
35.59	28.4	1.67E-04	8.46E-03	7.90E-03
38.59	31.4	-3.76E-04	5.99E-03	6.23E-03
45.59	38.4	2.44E-04	2.67E-03	2.75E-03
48.59	41.4	8.90E-05	1.89E-03	1.96E-03

Table 7.8: TH. NOISE TEST: Montecarlo results. Dynamic case B.

S/N_0 (dBHz)	P_R/N_0 (dBHz)	Phase error (rad)		
		Mean	Theoretical sigma	Computed sigma
33,16	26.0	9.50E-04	1.12E-02	1.10E-02
35.59	28.4	-4.69E-04	8.46E-03	9.31E-03
38.59	31.4	7.14E-04	5.99E-03	5.84E-03
45.59	38.4	-1.37E-04	2.67E-03	2.95E-03
48.59	41.4	-2.18E-04	-2.18E-04	1.90E-03

Table 7.9: TH. NOISE TEST: Montecarlo results. Dynamic case C.

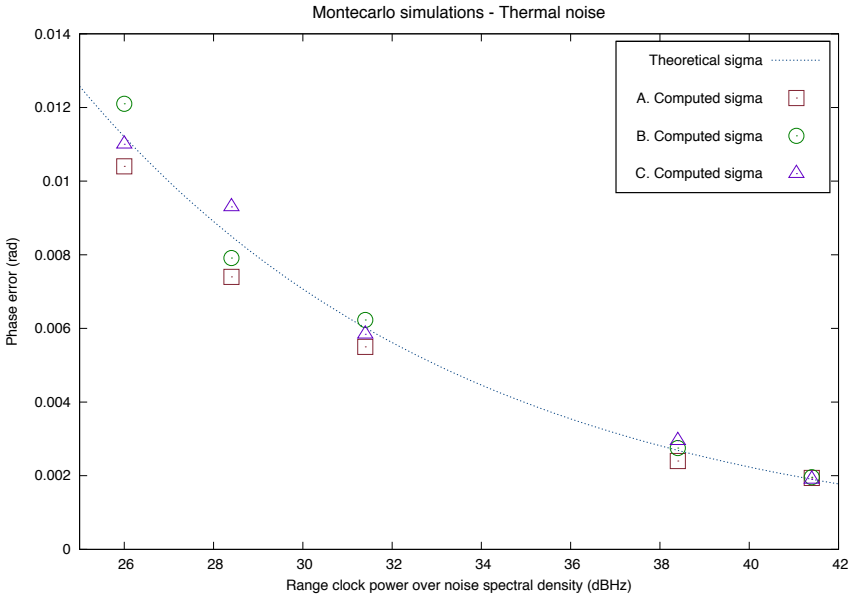

Figure 7.2: THERMAL NOISE TEST: Montecarlo results. Phase error standard deviation for different levels of thermal noise (Range clock power over Noise power density), and for different dynamic cases. The blue curve represents the theoretical behavior, while red squares are the computed phase standard deviation for dynamic A, green circles for dynamic B and purple triangles for dynamic C

On fig. 7.2 the computed error standard deviation, for the three dynamic cases, are reported together with the theoretical curve representing the relation beetwen the range measurement precision and level of noise. The figure clearly shows a full compatibility between theoretical values and computed ones. Furthermore, the mean values of the phase errors are always smaller than the corresponding standard deviations. These tests provide another assessment of the reliability of the system. No systematic or random errors are indeed introduced in the processing carried out by the software developed.

An additional test has been carried out looking to the relation between phase error and integration time. A Montecarlo with signals having a fixed level of noise ($35dBHz$) has been therefore performed and the phase has been estimated, incrementally, each second of the total 30s of integration time. Figure 7.3 shows the curve (red) made by the standard deviations of the estimated phases, second by second. Comparing it with the theoretical curve a full compatibility is found.

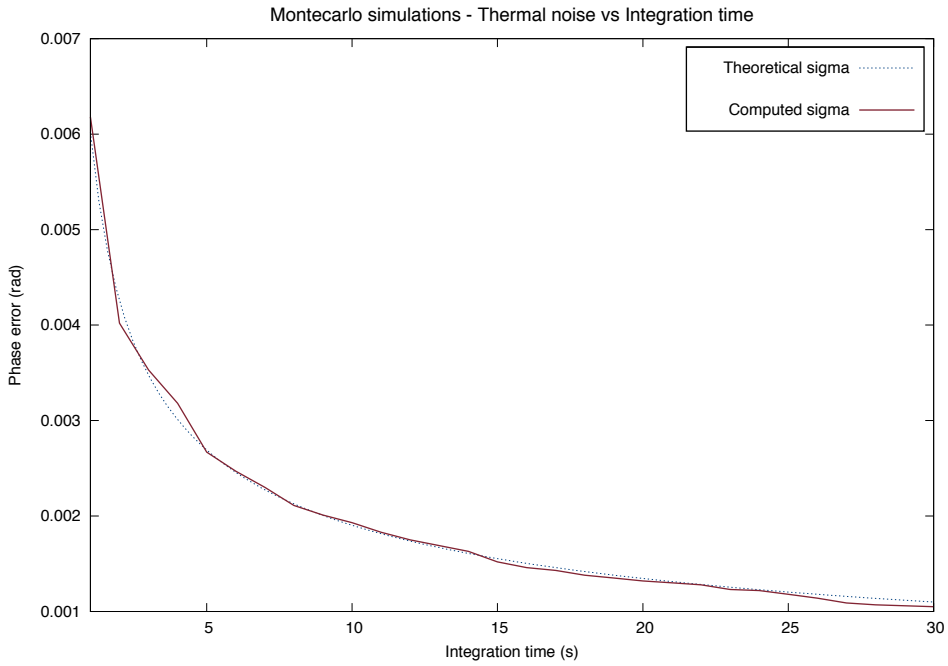

Figure 7.3: TH. NOISE TEST: Montecarlo results. Phase error standard deviation vs the integration time. In blue the theoretical curve while in red the computed values.

7.3 Computational optimization

Due to high sampling frequency required to perform range measurements with a PN code at high chip rate ($\approx 24MHz$), the computational load is very large. For this reason the software has been firstly analyzed to optimize the processing in terms of computational efficiency, and then has been deeply parallelized in order to drastically decrease the time necessary to carry out a measurement. Some tests have been, in the end, performed to investigate the time needed for every step of the correlation processing, to analyze quantitatively the benefits of the parallelization, and to assess the validity for operational use of the correlator developed.

Test setup

The setup used follows almost completely what already done in the other tests. The computational time obviously is not affected by the level of noise, type of code and dynamic. The crucial parameters have been chosen to simulate a realistic use of the software. The sampling frequency has been set to $100MHz$ (complex) and the quantization to 8 bit. Moreover, the test has been made simulating and correlating 5 seconds of data and extracting as result the needed computational time for correlating 1s of data (dividing by five). Obviously that is an approximation as some part of the processing are obviously not extensive and therefore they cannot be scaled, however they are the less computational expansive parts of the entire processing.

(a) Simulator Setup

PN Code type	BT4
Modulation Index	0.7 rad-pk
Carrier Frequency	32.5 GHz
Signal Type	Complex
Sampling rate	100 MHz
Quantization	8 bits
PN shapewave	Sinewave
PN Chip rate	24.2 MHz

(b) Correlator Setup

Integration time	5s
LPF bandwidth	50kHz
PLL Bandwidth	50Hz

Table 7.10: TIME TEST: General parameters setup.

The test has been made four times, using different level of parallelization: 1 thread (No parallelization), 2 threads, 4 threads and 8 threads.

Test results

The correlation process can be divided in four main steps:

1. Down-conversion and decimation
2. Demodulation and clock integration

3. Code integration

4. Code correlation

In table 7.11 and in figure 7.4 the time necessary to carry out each steps, and the overall process, using 1s of data is reported for different levels of parallelization. While the requested time in the first, in the second and in the fourth step decreases as the threads are increased; the third step, which is the code integration, is not currently parallelized and therefore it represents the lower bound of the needed correlation time. In a limit case where the number of threads are increased drastically, the necessary time for correlating 1s of data would equal the code integration time, that is 5 seconds.

In the following table are reported the results obtained:

	Processing time (s)			
	1 Thread	2 Threads	4 Threads	8 Threads
Down-conversion and decimation	14	7,5	4	2,5
Demodulation and Clock correlation	24	14	9	5
Code Integration	5	5	5	5
Component correlation	12	6	3	2
Total correlation process	55	32,5	21	14,5

Table 7.11: TIME TEST: results. Correlation processing time for 1 s of data and using different levels of parallelization.

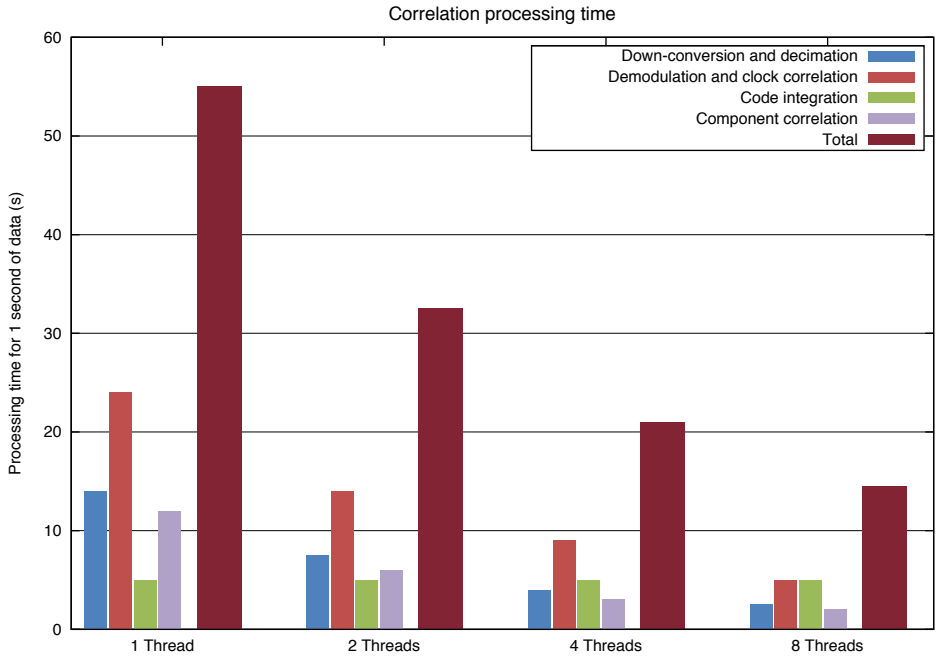

Figure 7.4: TIME TEST: Results. Correlation processing time for 1 s of data and using different levels of parallelization.

Chapter 8

Conclusions

Object of this work was the improvement of two different tracking systems used for navigation of deep space probes: ΔDOR and pseudo noise ranging.

The ESA ΔDOR correlator has been improved with the development of two new functionalities: wideband and Low-SNR. Concerning the first one (par.3.1), the spanned bandwidth strongly affects the achievable ΔDOR observables accuracy. Its increase is therefore a simple and effective way to improve the observables quality. However, the current hardware used at ESA ground stations limits the total bandwidth that can be acquired. To overcome that issue, it is possible to use different L-band down-converters and receivers in order to acquire different portions of spectrum. Since this approach, is however not compatible with the old and standard processing algorithm of the correlator, a new method has been developed, implemented and then tested.

The first tests have been carried out to investigate the correctness and the functionality of the new correlation algorithm. The first, preliminary, successful test consisted in a quasar-only acquisition while the second test consisted in a real ΔDOR acquisition, aiming to compare the new wideband method with the old one. ESA Venus Express (VEX) acquisition has been therefore carried out using different hardware configurations in order to simulate standard or wideband conditions. The correlation of the same data, by means of the two different methods, has provided results having a perfect agreement, within the one sigma level. The last test, on the other hand, consisted on a ΔDOR acquisition of the NASA deep space probe Juno, whose transponder is capable to use dedicated tones instead of telemetry harmonics. The acquisition, carried out on a wideband configuration, provides a spanned bandwidth of $38.2MHz$, more than four times the VEX standard one. Moreover, the use of dedicated tones results in a higher, about $20dB$, signal-to-noise (SNR) ratio of the external channels. The ΔDOR results show accuracy never reached before by ESA. The effect of thermal noise is indeed drastically reduced and the measurements error (one-sigma) is of about 40 picoseconds.

The second functionality (par.3.2) regards the possibility to carry out ΔDOR measurements with signal having very-low SNR. The current correlation algorithm, for what regards the spacecraft signal, is based on a digital phase-locked-loop (PLL) that limits the

possibility to acquire weak signal. A new algorithm has been therefore designed and implemented. This new correlation method, PLL-free, consists in an open loop integration driven by Flight Dynamics (FD) group predictions. The frequency estimate is obtained by means of FFT and peak search on the main channel, while the reconstruction of the other channels is carried out integrating blindly the signal and filtering it in the frequency domain. This method, suitable for each kind of signal, is strongly limited by the FD predictions accuracy, which determines the minimum filtering bandwidth achievable and affects the frequency and phase estimate accuracy. Several tests, aimed to assess the validity of the algorithm, have been performed. The new algorithm has been compared with the old one using real data with added noise and Montecarlo with simulated data at high SNR. Its performance has been tested also using Montecarlo simulations of data at very low-SNR. All tests have shown a full compatibility between the two algorithms and the errors obtained with simulations are in agreement with the theoretical ones. Furthermore, this new method resulted to be less time consuming.

The open loop correlator for pseudo noise (PN) ranging system, together with a simulator of the radio link, has been developed to have a an end-to-end simulator of the system, and the possibility to have a flexible and economic receiver to carry out ranging measurements with data collectable without great efforts or complex and expansive instrumentations. The tests have been carried out simulating the ranging system implemented in the ESA BepiColombo mission (24Mchip/s) and have been aimed to analyze the ranging correlator under different aspects. The first tests consisted in a simulation of noiseless signals under different conditions. The mean and the standard deviation of the phase estimate errors obtained are very small, providing time errors, due to numerical noise and quantization, under the picoseconds level, and therefore absolutely negligible. This assesses the correctness of the processing algorithm and its implementation. A series of Montecarlo simulations have been then carried out considering different conditions of noise (SNR) in order to investigate the performance of the system in terms of measurements precision. The measurements errors (standard deviation) obtained show a full agreement with the theoretical ones. Furthermore, the estimated phases are not biased from the real values. These results indicate the absence of random or systematic errors introduced by the correlation process, assessing the reliability of the developed system itself. The last investigated aspect regards the performance of the correlator in terms of computational optimization. Since the PN ranging systems are characterized by high frequencies, a software receiver has indeed to be investigated in terms of processing time. The correlator, developed using a parallel approach, has been therefore tested simulating realistic case and the results show that the parallelization provides good performance. Using 8 parallel threads, the correlation process needs 14 seconds for each second of data (200 millions samples). Augmenting the number of threads results in a hypothetical lower bound of 5 seconds. Although very far from real time processing, the developed open loop correlator results suitable to be used for operational purposes. Future enhancements of this open loop receiver are needed for computational optimization and processing time, considering the use of graphic processing units (GPU) or going towards the hardware implementation (FPGA development).

Appendix A

ESA mission: BepiColombo

The development of a PN ranging correlator (open loop) has began as part of the support activity to the ESA future deep space mission BepiColombo, in particular the Mercury Orbiter Radio-science Experiment (MORE). Consequently, the PN ranging system has been presented referring especially to this mission, as well as the software tests have been carried out using the baseline which will be used for it. This appendix has been written to give some details of the BepiColombo mission and its radio science experiment.

Bepicolombo is a dual spacecraft mission to Mercury carried out jointly between ESA and JAXA (Japanese Aerospace Exploration Agency). It is an interdisciplinary mission aiming to investigate the evolution and the environment of the planet nearest the Sun. The lunch, planned initially for the 2014 is actually delayed to 2015. The first spacecraft, the Mercury Planetary Orbiter (MPO), is led by ESA and is equipped with scientific instruments to study the Mercury interior, surface, exosphere and magnetosphere. Moreover, it will test Einstein's theory of general relativity. The second spacecraft, the Mercury Magnetosphere Orbiter (MMO), is led by JAXA and it will investigate the environment around the planet. The cruise phase of 6 years, characterized by the use of solar electric propulsion, will be followed by the orbit insertion, achieved using chemical propulsion, of the two spacecrafts in two different elliptic orbits (MPO orbit: $400x1508km$, MMO orbit: $400x11824km$). The scientific phase of the mission (orbiting without any maintanance) is nominally planned to be of 1 Earth year (an optional additional year doesn't need design margins).

The scientific objectives of the BepiColombo mission are (Benkhoff et al., 2010):

- Origin and evolution of a planet close to the parent star
- Mercury's figure, interior structure and composition
- Interior dynamics and origin of its magnetic field
- Exogenic and endogenic surface modifications, cratering, tectonics, volcanism
- Composition, origin and dynamics of Mercury's exosphere and polar deposits
- Structure and dynamics of Mercury's magnetosphere

- Test of Einstein's theory of general relativity

To contribute and give answers to the main scientific topics listed above, the MMO and MPO have been equipped with a great number of instruments or instruments suites (tab. A.1).

MPO instruments	
BELA	BepiColombo Laser Altimeter
ISA	Italian Spring Accelerometer
MGA	Magnetometer
MERTIS	The Mercury Radiometer and Thermal Infrared Spectrometer
MGNS	Mercury Gamma-Ray and Neutron Spectrometer
MIXS	The Mercury Imaging X-ray Spectrometer
MORE	Mercury Orbiter Radio-sicence Experiment
PHEBUS	Probing of Herman Exosphere by Ultraviolet Spectroscopy
SERENA	Search for Exospheric Refilling and Emitted Natural Abundances
SIMBIO-SYS	The Spectrometer and Imagers for MPO BepiColombo Integrated Observatory System
SIXS	Solar Intensity X-ray and particle Spectrometer
MMO instruments	
MDM	Mercury Dust Monitor
MAG	Magnetometer
MPPE	Mercury Plasma/Particle Experiment
MSASI	The Mercury Sodium Atmospheric Spectral Imager
PWI	Plasma Wave Investigation

Table A.1: BepiColombo scientific instruments.

The radio-science experiment, MORE, addresses scientific goals in geodesy, geophysics and fundamental physics. It aims to (Genova et al., 2012)

- determine the gravity field of Mercury (coefficients of spherical harmonics expansion up to degree and order 25) and the love number k_2
- estimate the rotational state of Mercury
- determine the post-Newtonian parameters, the mass and the oblateness of the Sun and the upper limits to the temporal variation of the gravitational constant G.

To achieve these scientific results, BepiColombo mission will be supported by the most advanced interplanetary tracking system ever built. The MPO will be equipped with a Ka/Ka Transponder (KaT) and a Deep Space Transponder, provided both by the Italian Space Agency, to enable a multi-frequency[1] radio link at X ($7.2GHz$ uplink/$8.4GHz$ downlink) and Ka band ($34/32.5GHz$). The others fundamentals components in the tracking system are the on-board high antenna of $1.2m$ of diameter and the highly stable Hydrogen

[1]Configuration already exploited by the Cassini mission (Bertotti et al., 1993; Tortora et al., 2004).

masers at the ground stations. Furthermore the range measurements will be provided using, for the first time, a ranging system based on pseudo noise code with $24Mchip/s$. The measurements accuracies achievable using this advanced tracking system are $0.003mm/s$ (at $1000s$ integration time) for range rate and $20cm$ (two-way) for range (Iess and Boscagli, 2001). Not only these radio tracking observables are necessary for the experiment. ISA (accelerometer) information will be also used to remove the non-gravitational accelerations effects, improving the orbit determination. Furthermore, optical images from the high resolution camera ($5m$ pixel size at pericenter), together with the accurate MPO orbit reconstruction ($0.1 - 1m$ in the radial position) and precise attitude reconstruction ($1 - 2arcsec$), will permit to carry out the rotational experiment, aiming to determine the rotational state of the planet (Genova et al., 2012).

Appendix B

Phase estimate through I and Q integration

This appendix reports an analysis of the structure and performance of an open loop phase estimator. What follows refers to Boscagli et al. (2008).

Consider a received baseband signal of angular frequency ω

$$s_{input}(t) = \begin{cases} A\sin(\omega t + \theta), & \text{sinewave shaped} \\ A\mathbf{sgn}\left(\sin\left(\omega t + \theta\right)\right), & \text{squarewave shaped} \end{cases} \tag{B.1}$$

The unknown phase θ can be estimated with an I and Q integration:

1. Mixing the input signal with two orthogonal reference signals characterized by the same angular frequency ω
2. Evaluating the integral of the resulting signals: in-phase and quadrature components
3. Comparing the two averaged in-phase and quadrature components

Since the reference signals can be

$$\begin{aligned} s_{ref_I}(t) &= \begin{cases} \sqrt{2}\sin(\omega t), & \text{sinewave shaped} \\ \mathbf{sgn}\left(\sin\left(\omega t\right)\right), & \text{squarewave shaped} \end{cases} \\ s_{ref_Q}(t) &= \begin{cases} \sqrt{2}\cos(\omega t), & \text{sinewave shaped} \\ \mathbf{sgn}\left(\cos\left(\omega t\right)\right), & \text{squarewave shaped} \end{cases} \end{aligned} \tag{B.2}$$

three cases are possible:

- Sine-Sine Matched case
- Square-Square Matched case
- Sine-Square Mismatched case

We consider firstly the case of a noiseless signal and a sine-sine matched case. The in-phase and quadrature components of the resulting signal coming from the beating of the input one with the reference signals are

$$\begin{aligned} I_{sin-sin} &= A\sin(\omega t+\theta)\sqrt{2}\sin(\omega t) = \frac{A\sqrt{2}}{2}\left[\cos(\theta)-\cos(2\omega t+\theta)\right] \\ Q_{sin-sin} &= A\sin(\omega t+\theta)\sqrt{2}\cos(\omega t) = \frac{A\sqrt{2}}{2}\left[\sin(\theta)+\sin(2\omega t+\theta)\right] \end{aligned} \tag{B.3}$$

After the mixing, these components are averaged (integrated) for a certain time T providing

$$\begin{aligned} \bar{I}_{sin-sin} &= \frac{A\sqrt{2}}{2}T\cos(\theta) \\ \bar{Q}_{sin-sin} &= \frac{A\sqrt{2}}{2}T\sin(\theta) \end{aligned} \tag{B.4}$$

The unknown phase is finally easily estimated comparing these two values

$$\theta = \arctan\left(\frac{\bar{Q}}{\bar{I}}\right) \tag{B.5}$$

Considering now the noise, the input at the phase detector are

$$\begin{aligned} \bar{I}_{noise} &= \bar{I}+N_i \\ \bar{Q}_{noise} &= \bar{Q}+N_Q \end{aligned} \tag{B.6}$$

with N_I and N_Q statistically independent Gaussian variables with zero mean and variance

$$\begin{aligned} \sigma_I &= \sqrt{\frac{N_0}{2}T} \\ \sigma_Q &= \sqrt{\frac{N_0}{2}T} \end{aligned} \tag{B.7}$$

The standard deviation of the phase estimate is given by

$$\sigma_\theta \approx \left[\left(\frac{\partial\theta}{\partial\bar{I}}\right)^2\cdot\sigma_I^2+\left(\frac{\partial\theta}{\partial\bar{Q}}\right)^2\cdot\sigma_Q^2\right]^{1/2} \tag{B.8}$$

Computing

$$\begin{aligned} \frac{\partial\theta}{\partial\bar{I}} &= -\frac{\bar{Q}}{\bar{I}^2+\bar{Q}^2} \\ \frac{\partial\theta}{\partial\bar{Q}} &= \frac{\bar{I}}{\bar{I}^2+\bar{Q}^2} \end{aligned} \tag{B.9}$$

and considering eq. B.7, eq. B.8 becomes

$$\sigma_\theta \approx \left[\left(-\frac{\bar{Q}}{\bar{I}^2 + \bar{Q}^2} \right)^2 \cdot \frac{N_0}{2} T + \left(\frac{\bar{I}}{\bar{I}^2 + \bar{Q}^2} \right)^2 \cdot \frac{N_0}{2} T \right]^{1/2} = \sqrt{\frac{N_0 T}{2}} \cdot \frac{1}{(\bar{I}^2 + \bar{Q}^2)^{1/2}} \tag{B.10}$$

Substituting the value of eq. B.4 into eq. B.10, and remembering the definition of the signal amplitude $P = A^2/2$, the standard deviation of the estimated phase is found

$$\sigma_{\theta_{sin-sin}} = \sqrt{\frac{1}{2P/N_0 \cdot T}} \tag{B.11}$$

Mixing the sinewave input signal with a squarewave shaped reference one, we have as I and Q components of the resulting signal

$$\begin{aligned} I_{sin-sq} &\approx A \sin(\omega t + \theta) \frac{2}{\pi} \sin(\omega t) = \frac{2A}{\pi} \left[\cos(\theta) - \cos(2\omega t + \theta) \right] \\ Q_{sin-sq} &\approx A \sin(\omega t + \theta) \frac{2}{\pi} \cos(\omega t) = \frac{2A}{\pi} \left[\sin(\theta) + \sin(2\omega t + \theta) \right] \end{aligned} \tag{B.12}$$

and after the integral

$$\begin{aligned} \bar{I}_{sin-sq} &= \frac{2A}{\pi} T \cos(\theta) \\ \bar{Q}_{sin-sq} &= \frac{2A}{\pi} T \sin(\theta) \end{aligned} \tag{B.13}$$

Since the phase delay is estimated in the same way of Sine-Sine case

$$\theta = \arctan \left(\frac{\bar{Q}_{sin-sq}}{\bar{I}_{sin-sq}} \right) \tag{B.14}$$

we can substitute the I and Q value (eq. B.13) directly into eq. B.10, finding the expression for the standard deviation of the estimated phase in case of sine-square mismatched

$$\sigma_{\theta_{sin-sq}} = \pi \sqrt{\frac{1}{16P/N_0 \cdot T}} \tag{B.15}$$

In case of square-square matched case, the averaged in-phase and quadrature components are

$$\begin{aligned} \bar{I} &= \frac{A}{\sqrt{2}} T \left[1 - \frac{2\theta}{\pi} \right] \\ \bar{Q} &= \frac{A}{\sqrt{2}} T \left[-\frac{2\theta}{\pi} \right] \end{aligned} \tag{B.16}$$

and the phase delay is given by

$$\theta = \frac{\pi}{2}\left(\frac{-\bar{Q}_{sq-sq}}{\bar{I}_{sq-sq} - \bar{Q}_{sq-sq}}\right) \tag{B.17}$$

Computing the new partial derivatives of θ with respect to I and Q component, and substituting these values into B.8 we find

$$\sigma_{\theta_{sq-sq}} = \frac{\pi}{2}\sqrt{\frac{1}{2P/N_0 \cdot T}}\sqrt{\left(1 - 2\frac{\theta}{\pi}\right)^2 + \left(\frac{2\theta}{\pi}\right)^2} \tag{B.18}$$

The function

$$f(x) = \sqrt{(1-x)^2 + (x)^2} \tag{B.19}$$

assumes values from $0.5\sqrt{2}$ to 1, for $0 \leq \theta \geq \frac{\pi}{2}$. The standard deviation can be therefore written

$$\frac{\pi}{4}\sqrt{\frac{1}{P/N_0 \cdot T}} \leq \sigma_\theta \leq \frac{\pi}{2}\sqrt{\frac{1}{2P/N_0 \cdot T}} \tag{B.20}$$

Considering the relation between range (ρ), time (τ) and phase (θ) delay,

$$\sigma_\rho = \frac{c}{2} \cdot \sigma_\tau = \frac{c}{2} \cdot \frac{1}{2\pi f} \cdot \sigma_\theta \tag{B.21}$$

we can summarize the results found (eq. B.20, B.15, B.11) in terms of one-way range accuracy

	Time delay standard deviation
Sine-Sine Matched case	$\sigma_\rho = \frac{c}{4\pi f}\sqrt{\frac{1}{2P/N_0 \cdot T}}$
Sine-Square Mismatched case	$\sigma_\rho = \frac{c}{16 f}\sqrt{\frac{1}{P/N_0 \cdot T}}$
Square-Square matched case	$\frac{c}{16 f}\sqrt{\frac{1}{P/N_0 \cdot T}} \leq \sigma_\rho \leq \frac{c}{8\sqrt{2} f}\sqrt{\frac{1}{P/N_0 \cdot T}}$

Appendix C

Chip Tracking Loop performance

This appendix reports an analysis of the Chip Tracking Loop (CTL) structure and its performance in terms of phase estimate accuracy (closed-loop approach). What follows refers to Boscagli et al. (2008).

Since PN ranging code resembles a square-wave, the CTL is designed (fig. C.1) modifying a Data Transition Tracking Loop (DTTL). The in-phase integrator is controlled by the CTL NCO and it delivers to the Code Component Correlators the recovered chip. Since the ranging signal clock components is coherently related to the transmitted carrier frequency, an aided acquisition scheme can be used. The base frequency, obtained summing the nominal chip rate with the carrier loop error scaled by the ratio of the ranging chip rate by the up-link carrier frequency, is summed to the filtered loop error in order to tune the NCO frequency, used to drive the code generator blocks. Using that approach, the acquisition performance of the CTL is improved since it has to recover only the phase and not also the frequency.

The signal at the CTL input comes from the carrier quadrature channel and it can expressed as

$$r(i) = r(it_s) = A \sum_k a_k \cdot p(it_s - kT - \tau) + N_i \tag{C.1}$$

where

t_s is the sampling interval

A is the amplitude of the chip

T is the chip time

N_i is zero mean white Gaussian noise sample with variance

$$\sigma_i^2 = \frac{N_0}{2t_s} \tag{C.2}$$

τ is the random epoch to be estimated

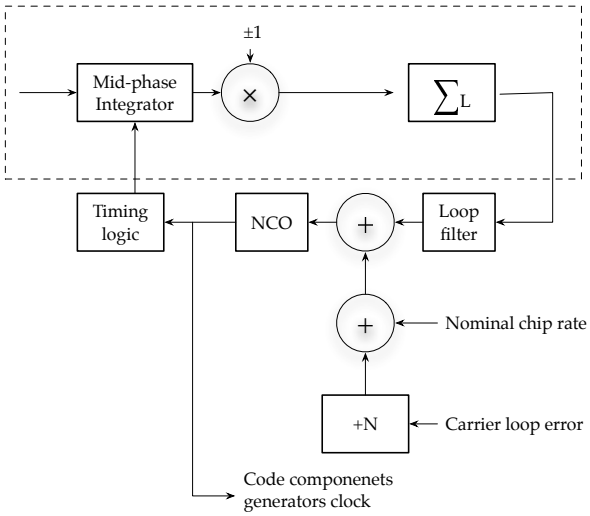

Figure C.1: CTL block diagram.

$p(t_i)$ is the square-wave functiona having value of 1 for $0 \leq t_i \leq T$ and having value 0 elsewhere

a_k represents the k-th chip polarity

The mid-phase integrator represents a solution matched to the signal for the phase error estimation. The input symbols have their leading edge at ...$kT + \tau$,$(k+1)T + \tau$,..., and that the loop generated its leading edges at ...$kT + \hat{\tau}$,$(k+1)T + \hat{\tau}$,..., so the timing error ϵ is

$$\epsilon = \tau - \hat{\tau} \tag{C.3}$$

To determine the tracking performance of the CTL in terms of timing jitter σ_ϵ^2 is possible to use a linear theory. We firstly define the S-curve as the mean value of the error control signal condition on the timing error

$$S(\epsilon) = L \cdot E(Q_k|\epsilon) \tag{C.4}$$

where

$E(\cdot)$ is the statistical expectation

ϵ is the timing error

Q_k is the quadrature channel output

L is the accumulation length of the integrate&dump following the quadrature branch of the CTL

The mid-phase integrator output (fig.C.2) is

$$Q_k = \sum_{i \in C_k} r(i) = \sum_{i \in C_k} \{A[a_k \cdot p(it_s - kT - \tau)] + N_i\} \tag{C.5}$$

where

$$C_k = \left\{ i : \left(k - \frac{1}{2}\right) T + \hat{\tau} \leq it_s < \left(k + \frac{1}{2}\right) T + \hat{\tau} \right\} \tag{C.6}$$

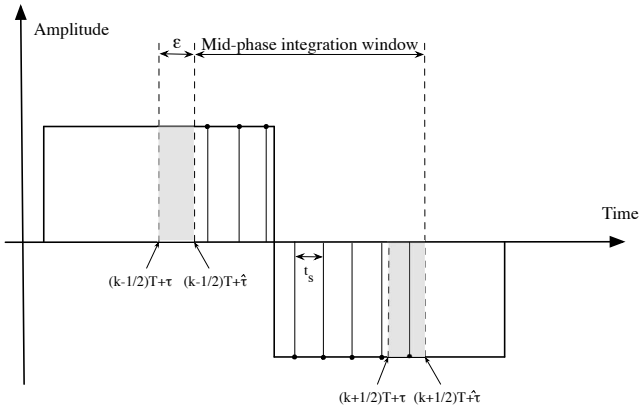

Figure C.2: Mid-phase integration.

The mean value of the output, after the multiplication by ± 1 in order to provide the right correction to the loop, is

$$E(Q_k) = 2A \cdot \left(\frac{\epsilon}{t_s}\right) \tag{C.7}$$

Substituting C.7 in C.4 we find a new expression, valid when loop is in tracking, for the S-loop curve

$$S(\epsilon) = 2AL \left(\frac{\epsilon}{t_s}\right) \tag{C.8}$$

Its slope at the origin represents the loop detector gain K_ϵ

$$K_\epsilon = \frac{\partial S(\epsilon)}{\partial \epsilon}|_{\epsilon=0} = \frac{2AL}{t_s} \tag{C.9}$$

When in tracking ($\epsilon \approx= 0$), the variance at the phase detector output is

$$\sigma_N^2 = L \cdot Var(Q_k()L\frac{N_0 T}{2t_s^2} \tag{C.10}$$

Using a linearized model of the CTL (fig.C.3), the loop error η can be written as

$$\eta = K_\epsilon \cdot \epsilon + N \tag{C.11}$$

being N the additive Gaussian noise. The timing jitter can be expressed as

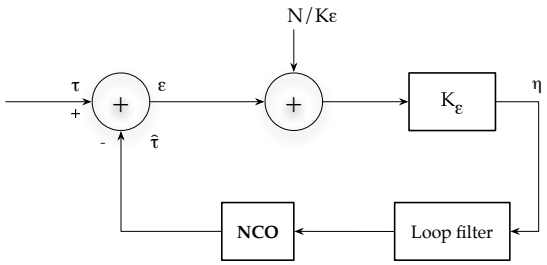

Figure C.3: CTL linearize model.

$$\sigma_\epsilon^2 = \frac{\left(\frac{S_N}{2}\right) \cdot 2B_L}{K_\epsilon^2} \tag{C.12}$$

where

B_L is the one side-loop bandwidth of the additive noise in the loop

S_N is the spectral density of the additive noise in the loop

$$\frac{S_N}{2} = \sigma_N^2 \cdot (L \cdot T) = L^2 \frac{N_0 T^2}{2t_s^2} \tag{C.13}$$

Using the last equations the CTL timing jitter becomes

$$\sigma_\epsilon^2 = \frac{\left(L^2 \frac{N_= T^2}{2t_s^2}\right) \cdot (2B_L)}{\left(\frac{2AL}{t_s}\right)^2} = \frac{N_0 T^2 B_L}{4A^2} \tag{C.14}$$

Considering the relation between the energy chip over noise spectral density ratio (E_C/N_0) and the ranging clock power[1] over noise spectral density ratio (P_{ck}/N_0)

$$P_{ck}/N_0 = \frac{1}{T}\frac{E_c}{N_0} = \frac{1}{T}A^2 T = A^2 \tag{C.15}$$

and considering that the frequency of the ranging clock component is half of the chip rate value ($f_{chip} = \frac{1}{T} = 2f_{ck}$) the variance of the timing jitter is

$$\sigma_\epsilon^2 = \frac{1}{16 f_{ck}^2}\frac{B_L N_0}{P_{ck}} \tag{C.16}$$

[1]Only the clock component is used for tracking the chip rate.

The one-way ranging jitter, being c the speed of light, can be finally written as

$$\sigma_{range_{sq-sq}}|_{CTL} = \frac{c}{2}\sigma_\epsilon = \frac{c}{8f_{ck}} \cdot \sqrt{\frac{B_L}{P_{ck}/N_0}} \tag{C.17}$$

If we consider an ideal sinewave shaped ranging signal (neglecting the losses due to channel filtering), the mean of mid-phase integrator output and the S-curve are

$$E(Q_k) = 2\sqrt{2}A\left(\frac{\epsilon}{t_s}\right) \tag{C.18}$$

$$S(\epsilon) = 2\sqrt{2}AL\left(\frac{\epsilon}{t_s}\right) \tag{C.19}$$

The loop gain becomes

$$K_\epsilon = 2\frac{\sqrt{2}AL}{t_s} \tag{C.20}$$

and the ranging jitter can be written as

$$\sigma_{range_{sin-sq}}|_{CTL} = \frac{c}{\sqrt{2}\cdot 8f_{ck}} \cdot \sqrt{\frac{B_L}{P_{ck}/N_0}} \tag{C.21}$$

Bibliography

Asmar, S.W., Armstrong, J.W., Iess, L., Tortora, P.. Spacecraft doppler tracking: Noise budget and accuracy achievable in precision radio science observations. Radio Science, 40, RS2001 2005;10.1029/2004RS003101.

Barbaglio, F., Ardito, A., Iess, L., Lanucara, M., Maddè, R., Mercolino, M., Rapino, G.. ESA DDOR enhancement: Agencies interoperability, wideband and low-snr functionality. 63rd International Astronautical Congress; 2012.

Benkhoff, J., van Casteren, J., Hayakawa, H., Fujimoto, M., Laakso, H., Novara, M., Ferri, P., Middleton, H.R., Ziethe, R.. BepiColombo-Comprehensive exploration of Mercury: Mission overview and science goals. Planetary and Space Science 2010;58:2–20.

Berner, J.B.. New tracking implementation in the deep space network. Tech Report, Jet Propulsion Laboratory; 2001.

Berner, J.B., Bryant, S.H.. Operations comparison of deep space ranging types: Sequential tone vs. pseudo-noise. IEEE Aerospace Conference Proceedings 2002;3:1313–1326.

Berner, J.B., Bryant, S.H., Andrews, K.S.. Future capabilities for the Deep Space Network. Jet Propulsion Laboratory, Space Ops; 2004.

Berner, J.B., Bryant, S.H., Kinman, P.W.. Range measurement as practiced in the Deep Space Network. Proceedings of the IEEE 2007;95:2202–2214.

Berner, J.B., Jayalar, S., Perret, J.D.. The NASA Spacecraft Transponding Modem. IEEE Aerospace Conference Proceedings 2000;7:195–209.

Berner, J.B., Layland, J.M., Kinman, P.W., Smith, J.R.. Regenerative pseudo-noise ranging for deep-space applications. Jet Propulsion Laboratory, TMO Progress Report 1999;42-137.

Bertotti, B., Comoretto, G., Iess, L.. Doppler tracking of spacecraft with multi-frequency links. Astronomy and Astrophysics 1993;269(1-2):608–616.

Border, J.S., Koukos, J.A.. Technical characteristics and accuracy capabilities of Delta Differential One-Way Ranging (DeltaDOR) as a spacecraft navigation tool. Proceedings of the RF and Modulation Subpanel 1E Meeting at the German Space Operations Centre; 1993.

Boscagli, G., Holsters, P., Simone, L.. End-to-end ranging jitter. Consultative Committee on Space Data Systems Space Link Services Ranging Working Group; 2006.

Boscagli, G., Holsters, P., Simone, L., Vassallo, E., Visintin, M.. Regenerative pseudo-noise ranging: Overview of current ESA's standardisation activities. 4th ESA International Workshop on Tracking, Telemetry and Command Systems for Space Applications; 2007a.

Boscagli, G., Holsters, P., Vassallo, E., Simone, L., Visintin, M.. An open and closed loop ranging jitter performance. Consultative Committee on Space Data Systems Space Link Services Ranging Working Group; 2008.

Boscagli, G., Holsters, P., Vassallo, E., Visintin, M.. PN regenerative ranging and its compatibility with telecommand and telemetry signals. Proceedings of the IEEE 2007b;95(11):2224–2234.

Bryant, S.. Using digital signa processor technology to simplify deep space ranging. IEEE Aerospace Conference Proceedings 2001;3:1277–1282.

CCSDS 414.0-G-1, . Pseudo-noise (PN) ranging systems: Recommendation for space data system standards. Green book CCSDS 414.0, Issue 1; 2010.

DeBoy, C.C., Haskins, C.B., Brown, T.A., Schulze, R.C., Bernacik, M.A., Jensen, J.R., Millard, W.P., Duven, D., Hill, S.. The RF teleccomunications system for the New Horizons mission to Pluto. IEEE Aerospace Conference Proceedings 2004;3:1463–1478.

ESA-ESTEC, . Space engineering, Ranging and Doppler tracking. volume E-50-02A. European Cooperation For Space Standardization (ECSS), 2005.

Genova, A., Marabucci, M., Iess, L.. A batch-sequential filter for the BepiColombo radio science experiment. Journal of Aerospace Engineering, Sciences and Applications 2012;IV(4):17–30.

Haskins, C.B., Duven, D.J., DeBoy, C.C., Jensen, J.R.. First deep-space flight demonstration of regenerative pseudo-noise ranging. IEEE Aerospace Conference Proceedings 2012;.

Iess, L.. MORE Science Performance Report (SPR). 2007.

Iess, L., Benedetto, M.D., Marabucci, M., Racioppa, P., Tortora, P., Corbelli, A., Fabbri, V., Graziani, A., Mariotti, G., Zannoni, M., James, N., Brown, A., Westcott, M., Simone, L., Colamarino, C.. Astra, interdisciplinary study on enhancement of end-to-end accuracy for spacecraft tracking techniques. European Space Operation Centre (ESOC) study; 2012.

Iess, L., Boscagli, G.. Advanced radio science instrumentation for the mission bepicolombo to mercury. Planetary and Space Science 2001;49(Issued 14-15):1597–1608.

Iess, L., Palmerini, G., Tortora, P., Persi, P., Mercolino, M.. Error analysis for Bepi Colombo radio science experiment. 2002.

Iess, L., Puyuelo, R.A., Ardito, A., Comoretto, G., Lanucara, M., Maddè, R., Mercolino, M., Rapino, G., Sensi, M., Tortora, P.. The European Delta-DOR correlator. 57th International Astronautical Congress; 2006.

James, N., Abellò, R., Lanucara, M., Mercolino, M., Maddè, R.. Implementation of an ESA delta-DOR capability. Acta Astronautica 2009;64:1041–1049.

Kinman, P.W.. Delta-Differential One Way Ranging System. DSMS Telecommunications Link Design Handbook. Jet Propulsion Laboratory, module 210; 2004.

Kinman, P.W.. Sequential ranging. DSMS Telecommunications Link Design Handbook. Jet Propulsion Laboratory, module 203B; 2009.

Kinman, P.W., Berner, J.B.. Two-way ranging during early mission phase. IEEE Aerospace Conference Proceedings 2003;3:1441–1455.

Maddè, R., Morley, T., Abellò, R., Lanucara, M., Mercolino, M., Sessler, G., de Vicente, J.. Delta-DOR, a new technique for ESA's deep space navigation. ESA bulletin 2006;128.

Martin, R., Warhaut, M.. ESA's 35-meter deep space antennas at New Norcia/Western Australia and Cebreros/Spain. IEEE Aerospace Conference Proceedings 2004;2:1124–1133.

Massey, J.L., Boscagli, G., Vassallo, E.. Regenerative pseudo-noise (PN) ranging sequences for deep-space missions. International Journal of Satellite Communications and Networking 2007;25(Issue 3):285–304.

Resch, G., Jacobs, C., Keihm, S., Lanyi, G., Naudet, C., Riley, A., Rosenberger, H., Tanner, A.. Calibration of atmospherically induced delay fluctuations due to water vapor. NASA/CP-2000-209893, International VLBI Service for Geodesy and Astrometry, General Meeting Proceedings; 2000.

Rife, D.C., Boorstyn, R.R.. Single-tone parameter estimation from discrete-time observations. IEEE Transactions on Information Theory-TIT 1974;20(5):591–598.

Ruggier, C.J.. Psuedo-noise and regenerative ranging. DSMS Telecommunications Link Design Handbook. Jet Propulsion Laboratory, module 214; 2004.

Simone, L., Gelfusa, D., Comparini, M.C.. On-board regenerative ranging channel: Analysis, design and test results. 3rd ESA Workshop Tracking, Telemetry Command System Space Application; 2004.

Tausworthe, R.C.. Tau Ranging Revisited. The Telecommunications and Data Acquisition Progress Report 42-91, Jet Propulsion Laboratory; 1987.

Tausworthe, R.C., Smith, J.R.. A simplified, general-purpose deep space ranging correlator design. The Telecommunications and Data Acquisition Progress Report 42-92, Jet Propulsion Laboratory; 1987.

Thornton, C.L., Border, J.S.. Radiometric Tracking Techniques for Deep-Space Navigation. Deep Space Communications and Navigation Series, JPL pubblication, 2000.

Tortora, P., Iess, L., Bordi, J.J., Ekelund, J.E., Roth, D.C.. Precise Cassini navigation during solar conjunctions through multifrequency plasma calibrations. Journal of Guidance, Control, and Dynamics 2004;27(2):251–257.